Analysis and Design Consideration of Millimeter-wave

Rectangular Dielectric Resonator Antennas

BY

SHANSHAN ZHAO
B.S., Nanjing University of Sci. & Tech., China, 2010

THESIS

Submitted as partial fulfillment of the requirements
for the degree of Doctor of Philosophy in Electrical and Computer Engineering
in the Graduate College of the
University of Illinois at Chicago, 2015

Chicago, Illinois

Defense Committee:

H. Y. David Yang, Chair and Advisor
Vitali Metlushko
Junxia Shi
Zheng Yang
Jing Liang, Google Inc.

ACKNOWLEDGEMENTS

I would like to express my gratitude to my advisor, Prof. H. Y. David Yang for his mentorship. He approved enough flexibility in conducting research projects which has helped me broaden my knowledge and grow as an independent researcher. On the other hand, he also provided insightful discussions and suggestions to guide my research efforts in the right direction. I would thank Prof. Danilo Erricolo, Prof. Sharad R. Laxpati and Prof. Piergiorgio L. E. Uslenghi who have helped me throughout my thesis-related course work at UIC and generously shared their immense knowledge and experience in research and academic matters such as technical writing and lab equipment operation. I am grateful to Prof. Vitali Metlushko, Prof. Junxia Shi and Prof. Zheng Yang for taking their precious time in the summer to serve on my defense committee. I appreciate the opportunity provided by Prof. Rashid Ansari of being a lecturer in the class. This not only enhanced the fundamental knowledge in my area, but also sharpened my professional lecturing skills. I thank Dr. Jing Liang who generously agrees to take his time from work to be my committee member and for the brief time we worked together, he has provided his professional opinions on many technical discussions. I leant a lot from my former lab mate Dr. Haijiang Ma who is always there whenever I need guidance in academy or in industry. I am thankful to my working experience in Tensorcom, Inc which provides me the opportunity to get familiar with the cutting-edge technology for high speed wireless personal and local area networks and make my work meaningful and practical in the real world. Special thanks to Jacobs School of Engineering, UCSD for providing the equipment for all the 60GHz antenna test. I thank Martha Salinas and George Ashman who has retired from UIC for their help regarding the lab equipment and TA courses. I thanked all the professors who I have been served

as teaching assistant to. They have broadened my academic views in different areas which helped to inspire different ideas. I thank all the staff, especially Ala Wroblewski, Tina Alvarado, Erica Plys, Evelyn Reyes and Mihai Bora in the Electrical and Computer Engineering department, UIC for providing solutions to the administrative and financial issues.

I also enjoyed a lot of help from my colleagues Negishi, Tadahiro, Dr. Picco, Vittorio and Rui Yang. I am thankful to all my friends in and around Chicago who have made my graduate life a more delightful experience than it was probably supposed to be.

Finally, I express my sincere gratitude to my parents, without whom none of my efforts would have been fruitful. Their unwavering support and care has been my greatest source of encouragement and inspiration.

SZ

TABLE OF CONTENTS

TABLE OF CONTENTS (continued)

TABLE OF CONTENTS (continued)

LIST OF TABLES

TABLE PAGE

LIST OF FIGURES

FIGURE PAGE

LIST OF FIGURES (continued)

FIGURE PAGE

LIST OF FIGURES (continued)

FIGURE PAGE

LIST OF FIGURES (continued)

FIGURE PAGE

LIST OF ABBREVIATIONS

DR	Dielectric Resonator
DRA	Dielectric Resonator Antenna
AiP	Antenna-in-Package
LTCC	Low Temperature Co-fired Ceramics
EMI	Electromagnetic Interference
FDTD	Finite-Difference Time-Domain
MoM	Method of Moments
VSWR	Voltage Standing Wave Ratio
CPW	Coplanar Waveguide
SIP	System-in-Package
UWB	Ultra-Wideband
WPAN	Wireless Personal Area Network
PHY	Physical Layer
FCC	Federal Communications Commission
EIRP	Equivalent Isotropically Radiated Power
WLAN	Wireless Local Area Network
CMOS	Complementary Metal-Oxide Semiconductor
LCP	Liquid Crystal Polymer
SIW	Substrate Integrated Waveguide
LTSA	Linear Tapered Slot Antenna
HMSIW	Half-Mode Substrate Integrated Waveguide
MIC	Microwave Integrated Circuit
MMIC	Monolithic Microwave Integrated Circuit
HD	High Definition
HFSS	High Frequency Structural Simulator
DWM	Dielectric Waveguide Model
PML	Perfect Matching Layer

LIST OF ABBREVIATIONS (continued)

EBG	Electromagnetic Band Gap
WiGig	Wireless Gigabit
MEMS	Microelectromechanical Systems
CTE	Coefficient of Thermal Expansion
PTFE	Polytetrafluoroethylene
AUT	Antenna Under Test
SoC	System-on-Chip
AoC	Antenna-on-Chip
DRAM	Dynamic Random-Access Memory
BGA	Ball Grid Array

SUMMARY

In last century, Dielectric Resonator (DR) has first been widely used in military world. Applications include filters, oscillators and other electronic components. In order to maintain the high-Q quality, it is usually enclosed in a metal box. Later, by removing the shield which is usually used for radiation prevention and applying lower dielectric constant materials, DRs have been brought to attention that they could also be treated as effective radiators. It is then widely accepted as a good antenna after a series of publications on cylindrical, rectangular and hemispherical dielectric resonator antennas (DRAs) published by Long et al. in 1983. Since then, the research topics on DRA have been driven into diverse directions. Efforts have been made for enhancement in bandwidth, compactness, polarization diversity, directivity, multifunction and so on. Traditionally, dielectric resonator antenna has been used in microwave range and advantages including small size, low loss, light weight, relatively wide bandwidth, ease of excitation and integration. Although many other shapes are developed over the years for different functionality, the most popular one is cylindrical for its ease of fabrication in microwave range and less mode density. Recently, mm-wave range, especially 7G unlicensed band around 60GHz has been brought to attention and considered as the spectrum for next generation mobile communication system. The advantages of using this band include large bandwidth available, compact size with attractive directivity and higher security. Taken into account the demand of high speed, ease of integration and operation, a high-gain low-profile antenna with end-fire radiation pattern is required.

Among all the shapes, rectangular DRA is much easy to fabricate in mm-wave range and has two degrees of freedom which is a good candidate for 60GHz high-speed Antenna-in-Package (AiP) design. By making it low-profile, it can provide end-fire radiation pattern which is convenient for operating the portable devices. However, no thorough study has been carried out for the antenna design of such applications in mm-wave range.

Previous researches have been focusing on the broadside radiation with nearly omni-directional pattern in which the DRA is excited at its lowest TE mode with a backside finite ground. This model is not suitable for end-fire antenna with planar excitation. In this thesis, theoretical method for mode study has first been chosen and proven its validity for eigenmodes in the DRA. Then a more practical model with planar excitation suitable for board integration in mobile system is presented and the characteristics equations are revised and applied to this new model to determine the modes excited in it. The industrial mainstream material LTCC is used as the substrate for most of the examples.

For the gain enhancement, previous methods either require much larger area or use the fundamental mode. The best choice in this scenario is to adopt higher order modes. However, the model under study is still ground-backed and no thorough design guide has been provided using end-fire gain as a criteria. This is the main purpose of this thesis. As for the low-profile DRA with relatively low dielectric constant, the most distinctive property is that it shows both the characteristics of dielectric resonator antenna and surface-wave antenna. Using end-fire gain as a criteria, the knowledge of surface-wave antenna is first applied to study the performance of the

antenna with different dimensions. Then the standing-wave modes of DRA bring certain variation to the gain curve. Various situations are discussed such as single-mode and degenerate-mode operation. Finally, the design rule of thumb is suggested and design curve is provided for preliminary end-fire antenna design using low temperature co-fired ceramics (LTCC) in 60GHz. Another popular material of Rogers 4350 is used as the substrate material to illustrate the potential effect of additional directors. Off-centered feeding is also investigated and solutions of beam tilt are discussed.

Based on these rules, several single antennas using different materials are fabricated and the results are discussed. In order to illustrate the advantages of the proposed antenna, it is compared with the performance of a linear tapered slot antenna. The ultimate goal of achieving sufficient gain in practical use is to integrate the antenna into communication system and use beamforming technique. Flip-chip technology is chosen to form the 1-by-1 T/R antenna system and certain measured and simulated data are compared. Eventually, 2-by-2 T/R antenna arrays can be integrated into the AiP system. By carefully design the property of antenna element, one can achieve beamforming system with different maximum gain and scanning range. This thesis serves as a design guide for low-profile high-gain rectangular DRA with end-fire pattern and planar excitation in 60GHz.

.

1. INTRODUCTION

1.1 Introduction of Dielectric Resonator Antennas

Dielectric Resonator (DR) has long been recognized valuable in designing filters, oscillators and other millimeter-wave components [1-4]. Theoretical studies have first been focusing on DR with high dielectric constant (ε_r > 20). Since the unloaded Q factor of the device is inversely proportional to tanδ and is usually very large [5], it is in general being treated as energy storage cavity rather than as a radiator. Due to its high permittivity, DRs are more compact than its metal cavity counterpart and more amenable to printed-circuit integration. In order to maintain a high Q factor and little radiation which are crucial for applications such as filters and oscillators, they are usually enclosed in metal cavities [6]. By removing the shield and applying lower dielectric constant materials, DRs have been brought to attention that they could also be treated as effective radiators. However, this idea had not been widely accepted until a series of papers on cylindrical, rectangular and hemispherical dielectric resonator antennas were published by Long et al. in the 1980s [7-9]. It was the first time that the theoretical and experimental study have been carried out systematically on the DRAs. Since then DRAs have received increasing attention in the past several decades. At the meantime, the most popular shape is cylindrical, as it is much easier and cheaper to fabricate than the others [10-17]. Since the last decade, new shapes, including conical, tetrahedral, hexagonal, pyramidal, elliptical, and stair-stepped shapes, or hybrid antenna designs, using dielectric resonator antennas in combination with microstrip patches, monopoles, or slots were also investigated for different applications [6]. Figure 1 shows a photo of DRAs with various shapes.

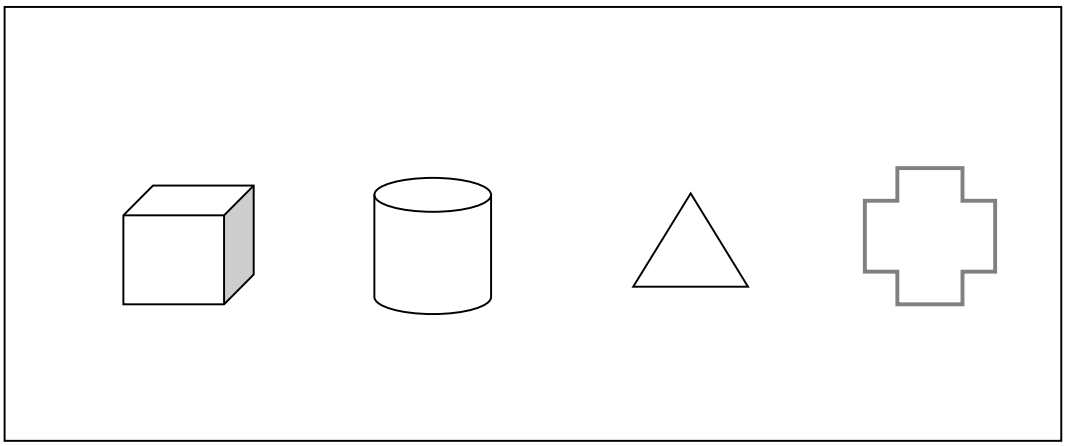

Figure 1 DRAs with various shapes

The parameters of interest relating to the DRA are discussed below.

1.1.1 Modes and Resonant Frequency

The basic quantity of a DRA is its modes and resonant frequencies. Further investigation that includes a DR with finite ground plane, where the latter serves as a mechanical support and the feed structure. Shielded DR is also of interest due to the EMI concern. This configuration will not only support 'DR' type modes, but also 'cavity' type modes.

Many methods have been developed for solving the modes inside a DR, depending on its shape. For instance, when it comes to the cylindrical DR, a simple magnetic wall model can provide a first-order solution that provides reasonably accurate predictions of the resonant

frequencies [7]. When a more accurate result is needed, mode matching method is an accurate numerical method [18], [19]. However, it is difficult to solve rigorously the modes in a rectangular DRA. Approximated methods, such as magnetic wall model and dielectric waveguide model can be applied. A more accurate FDTD method [20], [21] or MoM [4], [22] can be adopted for analyzing the aperture-coupled rectangular DRA. Nonetheless, it is time-consuming, memory intensive, and are not amenable to design or optimization.

Generally, According to Van Bladel [23], [24], for an arbitrarily shaped DR of high dielectric constant, if it satisfies:

$$\vec{\mathrm{E}} \cdot \vec{\mathrm{n}} = 0$$
$$\vec{\mathrm{n}} \times \vec{\mathrm{H}} = 0 \tag{1}$$

Then it is a confined mode. Otherwise, if it only satisfies $\vec{E} \cdot \vec{n} = 0$, it is a non-confined mode, where $\vec{n}$ is the unit vector normal to the body surface. The confined mode can only be supported by body of revolution, such as cylindrical and spherical DR. Thus, the rectangular DR can only support non-confined modes. For practical purposes, the theoretical and experimental investigations were limited to the fundamental (dominant) mode.

1.1.2 Radiation Pattern

Each mode of a DR antenna has a unique internal and external field distributions. Therefore, different radiation characteristics can be obtained by exciting different modes of a DR antenna [5]. An interesting feature of isolated DR antennas is that, in general, the different modes of a DR radiated like electric and magnetic multipoles such as a dipole, quadrupole, octupole, etc. The radiation pattern of a regular shape DR antenna can be predicted quite accurately without any extensive numerical computations [5].

As is mentioned of the concept of the confined and non-confined modes, it is necessary to discuss some interesting points of Van Bladel's theory. According to his theory, for a DR that supports the non-confined modes, the dominant fields that contribute to the radiation from non-confined modes is the magnetic-dipole fields. The other terms that contribute to the radiation are the electric dipole and higher-order magnetic and electric multipole fields. For instance, the lowest order mode of rectangular DR is known to radiate like a magnetic dipole. Once the pattern is determined, we could further discuss its other properties such as directivity, bandwidth and beam width.

1.1.3 Q Factor and Bandwidth

The impedance bandwidth of an antenna is defined as the frequency bandwidth in which the input VSWR of the antenna is less than a specified value S. The impedance bandwidth of a

resonant antenna, which is completely matched to a transmission line at its 'resonant frequency' is related to the total unloaded Q-factor (Q_u) of the resonator by the relation [5]:

$$\text{BW} = \frac{S-1}{Q_u\sqrt{S}} \tag{2}$$

For a DRA which has negligible dielectric and conductor loss compared to its radiated power, the total unloaded Q-factor (Q_u) is related to the radiation Q-factor (Q_{rad}) by the following relation [5]:

$$Q_u \approx Q_{rad} \tag{3}$$

Since the radiated Q-factor depends on the total stored energy and the power radiated by the DRA, the Q calculation is based on the field pattern at a certain mode. Certain approximations have to be made to derive the field and power. Thus, the mathematic expression of Q are usually found in literature for a specific case of DRA. Some may come from the approximate analysis. Other results come from curve fitting the numerical results from a rigorous numerical method [25].

1.1.4 **Excitation Schemes**

Since the actual modes existing in a DRA is determined by the excitation method used, feeding scheme needs to be chosen carefully in order to obtain a certain pattern or bandwidth requirement. Typical excitation schemes include [6]:

- By probe (vertical and horizontal) [7-9], [10-12]
- By dielectric image guide [26-28]
- By annular structure [29, 30]
- By microstrip line or CPW [31-36]
- By monopole or dipole [37-40]
- By slot [41-44]

1.1.5 **Other Topics**

With the enormous demand of wireless applications and service, many more researchers have begun investigating other possibilities that dielectric resonator antennas can provide. Further topics of interest lies in [6]:

- Low-profile and compact design [45, 46]
- Polarization implementation [47, 48]
- Linear and planar array [27, 48]
- Increased directivity [49, 50]

- Ultra-wide band/ multi-band [51, 52]
- Active/ tunable [53, 54]
- Effect of finite ground plane and shield [46, 54]
- Dual functions [55, 56]
- SIP integration [57, 58]
- Micro-machining fabrication technique etc. [59, 60]

1.2 Overview of Millimeter-wave Antennas

The demand of wireless local/personal area network (WLAN/WPAN) over the last decades is ever increasing. Standards such as 802.11a/b/g, ultra-wideband (UWB) and Bluetooth are all operated below 10GHz and the spectrum in the low gigahertz bands is likely to be overly congested in the near future [61]. Multimedia communications also requires high capacity with over subGbps transmission interfaces such as IEEE 1394 (100, 200, 400Mbps), Gigabit Ethernet and so on. It is an urgent issue that we consider moving up on the frequency scale to satisfy these needs.

The millimeter –wave region of the electromagnetic spectrum is commonly defined as the 30 to 300 GHz band. Utilization of this range for the design of data transmission and sensing systems has a number of advantages [62]:

- Large bandwidth permits a high data rate.

- Short wavelength allows the design of high directivity with a reasonable size. Thus compact systems with high resolution are feasible.

- Mm-wave can penetrate through fog, snow, dust better than infrared or optical waves.

- Finally, mm-wave transmitters and receivers lend themselves to integrated and monolithic design approaches, making RF heads which are compact and inexpensive.

There are plenty of available spectrum within the mm-wave range. Multiple factors need to be considered for a certain application. For instance, absorption by rain and atmospheric gases is the dominant effect in mm-wave range and it is obvious that the desired transmission range directly determines the operating frequency of an mm-wave system. Figure 2 shows the frequency dependence of mm-wave attenuation by atmospheric oxygen and water vapor. If large transmission distance is desired, low-attenuation windows a 35, 94, 140, 220 and 340 GHz can be chosen. However, if we choose the frequency near the steep absorption lines, it is not necessarily an inoperable band.

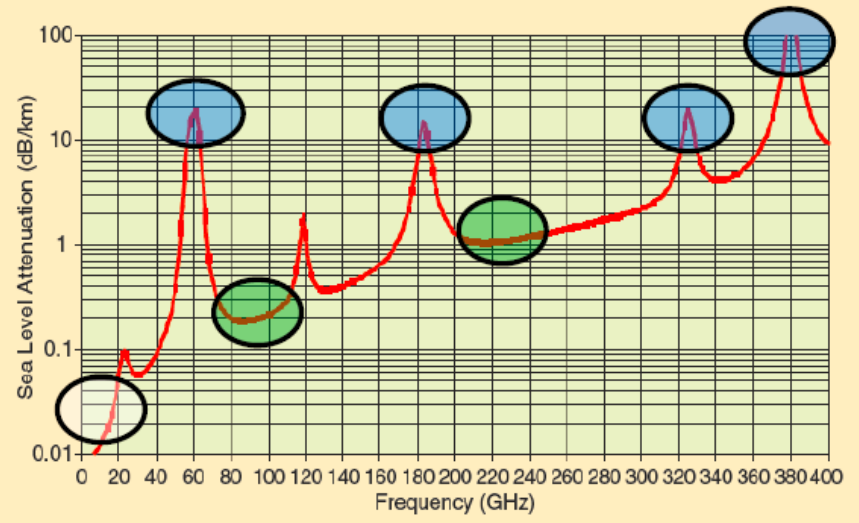

Figure 2 Attenuation of millimeter wave by atmospheric oxygen and water vapor

Among these bands, the unlicensed spectrum at the 60 GHz carrier frequency is proven to be at the spectral frontier of high-bandwidth commercial wireless communication systems as shown in Figure 3. Compared with microwave band communication, spectrum at 60 GHz is plentiful (frequencies of 57–64 GHz are available in North America and Korea, 59 – 66 GHz in Europe and Japan) [64]. In the past, the mm-wave system was primarily found in the military due to its high security as well as its ability to travel through dust and battlefield smoke with little attenuation, but its application has been extended to the civil sector in recent years [64]. In July 2003 the IEEE 802.15.3 working group for WPAN began investigating the use of the 7GHz of unlicensed spectrum around 60 GHz as an alternate physical layer (PHY) to enable very high-

data-rate applications such as high-speed Internet access, streaming content downloads, and wireless data bus for cable replacement [65]. The targeted data rate for these applications is greater than 2 Gb/s. Although the attenuation is more severe (20 dB larger free space path loss due to the order of magnitude increase in carrier frequency, 5–30 dB/km due to atmospheric conditions [66], and higher loss in common building materials [67]) resulting in the short communication distance, it actually benefits from the attenuation providing extra spatial isolation and higher implicit security. This also allows one to control the transmission distance by adjusting the frequency, thus 'overshoot' can be minimized to avoid unwanted interference. Furthermore, due to oxygen absorption, the FCC regulations allow for up to 40 dBm equivalent isotropically radiated power (EIRP) for transmission, which is significantly higher than what is available for the other WLAN/WPAN standards [65]. Moving to higher frequencies also reduces the form factor of the antennas. That is, for a fixed area, more antennas can be used, and the antenna array can increase the antenna gain. We could more easily grasp the control of varied-functional antenna design, such as point-to-point, point-to-multipoint, steerable beams due to different applications. The wide bandwidth, high allowable transmit power, design convenience and regulatory agencies' effort on spectrum allocation form a revolutionary markets on millimeter-wave antennas in the coming future.

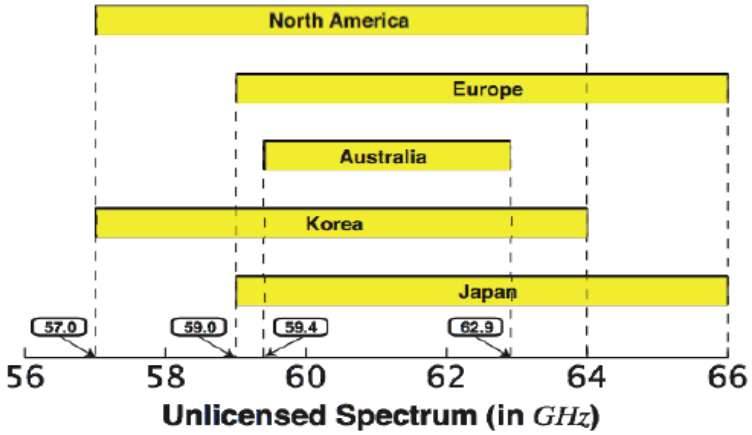

Figure 3 Unlicensed spectrum at the 60 GHz

The mm-wave antennas in the literature so far can be categorized roughly by different processes and different antenna types. For the simplest and lowest-cost solutions, single antenna-on-chip is attractive due to the maturely developed CMOS industry. However, we must overcome the challenges of low on-chip efficiencies (typically 10% or less [69]) and low gain (typical gains for single on-chip antennas without lenses are -20 to -10 dBi). For mm-wave point-to-point high-speed application, we favor the in-package antennas more which can provide us a relatively higher gain and efficiency due to its distance away from the chip. However, we still cannot ignore the lossy package interconnects (standard wire-bonds are limited to under 20 GHz [70]). For in-package antennas, package material with low dielectric constants will give the best gain-bandwidth products [71], but this must be weighed against other factors, including

manufacturing precision and available interconnect technologies (for example, wire-bonding, flip-chip, or coupling connections) [72], [73]. Popular package technologies include low-temperature co-fired ceramic (LTCC, $\varepsilon_r = 5.9 - 7.7$) [74], [75], fused silica ($\varepsilon_r = 3.8$) [76], liquid crystal polymer (LCP, $\varepsilon_r = 3.1$) [77], and Teflon ($\varepsilon_r = 2.2$) [72]. A number of challenges are also reported in 2010 by Kamet et al, including detuning of antennas due to the presence of packaging materials, difficulty in meeting mechanical and electrical reliability requirements, antenna interference from heat sinks, and possibly the high expense of packaging processes [78]. As for antenna types being investigated so far, Table I summarized antennas in terms of its gain, operation frequency, type and process. Popular structures include Yagi antenna, dipole antenna, patch antennas, inverted-F antenna, substrate integrated waveguide (SIW) antenna, linear tapered slot antenna (LTSA) and dielectric resonator antenna (DRA).

Fundamentally speaking, the choice of process and type of an mm-wave antenna is determined by its desired radiation pattern. This includes control over its direction and shape. For high-speed transmission, a system with high directivity is required with the assistance of beamforming and planar array technique. However, for certain mm-wave guidance and radar systems, fan-shaped radiation characteristics are required, and vehicular communication implies the use of omnidirectional antennas providing a circular symmetric pattern in the azimuth plane and moderate directivity in the elevation plane. Other mobile devices impose requirements on the direction of the main beam and the beam width. Polarization is another aspect needed to be taken into account when designing an mm-wave antenna.

Table I Summary of 60GHz antennas from literature

Reference	Gain (dBi)	Frequency (GHz)	Type and Process
[79]	3.6	61	Dipole, 150nm, pHEMT
[80]	3.2	60	Rectangular DRA, SOC
[81]	9	55-66	Rectangular DRA, SIP
[82]	-19	61	Inverted F, BEOL process
[83]	6	58.3-59.5	Yagi, LTCC ball grid array
[78]	5/ element	58.32-64.8	16 patch array, ball grid
[84]	4.9-6.9	45-75	LTSA backed with an air cavity on LTCC
[85]	10-12	55-61	2*4 array of SIW cavity-backed slot antenna

1.3 Advantages of Rectangular DRAs in Millimeter-wave Band

In general, the dielectric resonator antenna is simply made of dielectric material, whose loss can be made very small even at mm-wave frequencies. Another advantage of this is the size of the antenna is proportional to $\lambda_0/\sqrt{\varepsilon_r}$ with λ_0 and ε_r being the free-space wavelength and relative dielectric permittivity, respectively which in nature has a miniaturizing effect. Since the fundamental radiation schemes of DRA and microstrip antenna are both resonance, the former is usually considered as an alternative of the later. As compared to the microstrip antenna, they do share certain similarities. For instance, since the dielectric wavelength is smaller than the free-space wavelength by a factor of $1/\sqrt{\varepsilon_r}$, both of them can be made smaller in size by increasing

εr. Moreover, virtually all excitation methods applicable to the microstrip antenna such as probes, microstrip, slots, waveguides, substrate integrated waveguide (SIW), and half-mode substrate integrated waveguide (HMSIW) can be used for the DRA and the whole system is light-weighted. However, DRA has a much wider impedance bandwidth (~ 10 % for dielectric constant ε_r ~ 10) [13]. This is because the microstrip antenna radiates only through two narrow radiation slots, whereas the DRA radiates through the whole DRA surface except the grounded part. Since the whole body of the substrate is served as the radiator, it brings in more freedom in antenna design. For example, a trapezoidal DRA has been demonstrated with an impedance bandwidth of 55% and broadside radiation patterns with low cross-polarization [86]. Not only does the substrate material served as a radiator, it could also be used as packing cover [87]. Other advantages of the DRA include its compatibility with MIC's and ability to obtain different radiation patterns using different modes. All these features make the DRA an excellent antenna candidate for mm-wave systems.

Among all the shapes of DRA, rectangular one has not been as popular as the cylindrical one in the military and radar applications in microwave range. However, when it comes to mm-wave range, it becomes difficult to fabricate cylindrically-shaped resonators owing to their small size. Also, the modes in cylindrical DRA are purer and less dense than in the rectangular one which is more difficult to analyze because of the increase in edge-shaped boundaries. However, with the huge drive of the promising mobile communication market, more research efforts have been paid on investigating rectangular DRAs in the civil use since it is more convenient with an end-fire pattern which is easily achieved using this shape. In order to compare the geometries of

the DRAs, the dimensional degrees of freedom are considered [13]. For a DRA with rectangular cross section, two of the three dimensions (length, width and height) can be varied for a given resonant frequency and for a fixed dielectric constant. Hence, it has two degrees of freedom. Compared with the other two, cylindrical one has two degrees of freedom and hemispherical DRA has zero. The rectangular DRA offers practical advantages over the spherical and cylindrical shapes, due to the flexibility in choosing the aspect ratios [88].

1.4 Motivation

Dielectric resonator antennas have long been proven as an efficient and effective antenna in microwave range with the advantages of light weight, ease of excitement, ease of integration and etc. In the lower frequency range, they are usually excited in the lowest order mode and treated as an attractive alternative to other low-gain antennas such as microstrip antennas or dipoles. Multiple feeding schemes can be applied, among which the most popular one is the slot-coupling with a finite ground. In this case, the rectangular DRA behaves like a short magnetic dipole giving a broadside radiation with a relatively low gain.

Within the past several decades, mobile data traffic and device quantity are growing rapidly which exerts a great pressure on the system capacity. The current network traffic are video dominant which requires a large bandwidth to sustain the high speed and the newly-developed mobile devices, such as smart watch and fitness band, provide very limited space and majorly supported by the poorly-performed Bluetooth. Other demands such as low latency

access and low interference drove the transition of mobile communication system towards 5G in which mm-wave range is adopted. With the 7GHz unlicensed band at 60GHz, large bandwidth is achievable while high speed and low interference are obtained by the high-gain antenna. Traditionally, high-gain configurations include horn, lens and reflector antennas. However, it is quite difficult to integrate them to the MMIC in mobile devices. However, dielectric-based antennas such as surface-wave dielectric rod antennas or dielectric resonator antennas show a great number of advantages over a wide range of aspects.

When it comes to mm-wave range, simply scaling up the existing design in microwave range may not apply any more. Besides, with the newly developed needs in WPAN system, such as high-speed point-to-point communication system, certain high-gain end-fire radiator is in demand for ease of use especially for hand-held devices. However, most thorough studies are carried out with the broadside radiation. Current research focuses more and more on the model simulation instead of theoretical study due to the improvement of the full-wave simulation tool. It is believed that there is still a huge academic vacancy left to be filled in, especially the issue of how to use the theoretical tool as a guidance to optimize the mm-wave antenna system. Some preliminary practical antenna and system designs using rectangular DRA as an end-fire radiator have already shed light on its promising future and put into pre-commercial test. Such a practical WiGig system has great potential in next-generation wireless communication system applications including:

- Instantly HD video steam to your mobile phone, tablet, notebook, or HDTV

- Wireless sharing of high-resolution photos or video from your camera or HD camcorder
- Backing up GBs of data to a wireless hard drive in seconds
- Connecting a notebook to an projector without any cables

Thus, with all purpose, a thorough study on its behavior in mm-wave range is needed as guideline for the future design.

1.5 Objectives of the Thesis

Based on the previous research and the newly-emerged application requirements, this thesis will mainly focus on the understanding of low-profile end-fire rectangular resonator antenna with planar excitation which is suitable for board integration in mobile systems. It is obvious that the radiation pattern is determined by the modes excited within the DRA. Rigorous numerical methods are highly accurate, yet time-consuming which may not be applicable for practical usage. The purpose of this thesis is to first study the performance of the rectangular DRA in millimeter waves, and then apply it to the design of the 60GHz end-fire system. Thus an approximation method will be adopted and HFSS simulation for both eigenmodes and excitable modes with a certain feeding method will serve as proof of the validity of the analysis method. The analysis will be based on a more realistic model with a planar dipole excitation.

Once the analysis method has been established, the characteristics of a single center-fed DRA will be studied using the end-fire gain as the criteria. The effect on the end-fire gain of each element of the DRA structure will be investigated and finally a practical design curve will be provided for preliminary design. Based on this, other properties will be studied, such as the application of additional director and off-centered feeding. Several sample antennas will be implemented and test the theory.

At last, Antenna-in-Package (AiP) and flip-chip technology will be introduced to integrate the antenna into the system. Test and measured results will be compared. Based on the knowledge of the single antenna, a two-by-two antenna system will be presented with two operation modes.

In conclusion, this thesis will serve as design considerations and a guideline of mm-wave end-fire rectangular DRA system design.

1.6 Overview of the Thesis

The next five chapters of this dissertation are outlined below:

Chapter 2 first introduces several methods of analyzing the modes in rectangular DRA. The most efficient and practical one is proven to be dielectric waveguide model (DWM) method. In order to prove its validity, eigen-mode simulation using full-wave simulator HFSS is carried out for a certain DRA with fixed dimensions. However, the actual excitable modes in DRA are

determined not only by its dimension, but also by its feeding method. Thus a more practical model is introduced and proven to have practical use. Possible modes in the DRA are discussed and mode analysis is revised according to this new model. The simulated field distribution will be used to prove the accuracy of the method.

Chapter 3 focuses on the characteristic study of the DRA using end-fire gain as a main parameter. LTCC substrate is taken as an example for study. Although the rectangular DRA has a design freedom of two, the thickness of the DRA is proven to be the most sensitive dimension and it will greatly vary the properties of the antenna. The knowledge of surface-wave antenna is used to study the performance of the antenna since for an open cavity with a permittivity not high enough, these two antennas are very similar. Various situations are discussed under different thickness, or more accurately, different excited modes. Then design rule of thumb is suggested and design curve is provided for preliminary end-fire antenna design in 60GHz. Another popular material of Rogers 4350 will be used as the substrate material to illustrate the potential effect of additional directors. Off-centered feeding will also be investigated and solutions of beam-tilt will be discussed.

Chapter 4 presents several single antenna examples which have been simulated, fabricated and tested to prove the validity of the previous conclusions. Testing method will be introduced and results are compared.

Chapter 5 applies the knowledge of single DRA onto the mm-wave antenna system design. The idea of Antenna-in-Package is introduced as well as the flip-chip technology.

Several systems are fabricated and tested. Finally, the method extends to the linear array design and a two-by-two antenna system will be presented with two operation modes suitable for different end-fire applications.

Chapter 6 summarizes the results of this thesis and discuss the possible directions and challenges for future work.

2. MODE STYDY OF RECTANGULAR DRA

As an antenna, the most important feature is its radiation pattern. And when it comes to the radiation of dielectric resonator antenna, this feature is directly related to the modes excited within it. These modes also affect other properties of the antenna, such as bandwidth and cross-polarization level. Thus, it is crucial to thoroughly study the resonant modes of a certain-shaped DRA. As simple as the shape of a rectangle, the electromagnetic fields within the DRA is otherwise quite complex. An analytical closed-form solution for all but the hemispherical DRA does not exist. On the other hand, resonant frequencies of eigenmodes are also different for different excitation schemes, especially the one which is suitable for the mm-wave mobile devices. This chapter will focus on the mode study method of a rectangular DRA and developing a practical model.

2.1 Introduction of Analysis Methods

The analysis methods of a rectangular DRA can be generally divided into numerical and approximate methods. Over the years, various numerical techniques such as the Method of Moments (MoM) [89] or the Finite Difference Time Domain (FDTD) method [90] can be used to solve for these fields, but these techniques are time consuming, memory intensive, and are not amenable to design or optimization. Thus this section will focus on the approximate methods instead. Mainly, two approximate techniques have been reported in the literature for analyzing rectangular dielectric resonators.

2.1.1 Magnetic Wall Model Method

Magnetic wall model method was first introduced by Okaya and Barash [91]. An assumption has been made that the boundary coincides with a node or antinode of either the electric or magnetic field which is valid if the dimension is larger than the effective wavelength in the resonator. By solving the Maxwell equations assuming $\mu = 1$:

$$\nabla \times \mathbf{E} = -\dot{\mathbf{H}}$$
$$\nabla \times \mathbf{H} = \varepsilon \dot{\mathbf{E}} \tag{4}$$

The solutions of the three components of the electric field are in certain sinusoidal form. By applying the boundary condition, the expression for nonzero electric field can be found.

The name of 'magnetic wall model' originates from the boundary condition used for the solutions. The dielectric resonator is seen as a truncated part of an infinitely long waveguide. Then magnetic wall condition is applied to the terminated surfaces which is also called the open-circuit condition. By assuming the magnetic wall condition, it basically requires the fields near the surface to satisfy the following equations:

$$\mathbf{E} \cdot \mathbf{n} = 0$$
$$\mathbf{n} \times \mathbf{H} = 0 \tag{5}$$

However, Van Bladel has pointed out in [92] that the modes of a dielectric resonator can be divided into confined and non-confined types. The fields of confined type satisfy equation (5)

and yet can only be supported by spherical and cylindrical body. For rectangular one, it only meets the first condition of magnetic wall even when the dielectric constant of the resonator tends to infinity, thus proving the magnetic wall model not valid.

2.1.2 Dielectric Waveguide Model Method

Dielectric waveguide model (DWM) method is first proposed by Marcatili [93] to determine the guided wavelength of dielectric guides with a rectangular cross-section and then applied to determine the resonator frequency of rectangular DR by Itoh and C. Chang in [94]. Instead of using a magnetic wall condition on the terminal surfaces as in the previous method, proper impedance walls are applied. The isolated DR model of interest is shown in Figure 4. Again the DR is assumed to be a truncated section of an infinite dielectric waveguide having the same transverse dimensions.

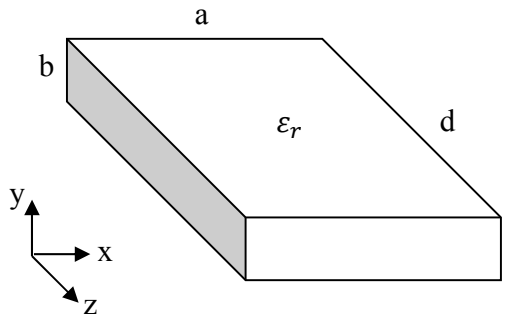

Figure 4 Isolated DR model

The first step would be solving the guided wavelength of an infinite dielectric waveguide. Based on the model in Figure 4 except that the wave is propagating along z direction, the cross-section field distribution is illustrated in Figure 5. For well-guided modes which usually occur in the DR with large permittivity, fields are assumed to distribute sinusoidally within the DR, decay exponentially outside the DR and little exist in shaded areas. When the guide is truncated with a length of d, a standing wave pattern is set up inside the dielectric in the z-direction as well. The standing wave pattern in x- and y-directions is still governed by the characteristic equations that are the same as those valid for the isolated infinite dielectric waveguide. According to Itoh [94], the terminated impedance is defined as:

$$Z_L = \frac{j\omega\mu}{\gamma} \tag{6}$$

with $$\gamma^2 = k_x^2 + k_y^2 - k_0^2$$

The nature of this equation determines the application of a DR. If $k_0^2 < k_x^2 + k_y^2 < \varepsilon_r k_0^2$ or $k_z^2 < (\varepsilon_r - 1)k_0^2$ in which case γ is real. The power within the DR will be fast attenuated in the air and radiation from it is negligible. This makes a good high-Q resonator. On the other hand, when $(\varepsilon_r - 1)k_0^2 < k_z^2 < \varepsilon_r k_0^2$ is satisfied, radiation occurs from two end surfaces. This can be explained using ray propagation as well. With k_z increasing, the incident angle of the rays at the end surface becomes less than the critical angle of total internal reflection and the radiation occurs as y becomes imaginary. This is the situation when the DR is used as an antenna.

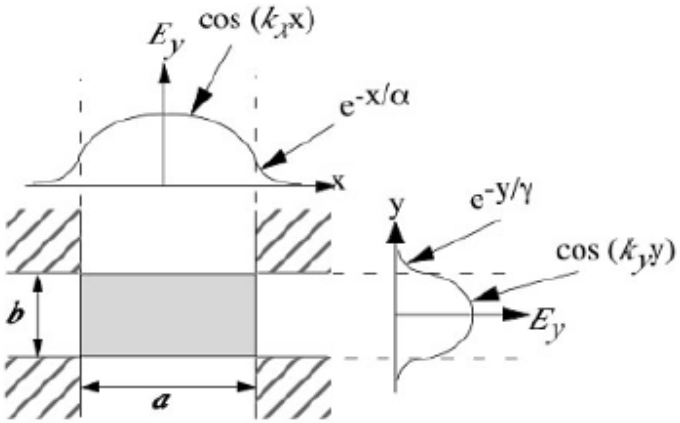

Figure 5 Cross-section field distribution

Here we assume the thickness b in y direction has the smallest dimension. Thus the mode within can be divided into families of TM^{y}_{mnl} f and TE^{y}_{mnl} modes where m, n, l denote the number of extremas in the x-, y-and z-directions inside the dielectric guide. Taken TE^{y}_{mnl} as an example, the characteristics equations are given in [95]:

$$k_y b = n\pi - 2\tan^{-1}(k_y / k_{y0}) \quad \text{n=1, 2, 3,…}$$

$$k_x a = m\pi - 2\tan^{-1}(k_x / \varepsilon_r k_{x0}) \quad \text{m=1, 2, 3,…} \tag{7}$$

$$k_z d = l\pi - 2\tan^{-1}(k_z / \varepsilon_r k_{z0}) \quad \text{l= 1, 2, 3,…}$$

where

$$k_{y0} = [(\varepsilon_r - 1)k_0^2 - k_y^2]^{1/2}$$

$$k_{x0} = [(\varepsilon_r - 1)k_0^2 - k_x^2]^{1/2}$$

$$k_{z0} = [(\varepsilon_r - 1)k_0^2 - k_z^2]^{1/2}$$

In the equations above, k_{x0}, k_{y0} and k_{z0} represent decay constants of the field along the x- and y-directions outside the dielectric guide and k_x, k_y and k_z represent the ones inside. k_0 is the free space wave number. Thus, the frequency at which k_x, k_y and k_z computed, as discussed above, also satisfy the separation equation $k_x^2 + k_y^2 + k_z^2 = \varepsilon_r k_0^2$, is the resonant frequency of the TE_{mnl}^{y} mode. Sometimes it is also designated as $TE_{m\delta l}^{y}$ mode since the thickness is, strictly speaking, only fraction of half wavelength and δ is defined as:

$$\delta = \frac{k_y}{\pi/b} \tag{8}$$

It is worth mentioning that the second and third equations in (7) are TM mode characteristic equations for a dielectric slab waveguide of thicknesses a and d, while the first equation is TE mode characteristic equations for a dielectric slab waveguide of thicknesses b and dielectric constant of ε_r [95]. There are two kinds of TE/TM mode solutions for a slab waveguide: even

mode and odd mode. For solution of TE modes, since this thesis focuses on the low-profile DRA which means the thickness of the DR is much smaller than the other two dimensions, n is always 1. For solution of TM modes, the possible value for m and l are determined by the boundary conditions. For instance, m and l are odd numbers when x=0 and z=0 planes are electric walls. For well-guided modes, the fields are confined within the resonator and a further approximation can be made:

$$k_x = \frac{m\pi}{a},\ k_y = \frac{n\pi}{b},\ k_z = \frac{l\pi}{d} \tag{9}$$

2.2 Theoretical and Simulated Eigenmodes

In last subsection, DWM method is assumed to be a good candidate for first-order approximation for mode study. By solving the characteristic equations, the theoretical resonant frequency at different modes can be calculated. Here, in order to verify the accuracy of this method, a DR example is presented with dimensions of a×b×d=4mm×0.7mm×7mm. This satisfies the assumption we made earlier that width a and length d is relatively larger than thickness b. The substrate material has a dielectric constant of 7.5 which is a typical value of LTCC (low temperature co-fire ceramic) which is a popular material used in mm-wave systems.

Also, for comparison, an HFSS eigenmode model is provided. PMLs are placed on left, right, up and down surfaces while master/slave boundary is applied on front and back as shown in Figure 6. By changing the phase offset between the master and slave boundaries, we can determine various modes via the field distribution within the DR. Since the eigenmode

simulation is time- and space-inefficient, we have to increase gradually the lower bound frequency to determine one mode at a time. Table II illustrates the comparison of the theoretical and simulated values of different modes calculated up to 60GHz. It is worth mentioning that since the dielectric resonator is enclosed by an air box, the eigenmode solver can solve both the resonance of the dielectric resonator and the metal box. If the air box is too close to the dielectric resonator, the default min frequency in the frequency setup will increase causing the missing of the modes with lower resonant frequency, such as the lowest order of TE mode TE_{111}^{y} with a theoretical resonant frequency of 27.4GHz. If you increase the dimension of the air box to several wavelength, the missing modes will gradually emerge. However, this will significantly increase the calculation time and space required. Also, here we ignore the fact that for thin substrate, the thickness is only a fraction of the half wavelength since this fraction is not easy to determine. By using n=1, as we can see in the table, the error is within tolerance.

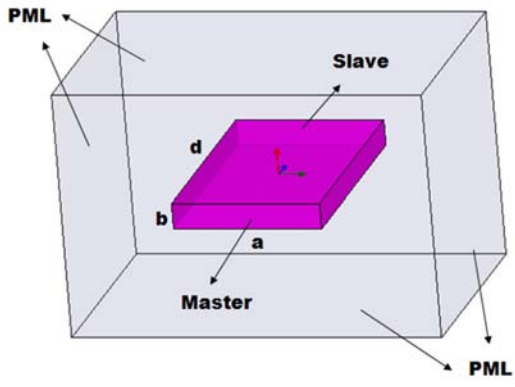

Figure 6 HFSS eigenmode model with dimensions of a×b×d=4mm×0.7mm×7mm

Table II Comparison of theoretical and simulated resonant frequencies of the DR

Mode	TE^{y}_{111}	TE^{y}_{112}	TE^{y}_{113}	TE^{y}_{212}	TE^{y}_{213}	TE^{y}_{214}
Theoretical fr (GHz)	27.4	33.5	40.5	45	50	55.5
Simulated fr (GHz)	27.1	33.1	41	41.7	49	55.7
Percentage error (%)	1.1	1.2	1.2	7.3	2	0.36

Strictly speaking, TE^{y}_{111} mode is not the mode that has the lowest resonant frequency. If we consider modes with other polarizations, TM^{z}_{111} mode and TM^{x}_{111} mode have resonant frequencies of 23.8GHz and 26.7GHz respectively. The reason why TE^{y}_{111} attracts more attention in literatures is due to the popular feeding method intended to use in practical applications. This will be addressed in the next section.

To give a clear idea of how the field is distributed, the fields for the TE^{y}_{112} mode of an isolated DRA in free space are shown in Figure 7. These fields are results of the HFSS eigenmode simulation. From the figure, we can see that these fields are similar to those produced by a short magnetic dipole.

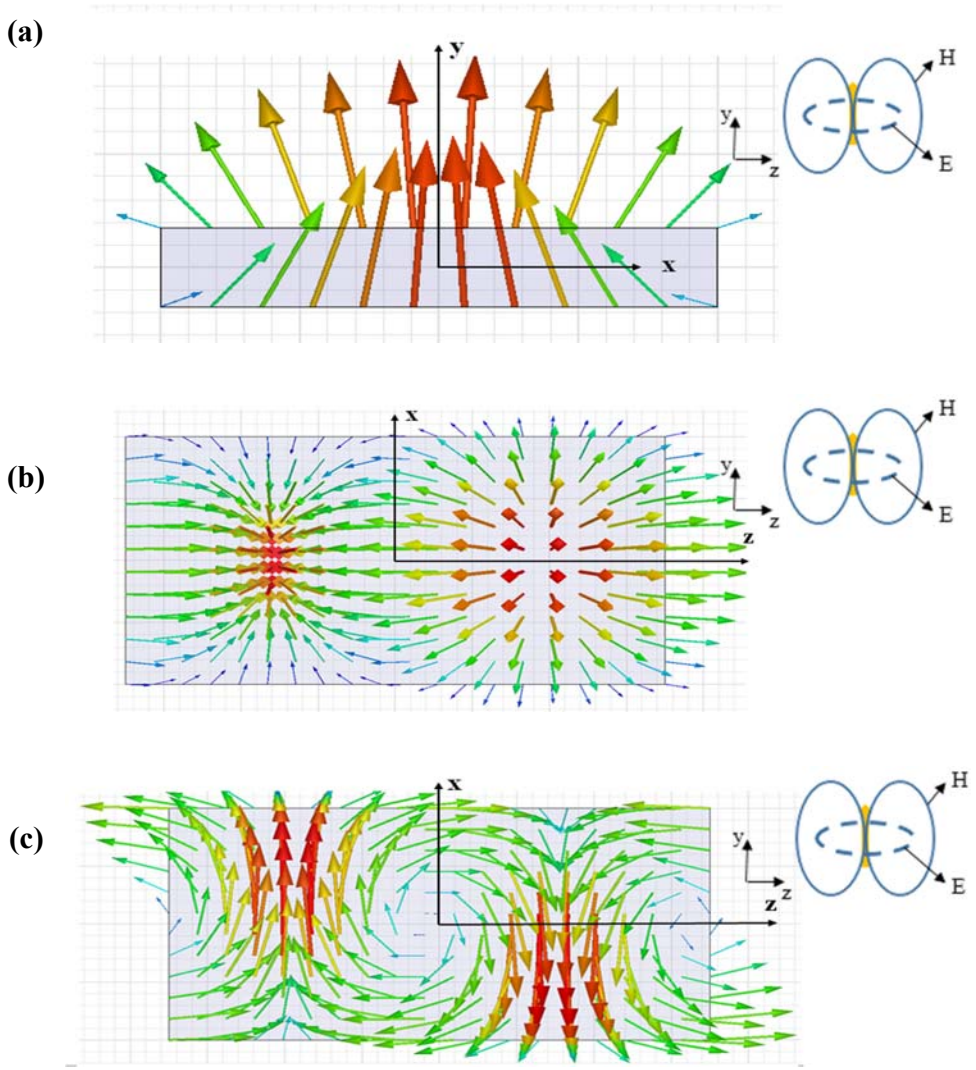

Figure 7 Fields distribution of TE^{y}_{112} (a) H field at z=0 (b) H field at y=b/2 (c) E field at y=b/2

2.3 Feeding Methods of Rectangular DRA

Up to this point, the DRAs were treated as being isolated in free space. The modes we acquired are eigenmodes. The equations that have been presented for the fields within the DRAs and their resonant frequencies do not take into consideration the method of coupling energy to the DRA. These coupling mechanisms can have a significant impact on the resonant frequency and Q-factor, which the above equations will fail to predict. The actual modes existed in a DR will be determined by its feeding mechanism and its location.

Here is some reviews on the coupling theory [13]. Given two electric current sources, J_1 and J_2 in a volume V enclosed by a surface S, which give rise to electric fields E_1 and E_2, respectively, and two magnetic currents M_1 and M_2 giving rise to magnetic fields H_1 and H_2, the general form of Lorentz Reciprocity Theorem is:

$$\oint_S (E_1 \times H_2 - E_2 \times H_1) \cdot dS = \int_V (E_2 \cdot J_1 - E_1 \cdot J_2 - H_2 \cdot M_1 - H_1 \cdot M_2) \cdot dV \qquad (10)$$

Which reduces to the following equation if S encloses all the sources [96]:

$$\int_V (E_1 \cdot J_2 - H_1 \cdot M_2) \cdot dV = \int_V (E_2 \cdot J_1 - H_2 \cdot M_1) \cdot dV \qquad (11)$$

Normally the DRA is excited by one source (J_1 or J_2, M_1 or M_2) and the coupling factor k between the source and the fields within the DRA can be determined by applying (8) with the appropriate boundary conditions. For an electric source J_1:

$$k \propto \int_V (E_2 \cdot J_1) \cdot dV \tag{12}$$

For a magnetic source M_1:

$$k \propto \int_V (H_2 \cdot M_1) \cdot dV \tag{13}$$

This indicates whatever source is used, it should be located in an area of strong electric or magnetic field within the DRA. It is thus necessary to have a good understanding of the field structures of the isolated DRA. The field distribution plotted in Figure 7 gives some idea of the TE_{11l}^{y} modes.

The excitation methods need to be chosen according to the specific applications. In this section, feeding methods will be divided into two categories with respect to the required direction of main beam. Also, in practice, the DRA excited in fundamental TE_{11l} modes are usually supported by a finite ground at the back. Using the image theory, if the thickness of the DRA is b, then it can be approximated by the one with thickness of 2b after removing the ground.

2.3.1 Feed for Broadside Radiation

Traditionally the DRA is widely used to provide a broadside radiation. There are multiple ways of feeding to achieve this pattern, each having their pros and cons.

2.3.1.1 Slot Aperture

The aperture coupling is an inductive type of coupling. One example is depicted in Figure 8 with the slot equivalent as a short magnetic dipole parallel to the length of the slot which excites the magnetic fields in the DRA. The aperture consists of a slot cut in a ground plane and fed by a microstrip line beneath the ground plane. The slot length should be large enough to achieve sufficient coupling between the DR and the feeding line. However, a large aperture might also resonate within the operation band, which usually results in a significant back lobe. Therefore, the slot size design is a tradeoff between proper coupling to the DR and avoidance of excessive back radiation. The tuning of the antenna can be achieved either by designing the microstrip stub to cancel out the reactive component of the slot or by properly offsetting the slot with respect to the DRA. The major advantage of using the aperture coupling is the easy integration with other printed circuit structure. Since it is relatively large in size for frequency blow L band, it has better behavior in higher frequencies. By making the feed network below the ground plane, it avoid spurious radiation from the microstrip line. It is also a simple way for DRA array feeding. The shape of the slot provides another degree of freedom to achieve certain improvement or feature in a specific aspect of performance, such as bandwidth or circular polarization [97]. Figure 9 shows some alternatives in slot shape.

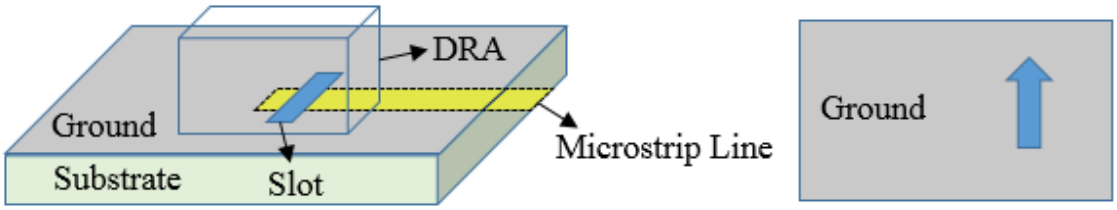

Figure 8 Slot aperture coupling to a rectangular DRA and its equivalence

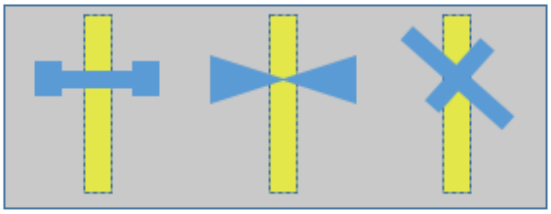

Figure 9 Coupling slots with different shapes

2.3.1.2 Coaxial Probe

For low frequency applications where the slot size is too big, the simplest way to feed a DRA is using a coaxial probe. It can excite the fundamental TE_{111} mode by either being placed adjacent to the DRA or embedded within it which also behaves like a short magnetic dipole as shown in Figure 10. However, unlike the slot coupling, the equivalent dipole is normal to the length of the probe. The impedance can be tuned by adjusting the probe height, radius and

location. To avoid unwanted radiation, normally the probe height does not exceed the one of the DRA. In some designs, a flat metallic strip on the side wall of the DR is used instead of a probe. The main advantage of coaxial probe excitation is that it allows direct coupling into a 50 Ω feeding system without a bulk feeding network.

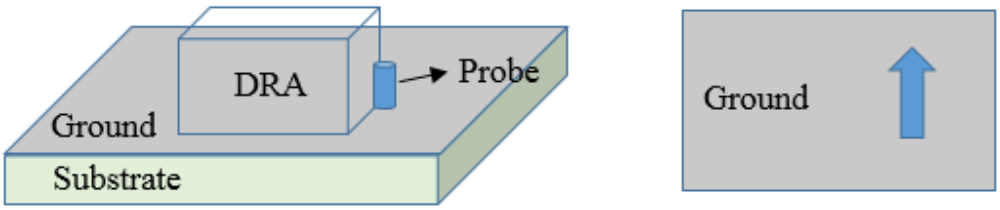

Figure 10 Probe-fed DRA and its equivalence

2.3.1.3 Microstrip Line

Another very simple method to couple energy to a DRA is through proximity coupling from a microstrip line. It can be placed outside or underneath the DRA as shown in Figure 11. The underneath part could also bend over onto the right side surface of the DRA behaving like a monopole as introduced in last subsection. The microstrip line excites magnetic field inside the DRA and produces a horizontal magnetic dipole mode. The coupling factor can be controlled by the distance of the DRA from the microstrip line as well as its dielectric permittivity. It shares some similarity as the slot coupling. First of all, as one a planar feeding, it can be easily

integrated to other printed circuits. Also, the size and shape of the open end can been tailored as a patch to achieve certain features such as matching network or wide bandwidth [98]. Figure 12 shows some alternative shapes of microstrip line. The main disadvantage of this coupling scheme is the spurious radiation due to the microstrip line. This translates into unstable radiation patterns and low polarization purity.

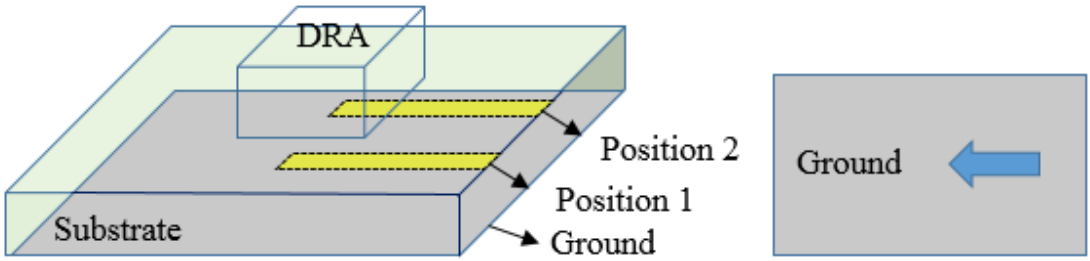

Figure 11 Mircostrip-fed DRA and its equivalence

Figure 12 Mircostrip line with different shapes

2.3.1.4 Coplanar Feeds

Coplanar feeds take the basic form of a loop or a slot as shown in Figure 13. It behaves in a way most similar to the coaxial probe. However, it has some fundamental advantage over the probe feeding. Since it is a planar structure, it does not require hole drilling inside the DR which reduces the interference resulted from the feed and the fabrication complexity. Also, it is easy to integrate like the microstrip case. The coupling level can be adjusted by the location of the feed. Again multiple shapes can be chosen for fine tuning as shown in Figure 14.

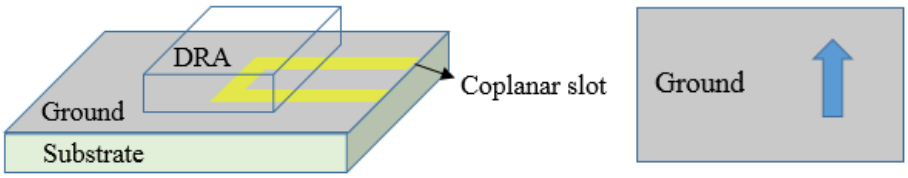

Figure 13 Coplanar-fed DRA and its equivalence

Figure 14 Coplanar feeds with different shapes

2.3.1.5 Dielectric Image Guide

As frequency goes into the mm-wave range, conductor loss becomes a more severe problem. Although isolated DRA is supposed to have no conductor loss, once the metal feed is introduced, the loss is unavoidable. An alternative way is to use dielectric image guide as shown in Figure 15. However, the coupling from the image guide to the DRA is relatively small and the feeding structure takes a large area compared with the methods introduced before. Thus, this method is usually used for a series feed to a linear array of DRAs [99].

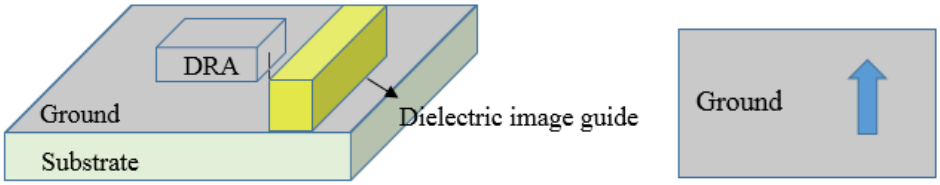

Figure 15 DRA fed with dielectric image guide and its equivalence

2.3.2 Feed for End-fire Radiation

In recent years, more and more focus has been paid to the end-fire radiation of the rectangular DRA since it is more user-friendly for the point-to-point beam forming application on the mobile device. Concerning the direction of the main beam, planar dipole is proven to be an effective feed. Figure 16 concludes some popular planar dipole structure to provide an end-fire pattern. Some of them are placed on the same layer, others takes two layers of the substrate.

The fundamental idea is to generate a 180 degree phase difference between two arms of the dipole. The shape is adjusted for the purpose of wider bandwidth [37], [38] or ease of excitation. Using this kind of planar structure, it is extremely easy to integrate the antenna to RF front-end circuit. Multiple technology, such as wire bond and flip chip, can be applied for the integration which will be addressed in another chapter. However, the spurious radiation introduced by the feeding dipole and the imperfect floating partial ground require additional care in the antenna design. This thesis will use this feeding structure for the end-fire DRA design.

Figure 16 Different planar dipole structure as feed for DRA

2.4 Model with Feed and Excitable Modes

As mentioned in the last section, the fundamental feeding structure of end-fire rectangular DRA is chosen to be planar or quasi-planar dipole. Based on this, one can further optimize the feeding scheme for a more realistic model and discuss the excitable modes in the DRA. Figure 17 indicates the process of developing the excitation model. Here we use the

second structure to the left in Figure 16. This is an antipodal structure with two arms of the dipole laying on different layers of the substrate. In order to suppress the backside radiation, a reflector with a slightly longer length is adopted on the lower layer connecting to one arm. Considering in reality, a G-S-G probe is used to excite the antenna system which requires a planar structure on top layer for proper landing, two ground pads pinned down to the partial ground on the lower layer and an extended microstrip line connecting to the other arm as signal line are added to form a complete antenna model. Using antipodal structure is the simplest way to excite a DRA since it does not require accurately offsetting the phase difference of two arms using delay line as for the coplanar dipole. It is automatically distributed on two layers separating the signal layer and the ground layer, the latter of which could in addition serve as the ground layer of the whole system. The tuning of the antenna is also simple as the transition part from the G-S-G contacts to the dipole could be adopted for this purpose. The only concern is that if the dipole is not vertically centered, the lengths of the two arms need to be slightly different to compensate for the different effective dielectric constants above and below the feed. To simplify the discussion, all the examples given in chapter 2 and 3 are under the condition of vertically-centered feed. It is also worth mentioning that in this chapter only the center-fed DRA is considered. The off-center feed will impose other problems which will be addressed in chapter 3.

Excitable modes in the DRA can be discussed based on this model. Here, certain assumptions need to be made beforehand. First of all, The DRA under study is low-profile which means the thickness b is much smaller than the width a and length d. According to the mode study of isolated DRA in section 2.1, TM^{y}_{mnl} and TE^{y}_{mnl} are the dominant modes since the

equivalent short dipole is supposed to be polarized along the shortest dimension especially under the first assumption. TM_{mnl}^{y} should be excited by vertical electrical dipole and TE_{mnl}^{y} should be excited by vertical magnetic dipole. Since it is excited by a horizontal planar dipole which generates a similar field distributions of a vertical magnetic dipole in the DRA, the excitable modes should be confined in the family of TE_{mnl}^{y}. For more practical concerns, since the thickness of the DR is much smaller than the other two dimensions, n is always 1 for excitable modes.

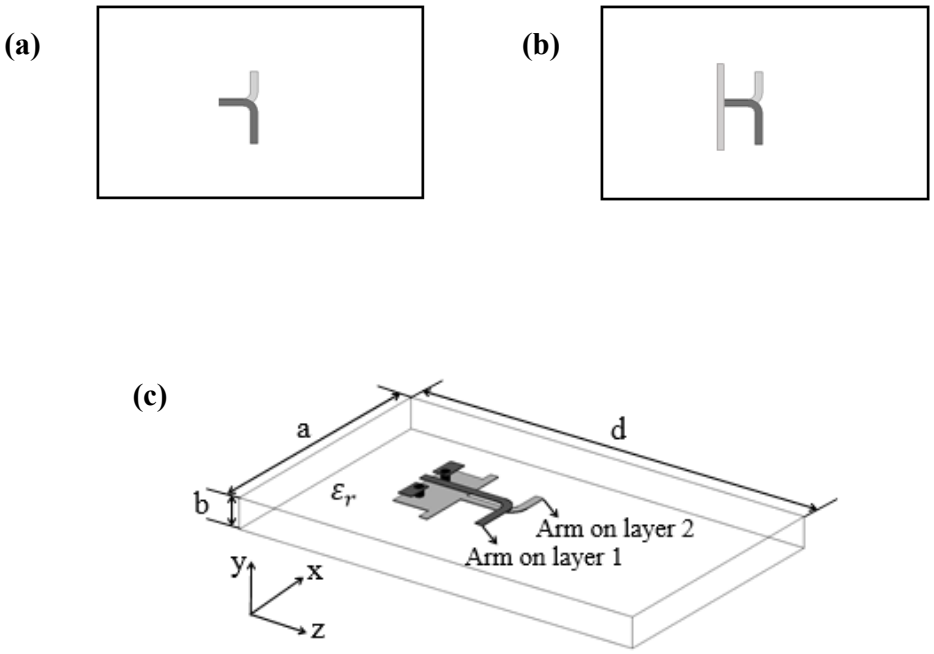

Figure 17 Development of excitation model (a) Single antipodal dipole (b) Dipole with reflector (c) Complete model with partial ground and G-S-G pads

The resonator frequency is purely determined by the three dimensions and the dielectric constant of an isolated DRA. However, now the DRA is inserted with feeding lines and certain adjustment needs to be made to determine the resonant frequency as well as the modes excited. Here another assumption needs to be made that the partial ground at the back of the feed is considered to be a very effective reflector and is able to reflect most of the backside radiation to the front. Thus it requires the distance between the reflector and the feeding dipole to be approximately quarter guided wavelength. In order to verify whether this is a valid assumption, an example is given using LTCC ($\varepsilon_r = 7.5$) as the substrate material with a × b × d =2mm × 0.35mm × 7.4mm. Detailed dimensions are shown in Figure 18 with d1=4mm, d2=0.69mm, d3=0.5mm, d4=2.21mm, l_{d1}=l_{d2}=0.452mm, l_r=1.248mm and w_g=0.944mm. The parameter Δx indicates the feed offsetting along its width. Since it is assumed that the DR is center-fed, here Δx=0. The dipole length is roughly half wavelength and the reflector is slightly longer than the dipole and placed roughly quarter wavelength away from the dipole. The partial ground area is chosen to be small enough not as an effective broadside radiator, but large enough to suppress most of the backside radiation which determines the minimum dimension of the ground pad. The location of the whole feeding structure is chosen randomly for general discussion. Later it will show that if the partial ground is an effective reflector, the location does not affect the end-fire performance. Figure 19 shows the magnitude distribution of the electric field of this example. It is quite clear that the backside radiation is efficiently suppressed by the partial ground and the magnitude ratio of the front- and back- radiation is approximately on the order of 10^4.

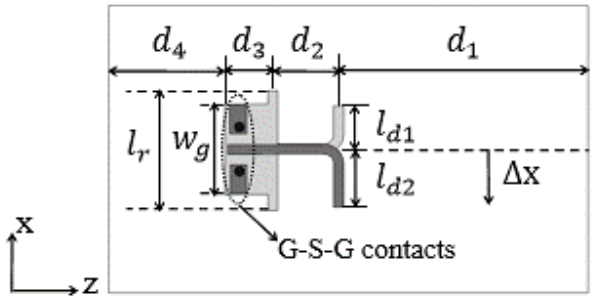

Figure 18 Detailed dimensions of the DRA model

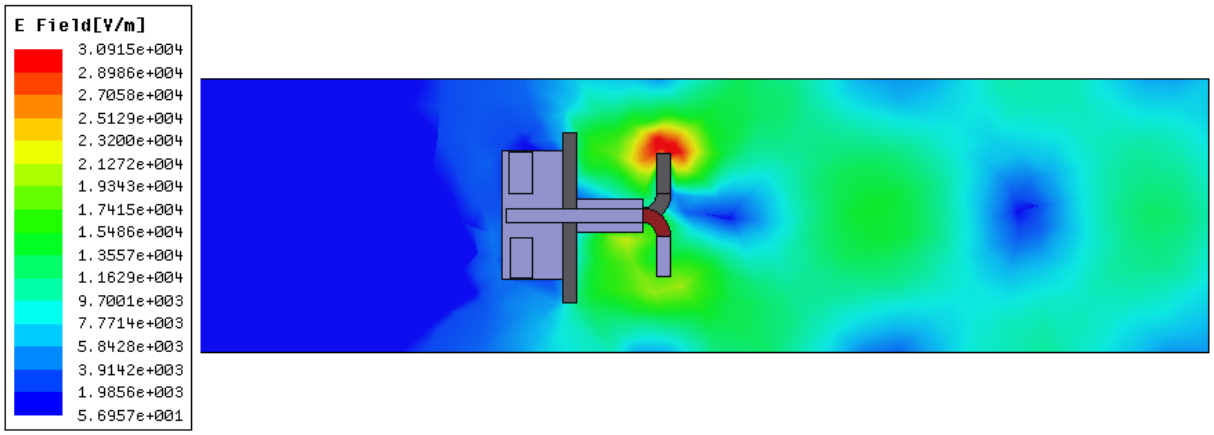

Figure 19 Magnitude distribution of the electric field

Another fact indicating the partial ground as an effective reflector lies in the gain performance of this DRA. Figure 20 illustrates two examples of the end-fire gain against the

length of the same DRA with different feed locations. They have cross section of a × b= 2mm×0.35mm and 2mm×0.8mm respectively. As it is pointed out that the location of the whole feeding structure is chosen randomly with different d4, thus if the partial ground is served as an effective reflector, the DR modes are built up only in the portion of the substrate in front of the reflector and the end-fire gain is related to d1+d2+d3 instead the total length d. Since d2, d3 are fixed, the trend of the end-fire gain against d1 should be the same for different d4 which is exactly the case in Figure 20. By comparing the two examples, it is obvious that for the second case with thicker substrate, the end-fire gain is more disturbed by location of the feeding structure. For thicker substrate, the surface wave is also much stronger. The partial ground becomes less and less effective and power starts leaking to the back. However, the trend of the end-fire gain for different d4 still matches. Thus, it can be concluded that the generosity of the mode analysis remains in spite of the location of the feeding structure.

(a)

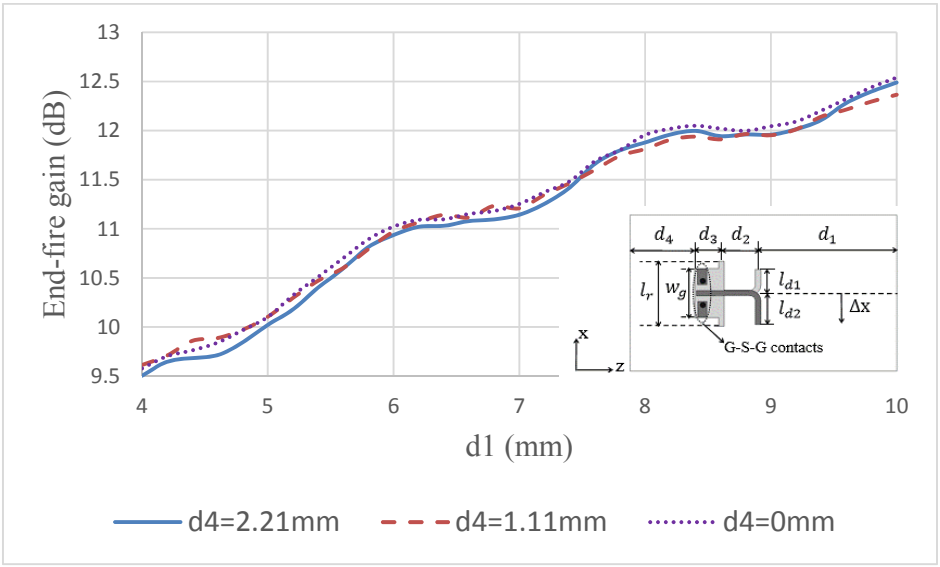

(b)

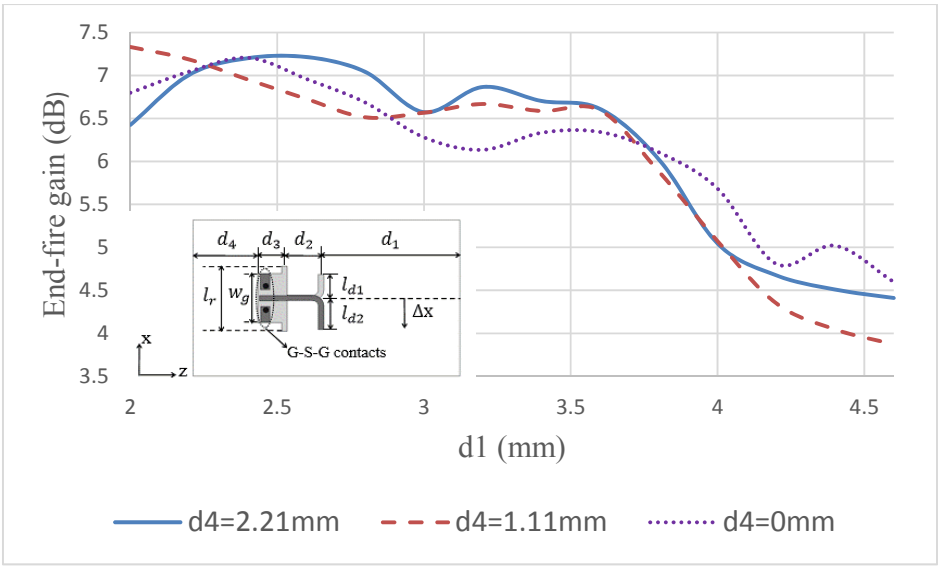

Figure 20 Gain performance of the same DR with different feed locations and a×b= (a) 2mm×0.35mm (b) 2mm×0.8mm

Once the feed of the DRA is specified, there are only certain TE^{y}_{m1l} modes which can be excited in the DRA with appropriate field distributions according to the feed. Recall that the broadside cases in section 2.3 that the DRA is usually supported by a finite ground. This finite ground is considered as a perfect conductor for mode study and the substrate thickness is doubled to estimate the resonant frequency of the DR if the ground is removed using image theory. Similarly, this assumption can be applied here for the end-fire case as well. Figure 21 indicates the equivalence of the model of interest. If the partial ground is considered as an infinite virtual perfect conductor and the distance between this perfect conductor to the end-fire edge of the DR is d_{eff}, then the model is equal to a center-fed DRA with a length of $2d_{eff}$ using image theory. In reality, the partial ground is not perfect, d_{eff} can be approximated with d1+d2+d3.

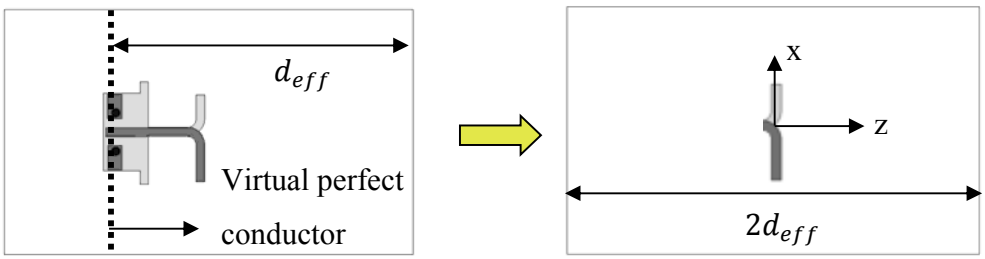

Figure 21 Equivalence of the model of interest

Once this equivalence has been made, certain restrictions need to be applied on the modes which can be excited in the DRA. It has been established in section 2.1 that the possible value for m and l are determined by the boundary conditions. When perfect conductor is present on plane z=0, only modes with l of odd value can be excited. Similarly, for center-fed DRA, plane x=0 is also considered as PEC since it is equivalent as a y-directed short magnetic dipole resulting in odd m as well. In conclusion only TE^{y}_{m1l} with odd m and odd l can exist in the proposed model.

2.5 Application of DWM on Model of Interest

DWM method is proved to be accurate in predicting the resonant frequency of isolated DRA in section 2.1. When excitation is included in the model, it is necessary to examine the validity of the method as well. Certain assumptions have already been made in last section to solve the characteristic equations (7) with $2\,d_{eff} \approx 2(d1 + d2 + d3)$ as the length. Three examples with different cross-section areas are made to be resonant at 60GHz and simulated using HFSS. They share the same dimensions of d2=0.69mm, d3=0.5mm, d4=0mm, l_{d1}=l_{d2}=0.452mm, l_r=1.248mm and w_g=0.944mm as indicated in Figure 18. Since d2 and d3 are fixed, by changing the value of d1, d_{eff} is changed accordingly with respect to a certain mode resonant at 60GHz for a DRA with a fixed cross-section area. Excited modes are determined by plotting the vector electric field distribution of plane y=0 as well as observing the maximas on the plot of end-fire gain versus d_{eff} and this is how the simulated d_{eff} is determined. This

approach will be reaffirmed in the next chapter. For indication, Figure 22 plots the E field distribution of TE_{115}^{y} mode for DRA with a×b=2mm×0.6mm. Table III compares the theoretical and simulated d_{eff} for three examples. Obviously the error is within tolerance indicating DWM method is still considered valid for studying DRA with inserted feed. In fact, it will be shown in the next chapter that accurate prediction of the excited modes in the low-profile DRA is not quite necessary since the modes only introduce small ripples on the end-fire gain plot for most desirable cases. However, it is useful to determine the DRA dimensions and avoid degeneracy.

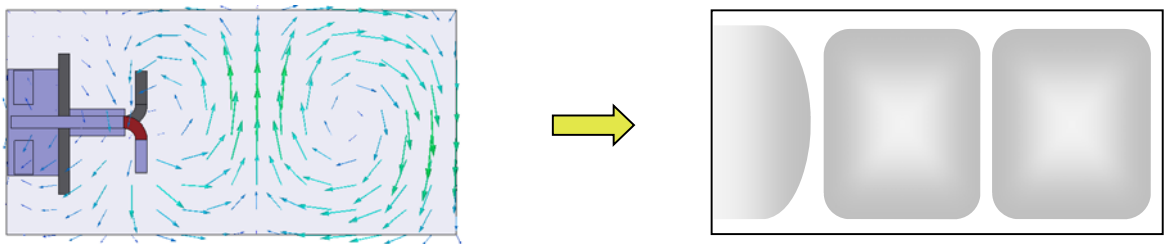

Figure 22 E field distribution of TE_{115}^{y} mode for DRA with a×b=2mm×0.6mm

Table III Comparison of theoretical and simulated d_{eff} for different modes of three DRAs resonant at 60GHz

DRA cross section (mm^2)	Mode	TE^{y}_{115}	TE^{y}_{117}	TE^{y}_{119}
a×b=2×0.6	Theoretical $\boldsymbol{d_{eff}}$ (mm)	4	5.6	7.2
	Simulated $\boldsymbol{d_{eff}}$ (mm)	3.8	5.6	7
	Percentage error (%)	5.3	0	2.9
a×b=2.5×0.35	Theoretical $\boldsymbol{d_{eff}}$ (mm)	5	7	9
	Simulated $\boldsymbol{d_{eff}}$ (mm)	5.2	6.9	8.6
	Percentage error (%)	3.8	1.4	4.7
a×b=4×0.35	Theoretical $\boldsymbol{d_{eff}}$ (mm)	4.3	6	7.7
	Simulated $\boldsymbol{d_{eff}}$ (mm)	4.8	6	7.8
	Percentage error (%)	10.4	0	1.3

The resonance we have seen so far cannot be taken for granted as results purely from the DR. The feeding dipole itself is a radiator as well. In order to figure out which is the dominant factor for the occurring resonance, two dipoles with different lengths are adopted as the feed of the same DRA with a×b×d=2mm×0.6mm×4mm. Figure 23 depicts the resonant mechanism of the dipole-fed DRA where the imaginary part of the input impedance is plot with frequency for l_{d1}=l_{d2}=0.452mm and l_{d1}=l_{d2}=0.855mm. Dipole resonances occur at frequencies where the dipole length is equal to a half wavelength. Since the dipole here is at the surface of the material, it is better we consider a wavelength corresponding to the effective dielectric constant ε_{eff} ≈5.4.

Thus the first dipole is roughly resonant in the 60GHz band and second dipole has a resonance frequency of 37.7GHz which is way lower than the 60GHz band. This is shown by an obvious resonance below 45GHz as the dashed line indicates. However, in both cases resonance occurs in 60GHz band. Thus the dominant modes responsible for radiation are entirely due to the dielectric resonance. However, by overlapping the two resonances resulted from dipole and DRA, the bandwidth of the antenna will be effectively enhanced since the solid line is closer to 0 over a large range of frequency.

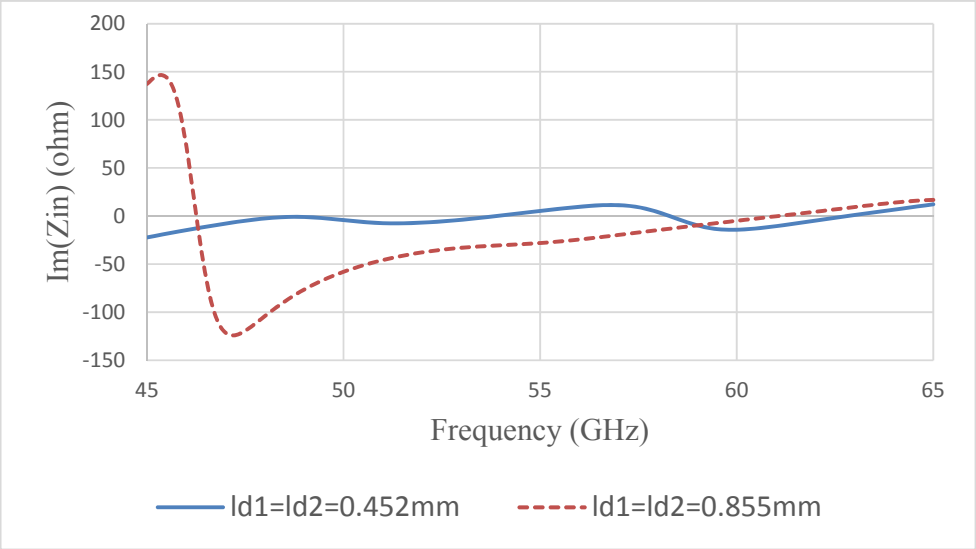

Figure 23 Resonance of DRA with feeding dipole of different length

2.6 Conclusions

In this chapter, several methods of analyzing the modes in rectangular DRA were introduced. In order for practical usage, first-order approximation of mode analysis is desired. The most efficient and practical one was proven to be dielectric waveguide model (DWM) method. Discussion was made on the nature of the characteristic equations. This method was first proven to be effective for predicting the resonant frequency of isolated DRA by comparing the theoretical results with the eigenmode simulation using EM full-wave simulator HFSS. The excitable modes within the DRA was determined by the simulated Q factor and the electric field distribution.

However, the actual excitable modes in DRA are determined not only by its dimensions, but also by its feeding method. Coupling theory was reviewed and various feeding methods for rectangular DRAs as well as their pros and cons were introduced for broadside and end-fire radiation. Based on the planer excitation suitable for mobile mm-wave devices, a new and more realistic model was developed for study. Necessary assumptions were made and examined to simplify the mode analysis. Based on this, excitable modes within such DRAs were discussed according to the low-profile structure and boundary conditions. DWM method was then applied to the center-fed DRA and HFSS simulations were carried out to prove its accuracy. Finally, it was shown that the modes responsible for the radiation were entirely due to the dielectric resonance instead of dipole resonance. However, by overlapping these two, the bandwidth of the DRA should be enhanced.

3. CHARACTERISTIC STUDY OF RECTANGULAR DRA

3.1 Introduction of Gain-enhancement Methods

Originally, study of DRA has been concentrated on the fundamental mode (TE_{111}^{y}) in which case the DRA radiates in broadside direction like a y-directed short magnetic dipole with a relatively low directivity. As the frequency moves up into mm-wave range, DRA providing higher directivity is in demand suitable for point-to-point communication. The straightforward way is to place the DR on a finite ground giving a gain of roughly 5dBi. This also saves at least 50% of the total volume. Over the years, multiple methods have been applied to enhance the gain of the DRA. Here is a brief review on some of the most popular ones for rectangular DRA.

3.1.1 Using Fundamental Mode

Being excited in its fundamental TE_{111}^{y} mode, the gain of the DRA can be enhanced in various ways. One of the methods is to stack the DRAs on top of each other as shown in Figure 24. This method was originally proposed to increase the bandwidth. Later on, it was also proven to improve the gain of the DRA in [100]. The design can be altered to either increase the bandwidth or gain or both. Introducing metal cavity is another way of increasing the gain. In [101], a shallow pyramidal horn with a height of 0.15 times the free space wavelength λ and a square aperture of dimensions $1.2\lambda \times 1.2\lambda$ has been adopted to increase the gain of a DRA to nearly 10 dBi as shown in Figure 25. Similarly as the stacking technique, a superstrate can be added above the DRA as illustrated in Figure 26. An example has been given in [102] with a

gain enhancement of 16 dBi for a square superstrate with dimensions of $3.2\lambda \times 3.2\lambda$. Finally, different radiation patterns can be achieved by changing the ground shapes such as incorporating the electromagnetic band gap (EBG) ground plane as shown in Figure 27. Other plane shapes such as cavity-corrugated, tin-can, transverse-corrugated, longitudinal-corrugated and strip-corrugated ground plane can also be applied [103]. From these illustrations, it is quite obvious that significant increase in the area and weight are required which is not suitable for mm-wave hand-held devices.

Figure 24 Stacked DRAs

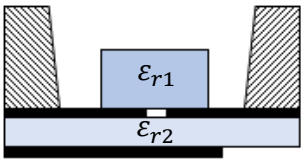

Figure 25 DRA inserted in a shallow pyramidal horn

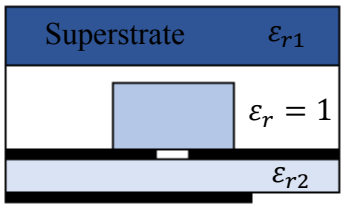

Figure 26 DRA with superstrate

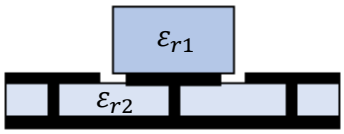

Figure 27 DRA on mushroom-like EBG ground plane

3.1.2 Using Higher-order Modes

In order to design compact system, higher-order modes can be excited to achieve the gain enhancement. This method was first used in multi-mode operations to enhance the impedance bandwidth [104-105]. Other applications include dual-band operation [106], circularly-polarized radiation [107] and so on. It has not been thoroughly studied for the gain enhancement until recent years. In [108], it is first applied on a ground-backed DRA and a directivity of almost 11 dB has been simulated for a DRA operating at 10.6 GHz. Higher-order mode is approximated by a set of short magnetic dipoles. By ignoring the mutual coupling between dipoles, simple array

theory is used for a radiation model of DRA and radiation pattern is plotted. The array model of TE_{115}^{y} mode is shown in Figure 28. Later in [109], recommended procedure for designing the higher-order mode DRAs is presented based on this theory. Furthermore, design curve of the aspect ratio is provided in order to avoid the mode degeneracy and the effect of fabrication error on the frequency shift of the DRA was also studied in [110]. To relax the precision problem of fabrication, it is proposed to obtain a larger DRA by designing it with its higher-order mode. However, in these papers, the model of interest is broadside-radiated and the procedure or curve presented is not practical for mm-wave low-profile design with end-fire pattern. Also, no study has been systematically carried out focusing on the end-fire gain performance and the optimization of the DRA design based on this target.

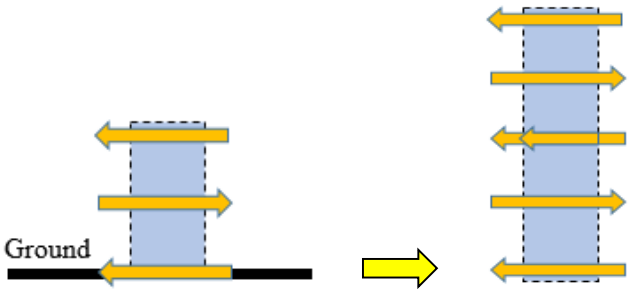

Figure 28 The array model of TE_{115}^{y} mode

3.1.3 Using Antenna Array

The ultimate way to increase the gain of the DRA in a large scale is to use antenna array, especially in mm-wave range since the total physical area occupied is relatively small considering the achievable gain. Broadside beam forming is typically achieved by planar patch arrays [111] or DRA arrays [6] and as for end-fire radiation, multiple configurations can be adopted such as dipole-fed DRA array [39] or SIW array [112]. Of course, the complexity and expense will be increased by using antenna array and it also leads to other issues in mm-wave band such as efficiency drop and proper feeding network design.

3.2 Methods of Studying End-fire Antennas

End-fire antennas are regarded as the one which support the dipole-type surface wave and the maximum direction of the radiation is parallel to the major dimension of the antenna. This radiation direction can be achieved by a particular single antenna structure such as Yagi, dielectric rod, horn and helix antenna, or achieved by antenna array. It is usually less bulky than the broadside antennas, thus one of its applications lies in the case where the space is limited. When it comes to mm-wave band, especially the hand-held mobile devices where concentrated beam is required for high-speed communication, end-fire antennas are assumed to be more user-friendly and easy for beam forming applications.

Over the years, many theories have been proposed to study the radiation mechanism of the end-fire antennas [113] which will be discussed here briefly.

3.2.1 Radiation Mechanism of Yagi Antennas

As the most classic end-fire antennas, Yagi antenna is first described in Japanese article in as early as 1927 and has been used worldwide since. It is very easy to construct and now very commonly used as TV antennas. The basic structure is shown in Figure 29. It is comprised of one driven element which is usually a dipole or folded dipole and directly fed (number N), one reflector to suppress the backside radiation (number N-1) and a series of directors placing along the end-fire direction (+z in this case) in front of the driven element (number 1 to number N-2). Experimental study has shown that the driven element is resonant with its length slightly less than λ/2 (usually 0.45–0.49 λ). The parasitic elements in the direction of the beam are somewhat smaller in length than the feed element. That is l_n is getting smaller and smaller along z, the lengths of which should be about 0.4 to 0.45 λ. The separation between the directors s_n is typically 0.3 to 0.4 λ, and it is not necessarily uniform as well. At last, the length of the reflector is slightly longer than the driven element with a distance of a quarter wavelength away from it for maximum reflection [114].

The mechanism of its radiation is quite straightforward. The directors actually carry a surface wave with a smaller phase velocity than the one in the air. This is equivalent as the wave traveling through a region of varied refractive index determined by the dimension and spacing of the directors which is comparable as a convergent lens. Also, the directors with gradually reduced length each resonant at a higher frequency. That means, at the operating frequency, the impedances of the directors are capacitive and the currents lead the induced emfs. Similarly the impedance of the reflector is inductive and the phase of the current lags the induced emf. Thus,

properly spaced elements with lengths slightly less than their corresponding resonant lengths (less than λ/2) act as directors because they form an array with currents approximately equal in magnitude and with equal progressive phase shifts which will reinforce the field of the energized element toward the directors. The longer reflector provides the proper reversed phase shift as well. In practical design, compromise needs to be made in number of directors used and end-fire gain. Also, this structure can be easily made planar for mobile devices integration. Another disadvantage is that the Yagi antenna is one of the few traveling antennas which have quite limited bandwidth.

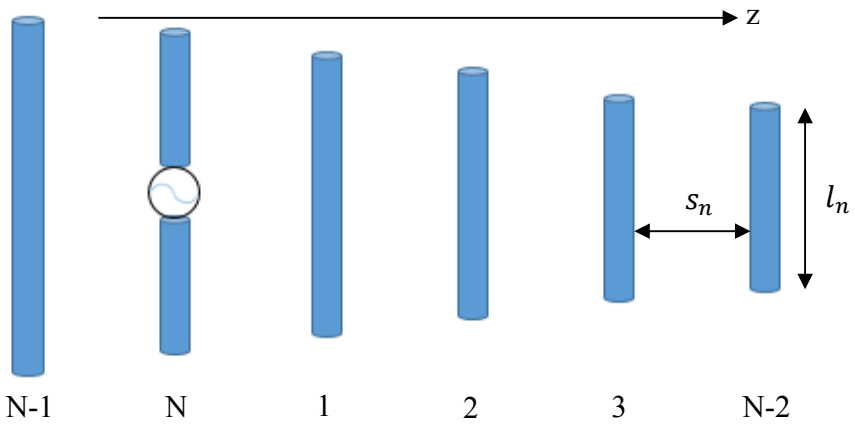

Figure 29 Basic structure of Yagi antenna

3.2.2 Mallach's Theory for Dielectric Rod Antennas

It has already been shown that the field distribution in the DRA is dipole-like and the wave traveling in it has a phase velocity less than that of a plane wave in free space. The overall radiation pattern is much similar to the one resulted from the end-fire antenna arrays. Thus a model according to this observation has been illustrated in Figure 30. Discrete radiation elements are placed along z direction with a phase difference ψ and a spacing of ΔL. The elements are assumed to radiate the same amount of power and the total pattern is calculated by adding each radiation together when ΔL approaches 0. The expression of the field strength is provided and the field pattern is plotted in [113]. The guided wavelength λ_g of the wave in the dielectric is determined by its dimension, for instance, the diameter of the cylindrical rod. An increase of rod diameter reduces the phase velocity of the wave. That is to say, a thin rod supports a spread-out wave traveling with nearly free-space phase velocity. On the contrary, a thick rod concentrated most of the power near the surface of the rod. It is easy to understand if one think of the extreme case of thin rod that is purely air in which λ_g becomes λ_0.

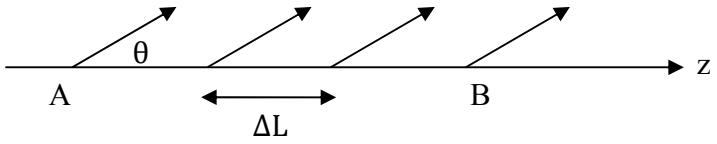

Figure 30 Illustration of Mallach's theory of dielectric rod antennas

There are two major objections to this theory. First of all, this mechanism of continuously energy loss suggests a leaky-wave radiation which is a fast wave structure and physically impossible in this scenario since the energy flow is along the rod toward its end-fire direction. Secondly, the theoretical result agrees poorly with the experimental one since it fails to predict the observed dependence of the beam width of the antenna on the length of the rod. The theory suggests that beam width should decrease steadily with increasing rod length, tending to zero as the length tends to infinity. However, as it will be shown in this chapter later, the beam width or the end-fire directivity is actually oscillating with the length.

However, it does not mean that this model of dielectric antenna has absolute no use. A similar model has been developed in [108-110] for a ground-backed DRA to estimate the radiation pattern in proving its enhanced-gain using higher order modes. Thus this theory could shed some lights on the qualitative study of DRA.

3.2.3 Brown and Spector's Theory

In [113], Brown and Spector have shown that an end-fire antenna, and in particular the dielectric rod, can be considered to support a non-radiating axial surface wave with radiation occurring at the discontinuities at the free end of the guiding structure and at the junction between this structure and the feed. This can be best visualized by a Dielectric rod example shown in Figure 31 compared with a horn antenna. So the major radiation occurs at two positions. Part of the power is directly radiated at the feed. Part of it is traveling along the

dielectric rod and radiates at the terminal. The terminal radiated field is considered to be distributed over an appreciable area of the radiating aperture. The total pattern is derived from the superposition of these two radiations. This mechanism is quite similar as the one of horn antenna. The horn antenna acts as a convertor between the guided wave in the feeding waveguide and the radiating wave in the free space. The radiated field at the opening of the horn is as well distributed on the aperture and the directivity is determined by the effective aperture A_e which is directly related to its physical aperture S by the aperture efficiency ε_{ap} as this:

$$\varepsilon_{ap} = \frac{A_e}{S} \tag{14}$$

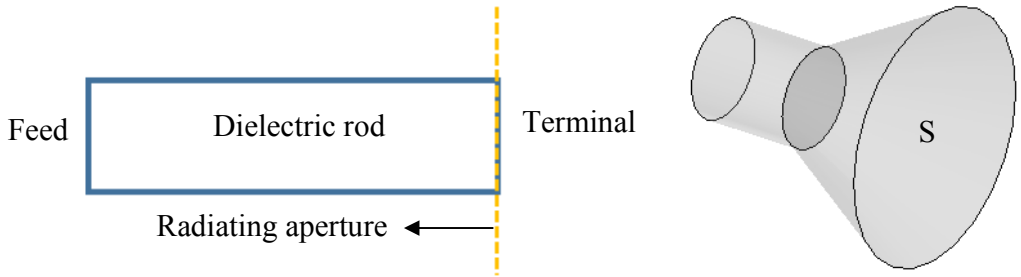

Figure 31 Radiation model of dielectric rod compared with horn antenna

However, there are obvious dissimilarities between the two antennas. This can be clarified using a more complete model describing the power distribution at the feed. For horn

antenna, at the discontinuity of the feeding waveguide and the flare part, power goes to three parts: wave traveling toward end-fire direction, power reflected and the reactive power. For dielectric rod, besides these three kinds of power generated, it also radiates power directly from the feed which is not present in the horn antenna since it is a sealed cavity. The proportion of the incident wave used to excite surface waves is known as the launching efficiency. One general rule is that the launching efficiency will increase as the surface wave is more restricted to the vicinity of its guiding structure. That is to say, if the dielectric rod has a very high dielectric constant which can be regarded as a well-guided rod, this direct radiation can be somehow neglected. However, in reality as the DR used as antenna, this assumption cannot be met. Thus it is necessary to include the direct radiation. In fact, the poor agreement of the theoretical and experimental data of the Mallach's theory results from the neglect of this wave. Usually, feed taper is applied to increase the efficiency of excitation. The body taper suppresses sidelobes and increases bandwidth. Because a reflected surface wave spoils the pattern and bandwidth of the antenna, a terminal taper is employed to reduce the reflected surface wave to a negligible value. Different approaches have been adopted to determine the launching efficiency of the feed. In [113], a trial-and-error method has been used to determine the value which gives the best agreement with experimental results. It has been found that this best agreement is obtained when 6% of the energy is assumed to be directly radiated by the feed. A transmission line model has been proposed in [115] to predict the launching efficiency of a waveguide-fed dielectric rod of uniform rectangular cross section. Experimental investigation has been carried out to determine the reflection coefficient, thus the ratio of impedances on the transmission line. However, until

now, there is no rigorous method available to determine the efficiency without the assistance of experimental data.

Another difference from these two antennas lies in the definition of the effective aperture. For horn antenna, the aperture area is well defined, while in the case of dielectric rod, it is not, though one can qualitatively discuss the change of effective aperture for different dimensions.

3.3 Gain Characteristics of Rectangular DRA

In general, antennas can be divided into two categories: standing-wave antennas and traveling wave antennas. For standing-wave antennas, such as center-fed linear wire antennas, no matter what the amplitude distribution is on the antenna, the phase distribution is assumed to be constant. That is, the sinusoidal current distribution of long open-ended linear antennas is a standing wave constructed by two waves of equal amplitude and 180° phase difference at the open end traveling in opposite directions along its length. The voltage distribution is also a standing wave with alternative maximum and minimum points to the current distribution. If an antenna is properly terminated so that the reflections are minimized if not completely eliminated, then the field on it appears a traveling wave pattern in current and voltage. Such antennas are considered as traveling-wave antennas. A progressive phase pattern is usually associated with the current and voltage distributions. Examples include long wire, V antenna, Yagi, dielectric rod or helix [114].

Just like standing wave antennas can be analyzed as traveling wave antennas with waves propagating in opposite directions. There is no distinctive boundary between resonant antennas and traveling-wave ones. In certain cases, one antenna can show properties from both parties. Thus, theories of two kinds of antennas can be combined together for a thorough analysis of, for instance, the model of a low-profile end-fire rectangular DRA in this thesis.

A traveling-wave antenna can be classified as a slow-wave structure or a fast-wave (leaky-wave) structure. It has been established in the last section that this model of interest supports dipole-like surface wave and the leaky wave is physically impossible. Thus, Brown and Spector's theory will be adopted here for the study of radiation mechanism.

There are all kinds of characteristics of an antenna which can be used as the goal of optimization. As it has been mentioned, end-fire gain of the DRA is a key parameter in realizing high-speed communication system. In this chapter, this property will be used as a major criteria for the antenna performance.

3.3.1 DRA with No Transverse Modes

It is known that the mode distribution of a rectangular DRA is affected by its aspect ratios. The cross-section dimensions determine the guided-wavelength. Along with the third dimension length, they further identify the modes excited, radiation pattern as well as other important parameters of the antenna. In chapter 2, according to the new model introduced and its boundary conditions, it has been established that the excitable modes in a dipole-fed DRA at

center with reflector are TE^{y}_{mnl} modes with odd-value m, l and n=1 for a low-profile structure. When the dimensions of the DRA are chosen improperly, other modes that are very close to the operating mode may be excited. In general, these degenerate modes have different radiation patterns and may undesirably increase the cross-polarized field or even distort the radiation pattern of the antenna. For instance, the desired modes in the DRA are the lowest TE^{y}_{11l} modes with l determined by the length d. However, if the width a of the DRA is chosen so that certain TE^{y}_{31l} modes are excited. Then the radiation pattern might be disturbed which will directly affect the end-fire gain. This can be considered as a result of 3-element horizontally place dipole array which will in theory widen the radiation toward the transverse direction. Such modes are thus called the transverse modes in this thesis. In order not to let the transverse modes disturb the generosity of the discussion, it is assumed in this section that no transverse modes are excited in the DRA of question if properly choosing the dimensions. Next section will examine the influence of the transverse modes on the end-fire gain.

According to the DWM method, the DR is considered as a truncated dielectric waveguide with the same field distribution on the cross section. In this case, wave number k_z along its length or the guided wavelength of the surface wave λ_g is determined by the cross-section dimensions. For a low-profile dielectric rod with very small thickness b, λ_g is very close to λ_0 which is the wavelength in free space. Thus the antenna behaves more like a surface-wave antenna. Brown and Spector's theory suggests that the radiation only occurs at discontinuities at the feed and the terminal. The total radiation pattern is the superposition of the two radiations.

These pattern determines the gain performance of the antenna. For an antenna with a fixed cross section, λ_g is determined. Changing the length of the antenna will change the phase difference between the waves radiating from feed and terminal resulting in varied end-fire gain.

In order to give some idea of the gain performance with the length d, one example based on the model introduced in chapter 2 have been shown in Figure 32 with its end-fire gain plot against the length. The cross section of this antenna is $\mathrm{a} \times \mathrm{b} = 2\mathrm{mm} \times 0.8\mathrm{mm}$ with LTCC of $\varepsilon_r = 7.5$ as the substrate. Other dimensions are d1=4mm, d2=0.69mm, d3=0.5mm, d4=0mm which indicates the ground is right at the edge, l_{d1}=l_{d2}=0.452mm, l_r=1.248mm, w_g=0.944mm and Δx=0 which indicates the feed is centered along its width. It is worth mentioning that all the length d in this chapter is referred to as the effective length d_{eff} of the model due to the non-ideal reflector which is approximated by d1+d2+d3.

A direct observation from the gain plot is that it is periodic with length d. That is to say, at certain length, the DR reaches a maximum value of end-fire gain and another length gives a minimum end-fire gain. The maximum gain one DRA can achieve is denoted as G_{max}. The main purpose of this section is to determine the length which gives G_{max} for a certain cross section and for DRA with different cross sections, how does G_{max} vary.

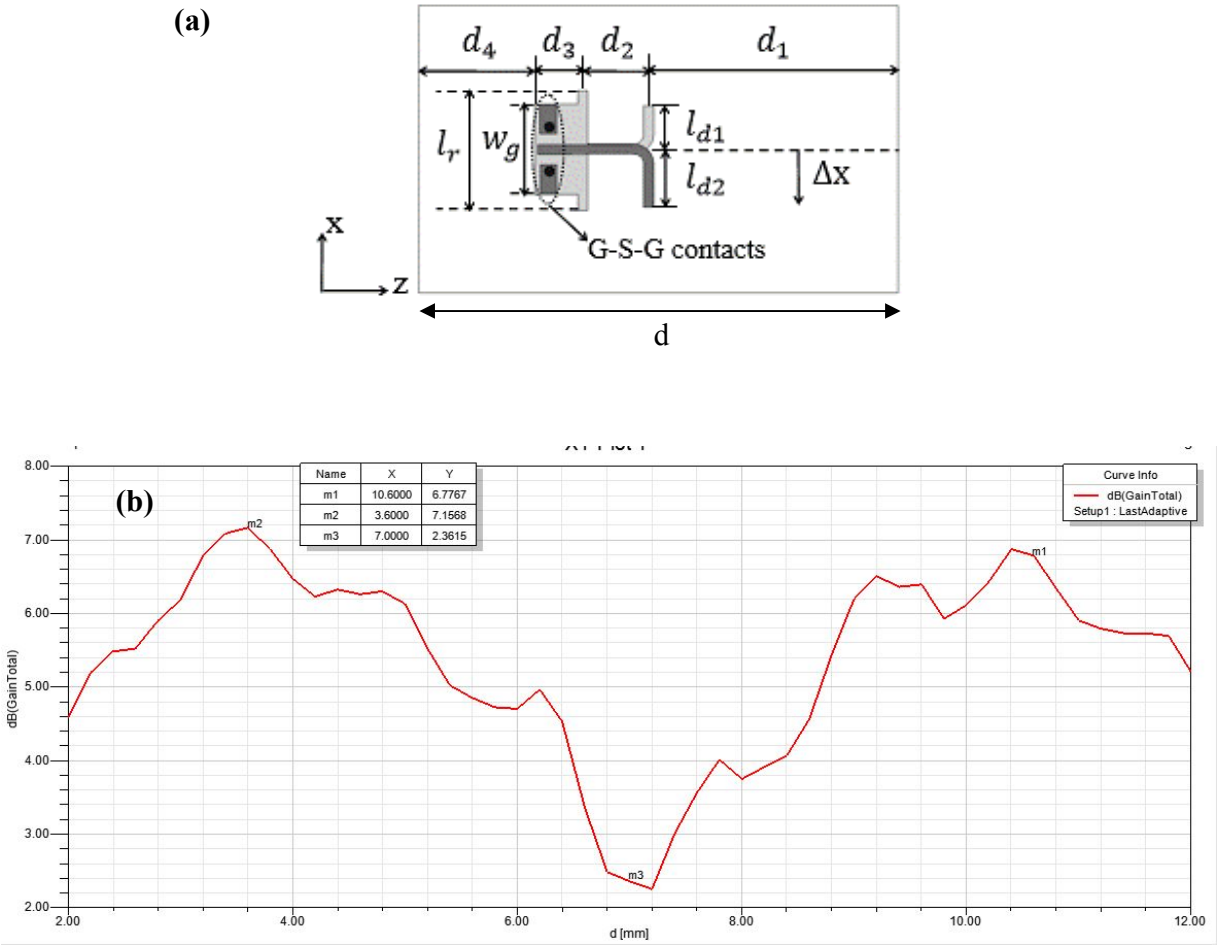

Figure 32 (a) model under discussion; (b) end-fire gain with length for antenna with a × b = 2mm × 0.8mm

A detailed radiation model for the low-profile DRA is illustrated in Figure 33. Before applying Brown and Spector's theory, several assumptions have to be made. The reflected or reactive fields associated at the feed and terminal are ignored. Also for a first-order

approximation, the element patterns radiated from the feed F(θ, ϕ) and the one from the terminal T(θ, ϕ) are considered the same. In this case, we only need to consider the pattern introduced by the phase difference between them. In fact, F(θ, ϕ) is a pretty broad cardioid shaped pattern and T(θ, ϕ) is a more focused version of that. The phase difference between the two radiators is:

$$\psi = k_z d - k_0 d cos\theta \tag{15}$$

in which k_z is the wave number in dielectric in z direction, k_0 is the wave number in free space, d is the effective distance between the feed and the terminal, θ is the angle away from the end-fire direction. This phase difference is a periodic term which means at a certain length d1 producing a ψ_1, there must be a another length d2 with a $\psi_2 = \psi_1 + 2k\pi$, hence the oscillating property of the end-fire gain. Of course practical design focus on the best performance with the smallest area. Thus all the discussions will be conducted within the first gain period.

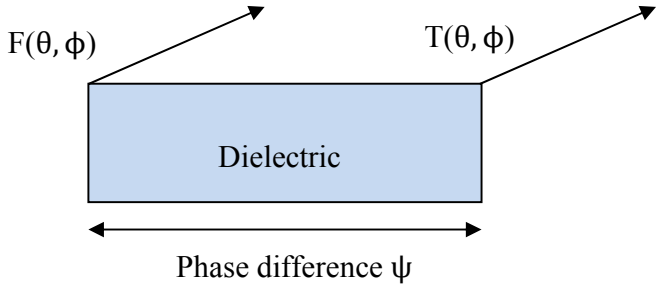

Figure 33 Detailed radiation model for the low-profile DRA

One of the most attractive advantages of the rectangular DRA is that it has two degrees of freedom for flexible design and board with different dimensions can resonate at the same frequency. It has already been established in [110] that by particularly choosing relatively bigger dimensions, the design is more tolerant to the fabrication error which is a crucial issue in mm-wave range since the antenna is so small that a little error might result in huge frequency shift or other parameter deterioration. Other efforts have been drawn to the wideband application, phase array and so on. Although, theoretical and experimental studies have been carried out to enhance the end-fire gain by exciting higher-order modes within the DR, it is not practical for low-profile planar excitation structure. In fact, such antennas have the characteristics of both surface-wave antenna and dielectric resonator antenna. Thus in this thesis, both theories have been applied for a thorough study of its gain performance and design optimization.

First of all, it is important to understand how the cross-section area of the substrate influences the gain performance. So the total radiation is a superposition of two parts from feed and terminal written as:

$$R(\theta, \phi) = F(\theta, \phi) + T(\theta, \phi) \tag{16}$$

in which the θ component of radiation pattern from the terminal can be approximated using this formula [116]:

$$T(\theta) = \frac{1}{\left(\frac{\lambda}{\lambda_g}\right) - cos\theta} \tag{17}$$

The ϕ component of T is narrowed by multiplication with the E-plane element factor (a dipole pattern modified by the effects of mutual impedance). Thus for qualitative discussion, these two component has the same trend and it is enough just to consider T(θ).

The pattern associated with equation (17) is one with no null or side lobes. Hence the total pattern R with all the nulls and side lobes is the result from the interaction between F and T. At certain ψ between them, the two radiation has cancellation effect which reduces the gain to minimum, whereas at other particular ψ, the superposition is constructive at the grazing angle resulting in a maximum gain. Moreover, equation (17) can be observed as the ideal case of the radiation without the disturbance introduced by F. Therefore, the distribution of T(θ) itself can give some idea of how large of G_{max} one DR can achieve with different cross-section areas.

DWM method indicates that once the cross-section area is fixed, the guided-wavelength λ_g is fixed within the substrate. By making this statement, the antenna is first be seen as a surface-wave antenna. Thus to change the cross section of the board is fundamentally changing the λ_g. Assuming this is a low-loss system and the gain is pretty close to the directivity which is inversely proportional to the beamwidth. Additionally the beamwidth is inversely proportional to the absolute value of the derivative of the pattern T(θ) at $\theta = \theta_0$. Since θ_0 is very close to the angle 0, $\sin\theta \approx \theta$ and $\cos\theta \approx 1$. To sum up, the gain is proportional to T(θ) as this:

$$G \propto \frac{\theta}{[\left(\frac{\lambda}{\lambda_g}\right) - 1]^2} \tag{18}$$

It indicates the end-fire gain increases with the guided-wavelength λ_g. In order to validate this statement, multiple examples have been adopted with different cross-section areas and λ_g is calculated using matlab and summarized in Table IV (at 60GHz where λ_0 is 5mm). In chapter 2, transcendental characteristics equations have been proposed for wave number calculation. However, it is easier to consider the antenna here as well-guided DRA for qualitative discussion. Under this circumstance, the relation between wave numbers and guided wavelength is

$$(\frac{2\pi}{\lambda_g})^2 = \varepsilon_r k_0^2 - \left(\frac{m\pi}{a}\right)^2 - \left(\frac{n\pi}{b}\right)^2 \tag{19}$$

Thus with either dimension getting bigger, the guided-wavelength will decrease and it is quite obvious from the Table that no matter for a series antennas with same width or same height, the end-fire gain decreases along with λ_g as expected.

Table IV G_{max} of DRA with different cross sections

Antennas with same width		λ_g(mm)	G_{max}(dB)	Antennas with same height		λ_g(mm)	G_{max}(dB)
a(mm)	b (mm)			a(mm)	b (mm)		
2	0.5	3.6	9.5	2	0.35	$\approx \lambda_0$	12
	0.6	3.2	8.16	2.5		4	11
	0.7	3	7.56	2.9		3.8	10.38
	0.8	2.8	7.26	4		3.4	10.36

However, it is worth pointing out that purely comparing the value of λ_g as an indicator of end-fire gain is misleading since in the actual situation, the feed radiation cannot be neglected along with other assumptions. For instance, the antenna of 2mm×0.5mm has a larger λ_g than the one with 4mm×0.35mm. However, the G_{max} it can provide is not as high. Another important observation is that the end-fire gain performance of the low-profile DRA is very sensitive to the thickness. This suggests a crucial design rule of thumb that if possible, thin substrate is always preferred for the gain optimization.

The physical meaning behind this scenario lies in the area of radiating aperture at the terminal end. For a surface wave having a λ_g quite close to λ_0 in the air, the wave is more loosely bounded to the substrate resulting in a larger effective radiating aperture providing a larger available gain. One drawback of such configuration is that this higher gain will require large area which sometimes limits its application.

The highest available gain is mainly varied with cross section while where this G_{max} occur remains a topic of interest. Large quantities of simulation results show that it actually occurs when the phase difference ψ between feed and terminal satisfies Hansen-Woodyard condition:

$$\psi = k_z d - k_0 d = \pi \tag{20}$$

The Hansen-Woodyard end-fire array is a special array designed for maximum directivity. In order to increase the directivity in a closely-spaced electrically long end-fire array,

Hansen and Woodyard analyzed the patterns and found that an additional phase shift of increases the directivity of the array over that of the ordinary end-fire array. Strictly speaking, this condition is valid only for discrete or continuous antenna with length much larger than the free-space wavelength. However, this condition is well-suited here with certain physical meaning. For a focused beam pattern at a small angle away from the end-fire direction, phase difference reaches near 180° with an effect of narrowing the beam. While when the length is getting longer until it reaches 360°which broaden the beam thus continuously making the gain oscillating with the substrate length as shown in Figure 32. Based on this, the gain performance with the substrate length can be analyzed. Equation (17) can be rewritten as

$$2\pi d(\frac{1}{\lambda_g} - \frac{1}{\lambda_0}) = \pi \tag{21}$$

For antennas carrying wave with smaller λ_g, although it has been proven that most likely the G_{max} will suffer from the dielectric cavity effect, it only takes a small length d to achieve this gain which is an advantage for antenna array design. Figure 34 shows two examples (antenna II and III) with different dimensions. Together with the antenna I shown in Figure 32, it is a clear demonstration of the maximum and minimum gain and the lengths they occur respectively for different dimensions. In summary, antenna I, II and III have λ_g of 2.8mm 3.2mm and 3.4mm with G_{max} of 7.16dB, 8.16dB and 10.36dB occurring at the length of 3.6mm, 4mm and 6mm. All simulation results agree with our conclusions.

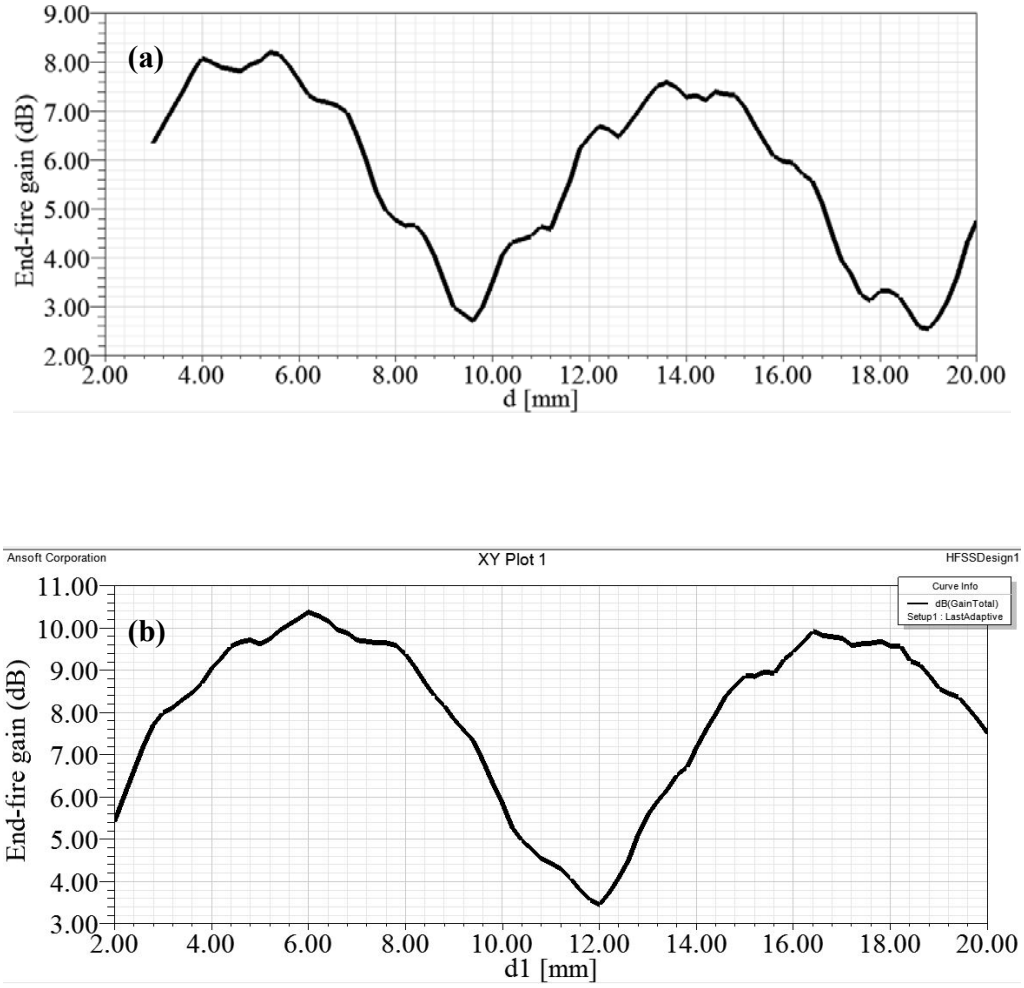

Figure 34 End-fire gain with length for (a) antenna II with $\mathbf{a \times b = 2mm \times 0.6mm}$ (b) antenna III with $\mathbf{a \times b = 4mm \times 0.35mm}$

Recall the low-profile DRA has both the properties of surface-wave antenna and dielectric resonator antenna. This can be clearly shown in comparing the gain trend of the three antennas mentioned above. If the cavity effect is stronger such as antenna I, modes start to play its role in

the radiation pattern and introduce more obvious ripple on the gain curve. All the small local maxima exist near resonances. This property will be addressed again and applied to determine the design curve in the following sections.

3.3.2 DRA with Transverse Modes

As it has been mentioned, degenerate modes in the DRA will disturb the radiation pattern. This most occurs mostly with wider boards in which TE_{31l}^{y} modes are possible. If they coexist in the DRA with TE_{11l}^{y} modes, the design rule introduced in the last section to predict the optimized board length for a highest available gain will not apply any more. More fluctuations will appear on the plots of gain versus substrate length. To illustrate this phenomenon. A LTCC-based model with cross-section area of a×b=4mm×0.8mm is presented and its gain performance against the length d is plotted in Figure 35. The two (largest and second largest) maximas are associated with TE_{115}^{y} and TE_{117}^{y} respectively. A quite deep null in the gain curve is due to the TE_{313}^{y} mode at d=4mm, the field distribution of which is plotted in Figure 36. This is not a strict TE_{313}^{y} mode since the center plane is not a perfect E plane. However, the transverse mode is clearly excited and strong enough to decrease the gain. This is another example of the importance of board thickness. However, thick board may be unavoidable as many layer stacking is necessary to route circuit traces for packaging the entire system. By making the substrate thick, it not only decrease the gain, the wave leaking backward is also stronger. For EMI concerns, shielding vias and proper routing are necessary to block the unwanted coupling. Severe

gain drop could occur over the band for thick substrate as well. It is also not recommended to make a substrate too wide since transverse modes are more likely being excited. Other issues including beam-tilting effect due to off-centered feed for wide board will be discussed later in this chapter.

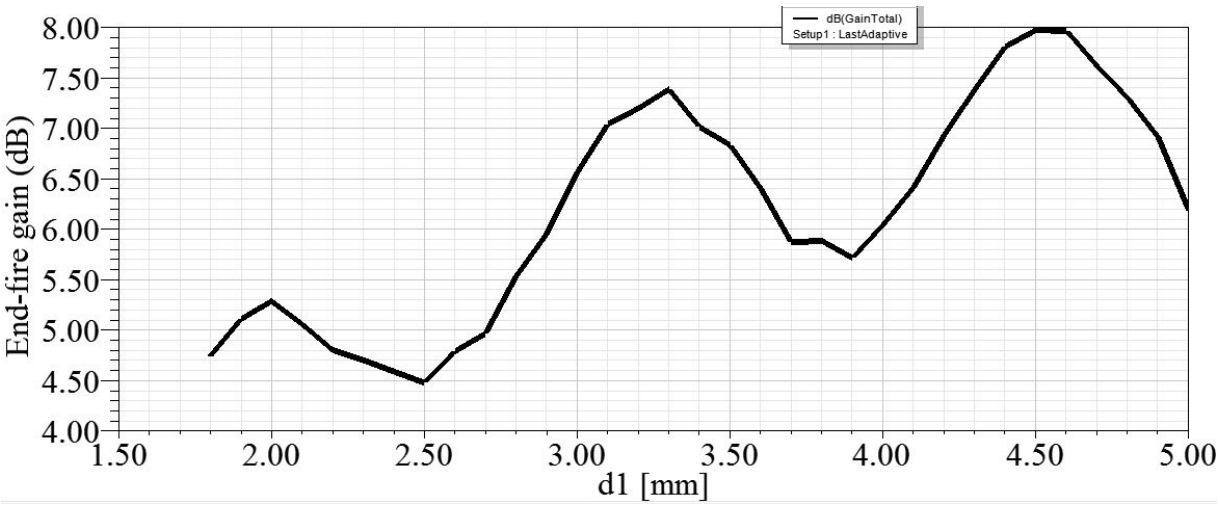

Figure 35 End-fire gain with length for antenna with $\mathbf{a \times b = 4mm \times 0.8mm}$

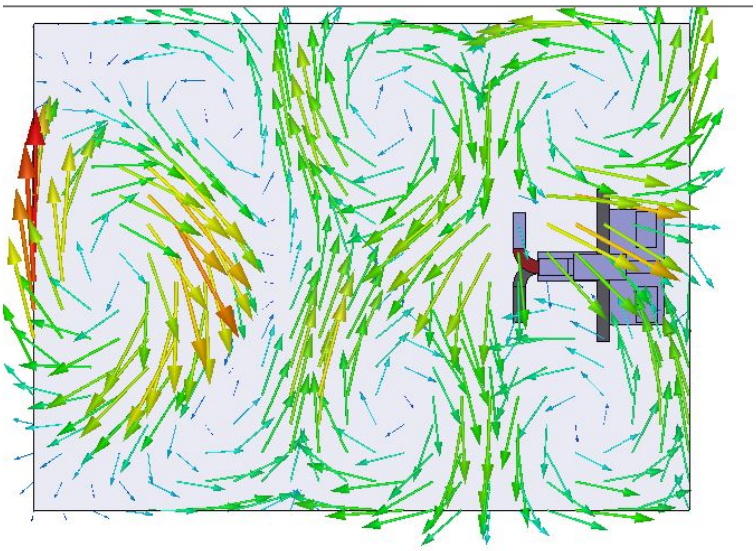

Figure 36 Field distribution of TE^{y}_{313} at d=4mm

3.4 Design Curve and Examples

Based on the investigations so far, it is practical to provide a design curve which can serve as a quick guideline in determine the dimensions of the 60GHz low-profile DRA design. With a prototype provided by the design rules, considerable time can be saved on the tedious HFSS simulation. However, fine tuning using simulation tool based on the prototype antenna is highly recommended for better gain optimization as well as improving other performance of the antenna, such as bandwidth and efficiency.

In last section, the optimized length of the substrate with a fixed cross section seems to occur when it can provide a 180 degree phase difference of the feed and aperture fields close to

the Hansen-Woodyard condition. While the DRA becomes thicker, cavity effects start to become noticeable in the gain curve. Thus the estimate of optimize board length from equation (21) needs to be modified to account for these modes.

Assuming the DRA is resonant at TE_{11l}^{y} mode with l being an odd number, this suggests the actual length d associated with this DR is $l\lambda_g/4$. Taken this into equation (21), the value of l is obtained as well as the length with this resonant condition:

$$l = \frac{2\lambda_0}{\lambda_0 - \lambda_g} \tag{22}$$

The mode which provides a phase difference closest to π is most likely to achieve the highest gain. Once the length d_{opt} (optimized d_{eff}) is determined, degenerate modes need to be carefully examined to avoid coexistence in the DR at the same frequency. Based on this idea, a practical design curve specifically prepared for the low-profile LTCC-based rectangular DRA at 60GHz is plotted in Figure 37. Since thickness is the most sensitive dimension, it acts as an independent parameter and several discrete values are chosen. For each set of width and thickness, there is an optimized length providing the highest end-fire gain. There are certain distinctive characteristics in the design curve that are worth mentioning. First of all, for the relatively thin substrate, there is an abrupt transition present when the width is narrower. Before the transition, the optimized length is much longer indicating a property of surface-wave antenna while after the transition, the d_{opt} does not change much and relatively short. This phenomenon does not apply to the thicker substrate since in this case, the dielectric resonance dominates no

matter how narrow the substrate is. In other words, this abrupt transition can be considered as the boundary between the behavior of surface-wave antenna and DRA. Secondly, the end of the curve is truncated abruptly. That is when the degeneracy occurs, further increase the width is not desired. Also, for thinner substrate, the maximum width reaching the degenerate point is wider. The optimized length is wider as well indicating a larger occupied area. Thus, a compromise needs to be made between the available space and maximum achievable end-fire gain.

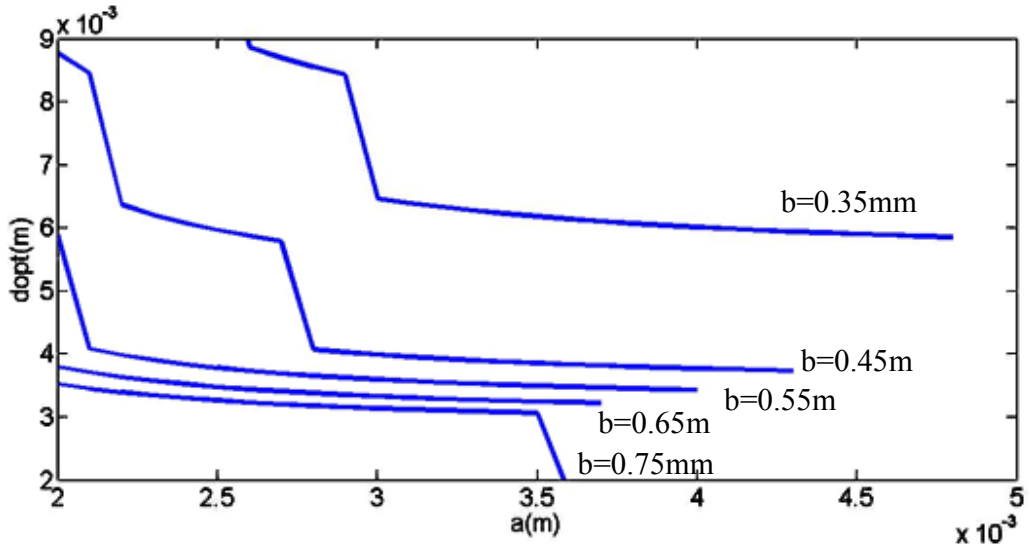

Figure 37 Design curve for low-profile LTCC-based rectangular DRA at 60GHz

In order to test whether this curve serves its purpose, one DRA is designed according to the plot with dimension of a×b×d=2.5mm×0.45mm×6mm. The simulated end-fire gain at 60GHz is 9.25dB. Parameter sweep has been performed near the predicted d_{opt} to check whether G_{max} is achieved. The end-fire gain versus d_{opt} is shown in Figure 38. The maximum value occurs exactly at d_{opt}=6mm. The field distribution displayed in Figure 39 indicates a TE_{117}^{y} mode which is what has been calculated using the formulas introduced. Several examples have been designed using the design curve. The error between the optimized and predicted value is within tolerance and the procedure is fast and accurate.

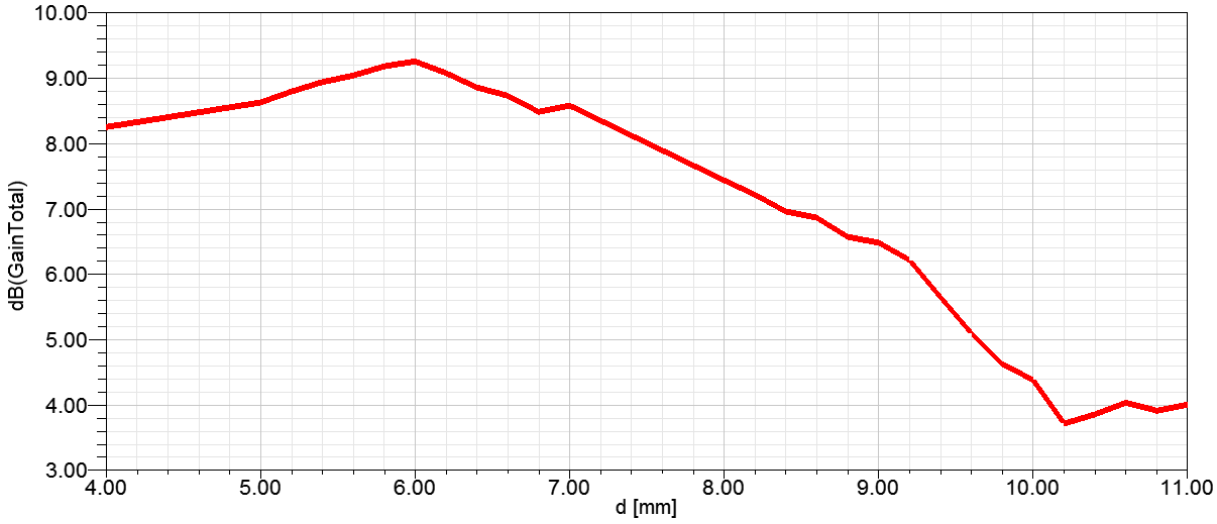

Figure 38 End-fire gain near the predicted d_{opt} with a×b×d=2.5mm×0.45mm×6mm

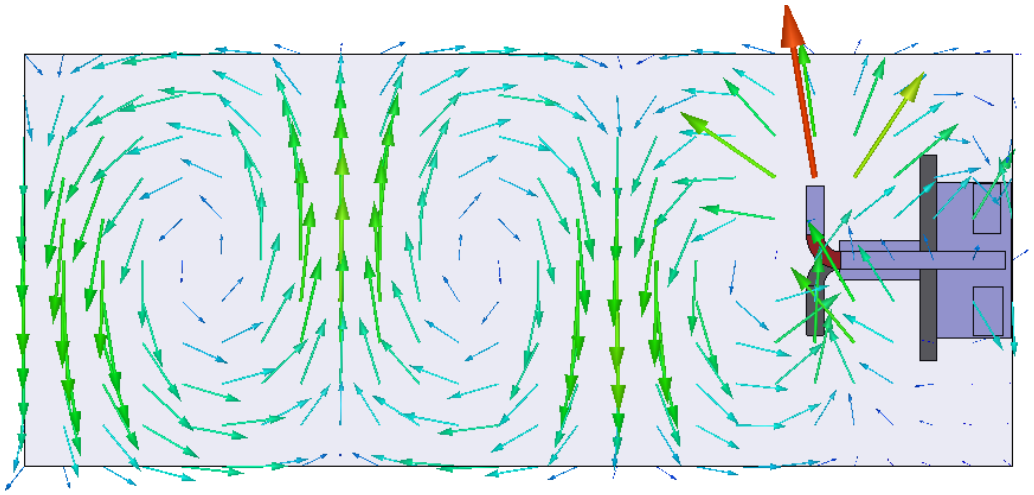

Figure 39 Field distribution of TE_{117}^{y} associated with d_{opt}

3.5 Director-assisted DRA

Quasi-Yagi antenna in a planar form is a popular structure when it comes to end-fire application in mm-wave. This kind of antenna contains a number of linear elements in front of the feeding dipole as directors to create a progressive phase distribution and direct the main beam forwardly. However, when it comes to the low-profile DRA, these directors may not work as expected. Moreover, in certain cases, they may even behave like reflectors and degrade the end-fire gain. In order to demonstrate this effect, one example has been applied here with a×b×d=4mm×0.35mm×6mm and $\varepsilon_r = 7.5$. The original end-fire gain is 10.36dB at 60GHz. Now one director is added in front of the feeding dipole as shown in Figure 40 in which l_{dr}=0.6mm and s=0.686mm. The length of the director and the distance between director and

feeding dipole is optimized to give the best result. The updated end-fire gain, however, drops to 10.22dB which indicates the director does not help enhancing the gain. Now consider a Rogers-based DRA ($\varepsilon_r = 3.66$) with the same board dimension. Since the dielectric constant is smaller, the feed dipole and the reflector should be scaled accordingly. The end-fire gain is originally 11.3dB. If the distance from director 1 to the driven dipole is s1, distance from director 2 to director 1 is s2 and the lengths of director 1 and director 2 are l_{d1} and l_{d2}, then adding one director with s1=0.846mm and l_{d1}=1.05mm gives 12dB and adding another director with s1=0.8mm and l_{d1}=1mm further boosts the gain to 12.2dB. Higher gain can be achieved if adding more directors and fine tune the parameters of the directors. This indicates the fundamental mechanism of the field distribution in the substrate. The wave carried by the substrate needs a progressive phase difference to propagate toward end-fire direction and then radiate at the terminal. This phase different can be provided by either the directors of the planar-Yagi or the dipole-like field of DR modes, whichever is dominant. If the dielectric modes are dominant and mainly responsible for the antenna radiation, then adding directors will only disturb the pattern instead of enhancing the gain. Vice versa, if the dielectric modes are too weak to sustain the surface wave, then additional directors are needed for maximum gain. Normally, the thinner substrate made of the material with lower dielectric constant could use the assistance of additional directors.

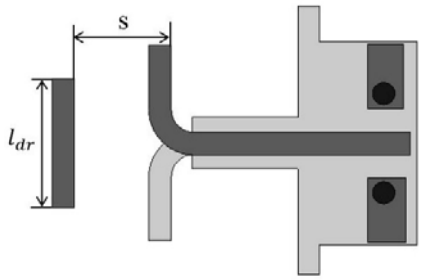

Figure 40 DRA with dimension of a×b×d=4mm×0.35mm×6mm and one director

3.6 Beam-tilting Effect

Of all the examples that have been discussed so far, the feeding dipole is always placed at the center of the transverse direction, that is $\Delta x = 0$ which is the offset distance from the center line of the feed to the center line of the DR. However, practically this condition can be easily compromised due to the board layout if the single antenna is integrated into the system or used as part of the linear array. The undesired effect in the radiation pattern is the main beam shift and degradation in the end-fire gain. Thus it is essential to evaluate the effect of an offset feed. Using LTCC as the substrate material, three antennas all resonant at TE_{117}^{y} mode with different dimensions and same offset are compared in the first three rows of Table V. The last two rows compares the results of the same antenna with different offset distance. End-fire gain is simulated at 60GHz. Antenna I, II and III have dimensions of a×b×d=2mm×0.35mm×8.6mm , 4mm×0.35mm×6mm, 4mm×0.8mm×4.5mm, respectively. Δx is positive if the feed moves toward -x direction. Figure 41 shows 3D radiation pattern of antenna III with Δx=1mm and its

field distribution. The main beam is clearly tilted toward the +x direction. The reason of this beam tilt is the unbalance radiation on the transverse direction. It has been established in the previous sections that within a short range of any dimension of the DR, the surface wave begins to build up resulting in an increased radiation in that direction. If the DR is center-fed, then the radiations in +x and –x directions are the same since the lengths in these two directions are the same. The main beam is therefore still in the end-fire direction. However, in the offset case where the feed is moved toward –x direction, the length toward the side of the feed in +x direction is longer resulting in a larger radiation. The superposition of radiations toward +x and +z direction causes the main beam away from the end-fire direction. From the dimension of the three antennas, it is quite clear that λ_g decreases as the number of antenna increases. That is to say, antenna III has the strongest dielectric resonant effect. Hence the tilt angle of the main beam in the last row of Table V is the largest and end-fire gain is degraded significantly to almost 0dB. Although Rogers-based examples are not shown here, it is not difficult to come to the conclusion that for the Rogers counterparts of these three antennas, the beam tilt is not as severe.

Table V Comparison of beam-tilting effect for different antennas with Δx

Antenna # and **Δx** (mm)	Angle tilt from end-fire (degree)	Maximum Gain (dB)	End-fire gain (dB)
I : **Δx**=0.35	6	11.20	11.07
II: **Δx**=0.35	8	10.37	9.94
III: **Δx**=0.35	10	7.88	7.36
III: **Δx**=1.0	32	6.01	0.43

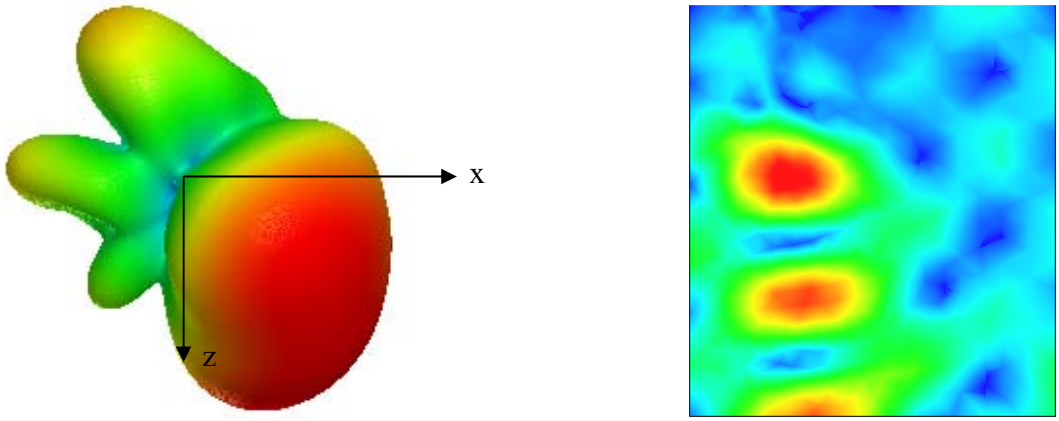

Figure 41 3D radiation pattern of antenna III with Δx=1mm and its field distribution

When the feeding dipole has to be placed off-centered, it is still possible to achieve end-fire main beam. One solution is to adopt air cavity. For instance, in certain AiP design, the front portion of the substrate board serves as the antenna while the back portion is used for the system routing. Thus the one can maintain the thickness of the back portion while adopt air cavity at the antenna part as shown in Figure 42, to decrease the effective thickness as well as the dielectric resonant effect. The major drawback of this approach is by introducing different thicknesses on the same board, the fabrication process is more complicated thus increasing the total cost of the system. Another more economic technique is to cut a gap on a wide board to tilt the beam back to end-fire direction. It could also increase the isolation between antenna elements if several antennas are placed horizontally on the same thick substrate and the gap cut in the middle when assembling a T/R antenna system or array. Thus this method is quite practical. Of course the gap

cannot be too narrow according to the tolerance of the design rules. Figure 42 shows a configuration using an air cavity with dimension of a1×b1×d1=3mm×0.3mm×4.5mm based on antenna III with Δx =0.35mm and in Figure 43 a gap with dimension of a1×b1×d1 =0.7mm×0.8mm×3mm is cut from the substrate. Table VI summarizes the results of these two solutions. Both methods manage to tilt the main beam back to the end-fire direction. However, the price to pay in both cases is the loss in mechanical strength.

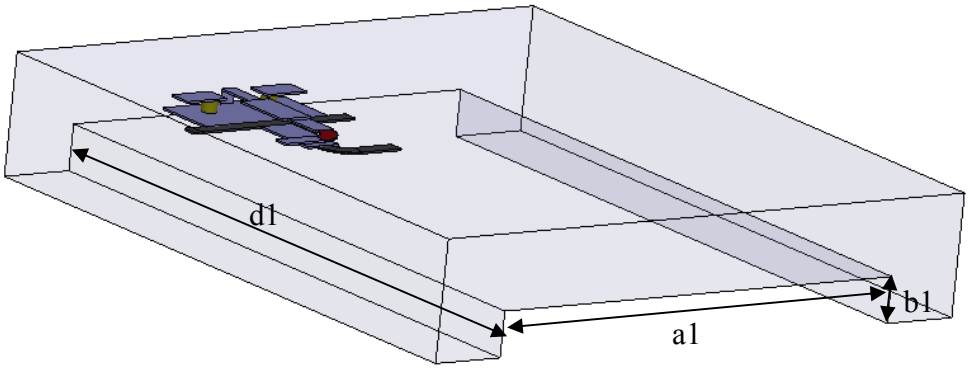

Figure 42 Antenna III with Δx=0.35mm and an air cavity of a1×b1×d1=3mm×0.3mm×4.5mm

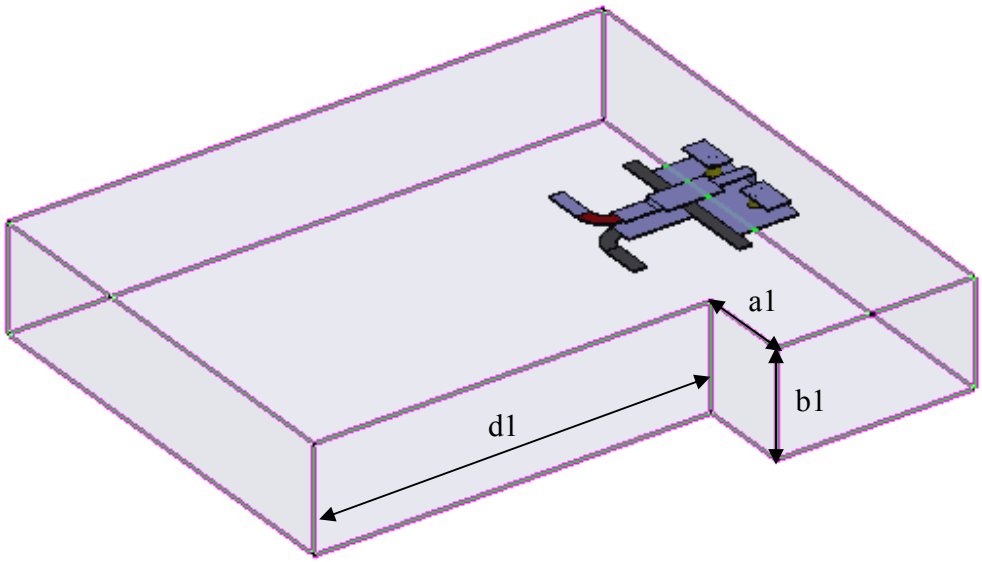

Figure 43 Antenna III with Δx=0.35mm and a gap of a1×b1×d1=0.7mm×0.8mm×3mm

Table VI Comparison of solutions to beam tilt

Antenna III $\Delta x = 0.35$mm	Angle tilt from end-fire (degree)	Maximum Gain (dB)	End-fire gain (dB)
original	10	7.88	7.36
with air cavity	4	8.00	7.89
with gap	4	7.71	7.63

3.7 Conclusions

This chapter focused on the characteristic study of the DRA using end-fire gain as a main parameter. Gain-enhancement methods were first introduced. For end-fire application, the method of using higher-order modes is more suitable. Then methods of studying end-fire antenna were introduced, among which the Brown and Spector's theory can be applied toward the mode of interest. LTCC substrate was taken as an example for study. Although the rectangular DRA has a design freedom of two, the thickness of the DRA was proven to be the most sensitive dimension and it will greatly vary the properties of the antenna. Since the low-profile surface-wave antenna and DRA with dielectric constant not high enough share some similar properties, the knowledge of surface-wave antenna was used to study the performance of the antenna. The radiation mechanism of DRA with no transverse mode was first studied. The properties of the gain curve was thoroughly investigated with respect to different dimensions of the DRA. Then design rule of thumb was suggested and design curve was provided for preliminary end-fire antenna design in 60GHz. An example antenna was designed using the curve to prove its validity. The disadvantages of DRA with transverse modes excited were also illustrated. Another popular material of Rogers 4350 was used as the substrate material to demonstrate the potential effect of additional directors. At last, off-centered feeding was investigated and solutions of beam-tilt was discussed.

4. SINGLE ANTENNA DESIGN

4.1 Review of Design Background

Operating at the 60 GHz spectrum and offering speeds of up to 7 GB/s, WiGig is the next-generation of high-speed wireless technology. The 60 GHz wireless band is desirable because very few devices and technologies currently use the 60 GHz band. Regulation of the 60 GHz band is minimal, and it allows very fast data transfer rates, compared to existing wireless options that operate in lower 2.4 GHz and 5 GHz wireless bands. The wireless sync-and-go applications include smart phones, tablets, laptops, digital cameras, storage devices, and more. With speeds more than 10 times faster than today's WLANs, the next-generation of wireless entertainment and networking becomes reality.

Among all the applications of WiGig, the attraction is the point-to-point high-speed wireless module which can cover the whole 7GHz of the 60GHz band. Point-to-point requires an end-fire communication in mobile devices. This also allows the convenience for customers to operate the device. High-speed demands a high-gain antenna and operating in mm-wave range requires a low-loss system which make a dielectric resonator antenna with proper excitation a good candidate to meet all the above requirements.

Three mainstream materials are used for the DRA design in this chapter. Low temperature co-fired ceramic (LTCC) devices are monolithic, ceramic microelectronic devices where the entire ceramic support structure and any conductive, resistive, and dielectric materials are fired in a kiln at the same time. It is first developed in the late 1950s and early 1960s to make

more robust capacitors. The technology was later expanded in the 1960s to include multilayer printed circuit board like structures. Typical devices include capacitors, inductors, resistors, transformers, and hybrid circuits. The technology is also used for a multi-layer packaging for the electronics industry, such as military electronics, MEMS, microprocessor and RF applications. LTCC devices are made by processing a number of layers independently and assembling them into a device as a final step. This differs from semiconductor device fabrication where layers are processed serially; each new layer being fabricated on top of previous layers. Low temperature co-firing technology presents advantages compared to other packaging technologies including high temperature co-firing: the ceramic is generally fired below 1,000 °C due to a special composition of the material. This permits the co-firing with highly conductive materials (silver, copper and gold). LTCC also features the ability to embed passive elements, such as resistors, capacitors and inductors into the ceramic package minimizing the size of the completed module. Thus, it is a perfect candidate for the Antenna-in-Package (AiP) design. For an LTCC board, the dielectric constant (5~8) is the highest which ensures a compact size. This is a benefit when designing beamforming system, nonetheless imposes an error tolerance issue if the size is too small. However, when substrate thickness is close to a quarter-wave electric length of the dielectric medium, the antenna placement becomes an important issue as the whole board is in effect a dielectric cavity resonator which restrict the maximum achievable gain. Other issues also begin to immerge such as beam-tilting or gain drop over the band.

Another choice is RO4000 series high frequency circuit materials produced by Rogers Corporation with a dielectric constant of 3.3~3.6. Since the selection of laminates typically

available to designers is significantly reduced once operational frequencies increase to 500 MHz and above, low dielectric loss allows RO4000 series material to be used in many applications where higher operating frequencies limit the use of conventional circuit board laminates. The temperature coefficient of dielectric constant is among the lowest of any circuit board material and the dielectric constant is stable over a broad frequency range. This makes it an ideal substrate for broadband applications. RO4000 materials coefficient of thermal expansion (CTE) is similar to that of copper which allows the material to exhibit excellent dimensional stability, a property needed for mixed dielectric multilayer boards constructions. The low Z-axis CTE of RO4000 laminates provides reliable plated through-hole quality, even in severe thermal shock applications. RO4000 series material has a Tg of >280°C (536°F) so its expansion characteristics remain stable over the entire range of circuit processing temperatures. RO4000 series laminates can easily be fabricated into printed circuit boards using standard FR-4 circuit board processing techniques. Unlike PTFE-based high performance materials, RO4000 series laminates do not require specialized via preparation processes such as sodium etch. This material is a rigid, thermoset laminate that is capable of being processed by automated handling systems and scrubbing equipment used for copper surface preparation. To sum up, the result is a low loss material which can be fabricated using standard epoxy/glass (FR-4) processes offered at competitive prices.

Also from Rogers Corporation, ULTRALAM 3850 laminate is a liquid crystalline polymer (LCP) material with the lowest dielectric constant of 2.9. These adhesiveless laminates are well suited for high speed and high frequency applications in telecommunication network

equipment, high-speed computer data links and other high performance applications. Besides the similar advantage of stable electric properties as RO4000, it allows use of thinner dielectric layer comparable with the LTCC technology with minimal signal distortion. As it has been pointed out that the thickness is the most sensitive dimension of all in the gain performance of the DRA, the thickness of each fabricated layer is thinner which means for a minimum total thickness, it could allow more number of layers. This is a crucial advantage for circuit routing in the system integration when realizing AiP. In addition, the LCP has a unique feature that it bends easily for flex and conformal applications, therefore offering design flexibility and maximizing circuit density requirements. To sum up, these three materials have their distinctive pros and cons and can be applied to the mm-wave antenna system design according to different applications.

In order to test the proposed theory in the previous chapter, several single antenna designs using the proposed materials are shown in this chapter. Both simulated and measured results are given for comparison of the performance of the antenna with respect to end-fire gain, impedance bandwidth, radiation pattern of co-and cross-polarization. These examples will provide a good idea of the meaning and future of this study. They also serve as the foundation of the mm-wave end-fire antenna system design including 1×1 TX/RX system and 2×2 beamforming system which will be proposed in the next chapter.

4.2 Measurement Setup

Since 60GHz system has a very small size, dealing with those slim lines can be really tricky. The radiation pattern is obtained using the set up shown in Figure 40(a) with the measured gain of AUT renormalized according to standard horn with -21dBi gain. The feeding method to the antenna system is through a very delicate G-S-G probe shown in Figure 40(b). Using the network analyzer we can obtain the return loss. Or if only the end-fire gain is desired, it is measured via the transformation of Friss equation. Figure 40(c) indicates the procedure of such measurement. Note that the antenna is placed over 5 wavelengths above the ground so that the ground has no noticeable effect. Also, the spacing between the transmitting and receiving antennas is above 8 wavelengths, thus both are operated in the far field zone. Suppose two identical AUT are used during test, the end-fire gain of a single antenna G_a can be extracted from measured S-parameters and Friss equation by:

$$2G_a = S_{21} + 20\log_{10}(\frac{4\pi r}{\lambda}) - 20\log_{10}(1 - |S_{11}|^2) \tag{23}$$

in which r is the distance between T/R antennas, λ is free space wavelength, S_{21} is the forward transmission coefficient, and $S_{11}$is associated with the return loss due to 50 Ω transmission line by:

$$S_{11} = \frac{Z_{in} - 50}{Z_{in} + 50} \tag{24}$$

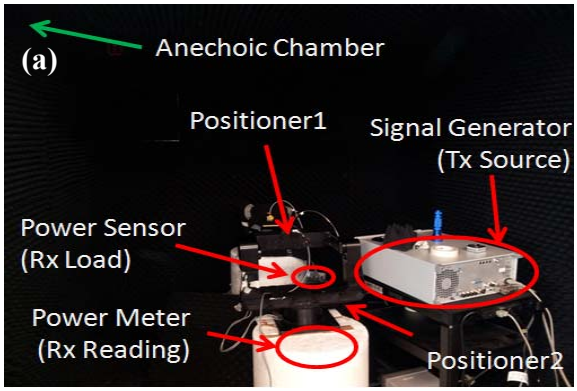

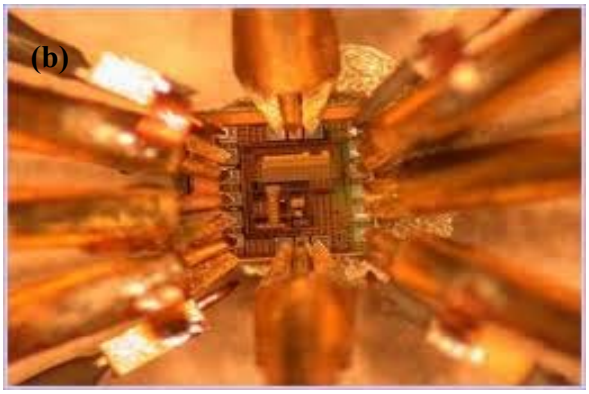

(c)

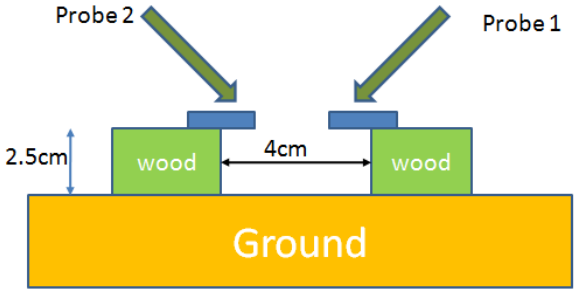

Figure 44 (a) Millimeter-wave test bench (b) G-S-G probe (c) return loss and gain measurement setup

4.3 Yagi on LCP Board

Based on the discussion in section 4.1, a proper end-fire antenna needs to be able to operate over 57-64 GHz band meaning it cannot be too narrow-band. The Q-factor of the system cannot be high resulting in the fact that a substrate material with a relatively low dielectric

constant compared with the regular DR design is desired. Although the most common and cheap substrate is FR4, the high dielectric loss especially at mm-wave range makes it less appealing. Thus, for a prototype antenna design, using the LCP material with a dielectric constant of 2.9 seems to be a good alternative with a potential of wideband performance.

When it comes to end-fire antenna, Yagi antenna is always the primary choice. This directional antenna is consisted of a driven element (typically a dipole or folded dipole) and additional parasitic elements (usually a so-called reflector and one or more directors). According to the discussion in chapter 3, the function of the directors is to provide progressive phase distribution along the end-fire direction similar as the dipole-like surface wave carried by the DRA. By applying the Yagi structure on LCP board, it is supposed to achieve a very substantial increase in the antenna's directionality compared to a simple dipole if the substrate is very thin. In Figure 45, the 6-element Yagi antenna is shown with the layout of top and bottom layers.

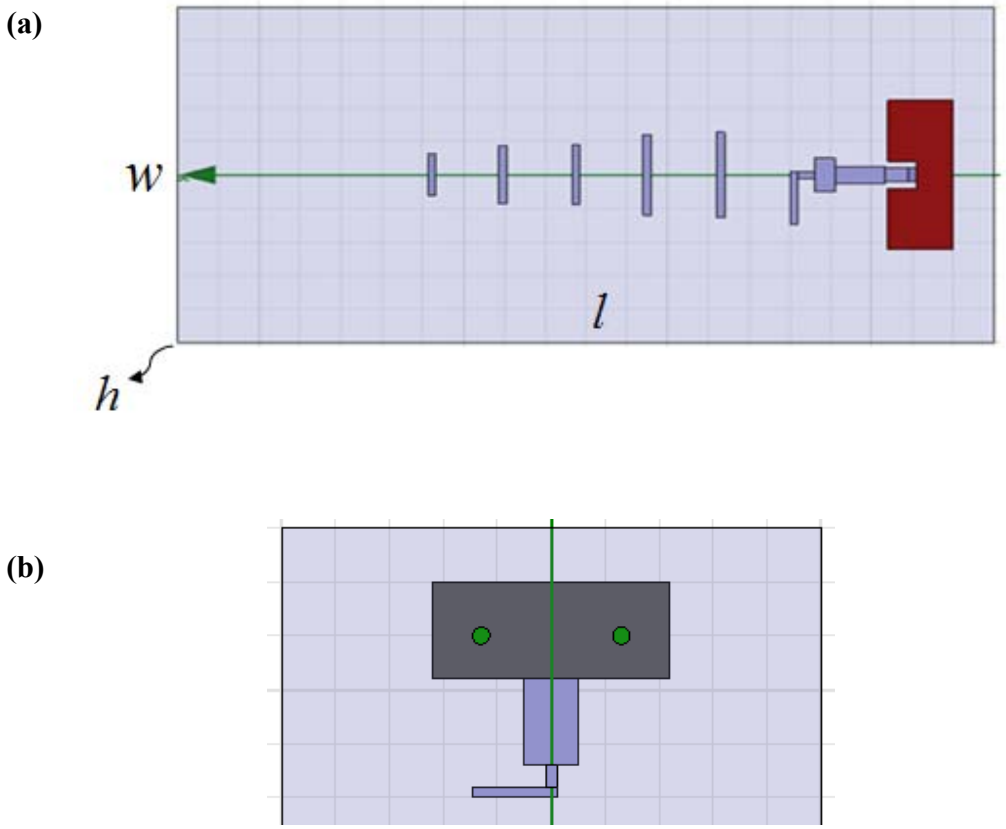

Figure 45 (a) Top layer (b) bottom layer of the two-layer structure of Yagi on LCP With dimension of $l \times w \times h$=11mm×5mm×0.254mm

Figure 46 zooms in on the details of the design. The whole structure is placed at the center of the substrate. The distance between directors and the length of directors are gradually decreased away from the feeding dipole and optimized using simulation. The dimensions of the two-layer structure is $l \times w \times h$=11mm×5mm×0.254mm with copper thickness of 0.034mm. The width of driven dipole and directors is 0.1mm. Initially the coplanar dipole is the best option

as feed. However, it will require the two arms of the dipole really close to each other. Due to the fabrication limit, they are spread into different lays with very short distance as shown in Figure 46(a). The upper arm serves as the signal line and the lower arm serves as ground, both of which are stretching to the CPW part. The lower ground is pinned up to form the G-S-G contacts for the probe to land on. The length from the feed to the dipole is adopted as a CPW to microstrp line transformer for impedance tuning in Figure 46(b). The patch on the backside serves both as the partial ground for the microstrip line and the reflector of the Yagi in Figure 46(c). Figure 47 shows the photo of top and bottom layers of fabricated antenna.

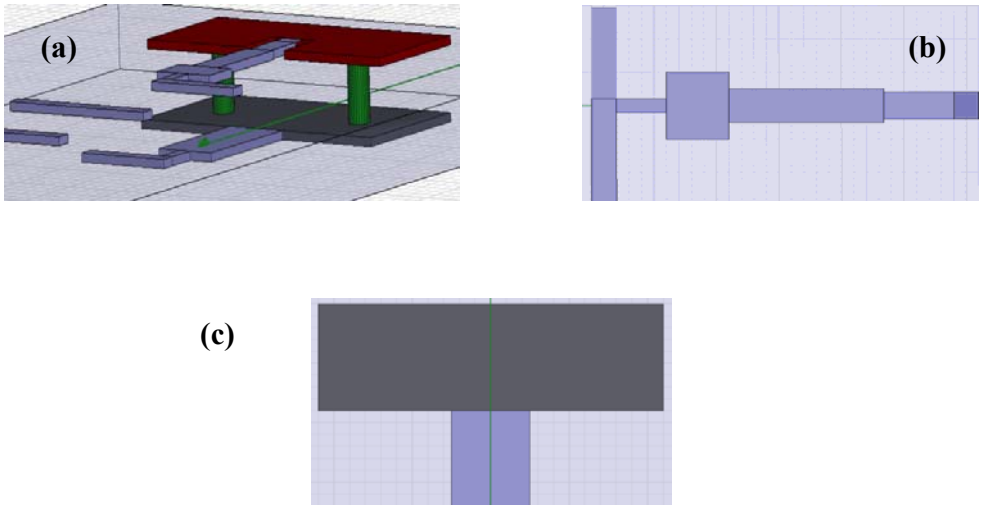

Figure 46 (a) Two-layer dipole feed (b) impedance matching (c) backside ground as reflector

Figure 47 Top and bottom layers of fabricated antenna

In order to examine the performance of this antenna, simulated results are obtained using HFSS as for all the simulated results in the following contents. Figure 48 shows the return loss from the test and simulation. Using a criteria of -10dB, the measured bandwidth is 7.2% (59.4GHz -63.8GHz). The simulated bandwidth is 9.8% (58GHz-64GHz) which is slightly wider than the measured one, but two seems to agree reasonably well.

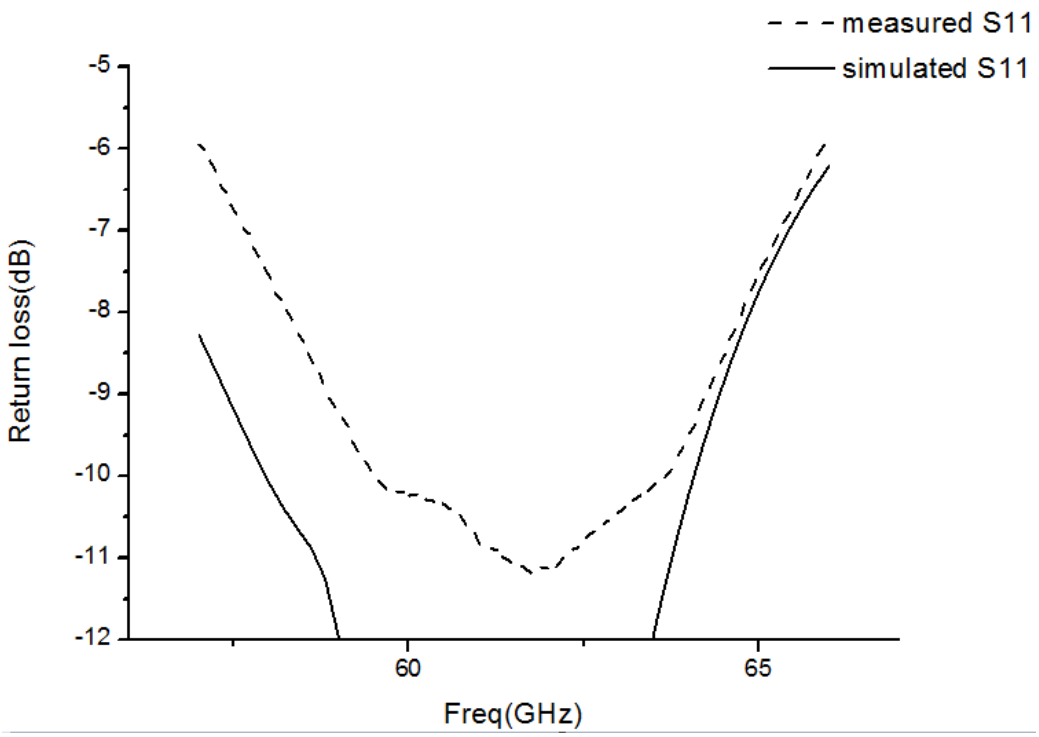

Figure 48 Simulated and measured return loss of Yagi on LCP

Radiation pattern at 61GHz and gain over the band are shown in Figure 49. From the simulated gain pattern, a clear end-fire radiation is observed with a maximum gain of 11.4dB which is very high for a single antenna at mm-wave band within a limited area. This makes this structure a good candidate for the high-gain end-fire application. An average measured gain of 10dB is maintained over the whole band and is very close to the simulated data which makes it a very promising element for the beam forming applications.

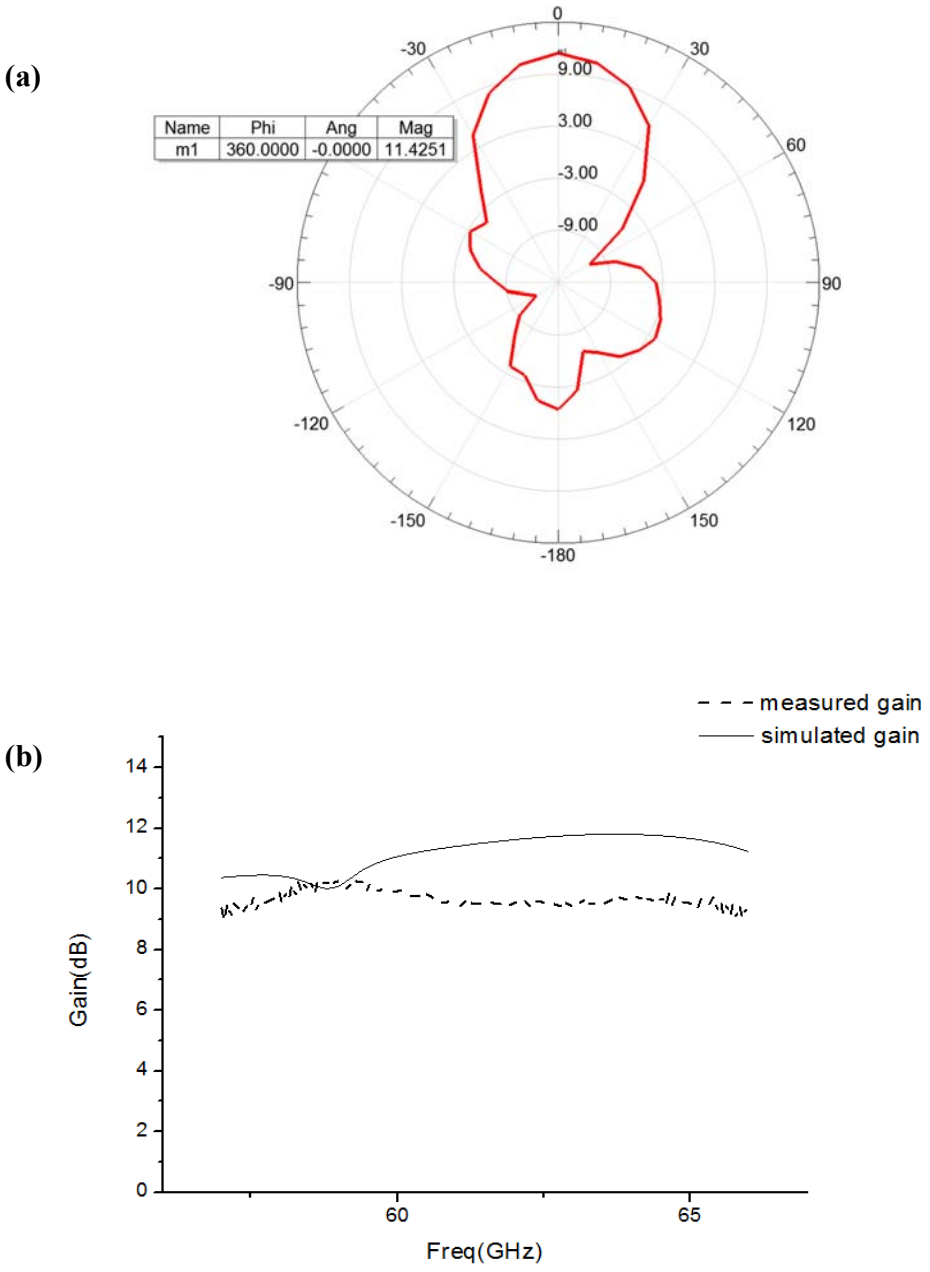

Figure 49 (a) Radiation pattern at 61GHz with 11.4dB end-fire gain (b) gain over the 60GHz band

Figure 50 shows the simulated radiation pattern of co- and cross-polarization. It can be seen that the E- and H-plane cross-polarization is approximately more than 17dB lower than the co-polarization.

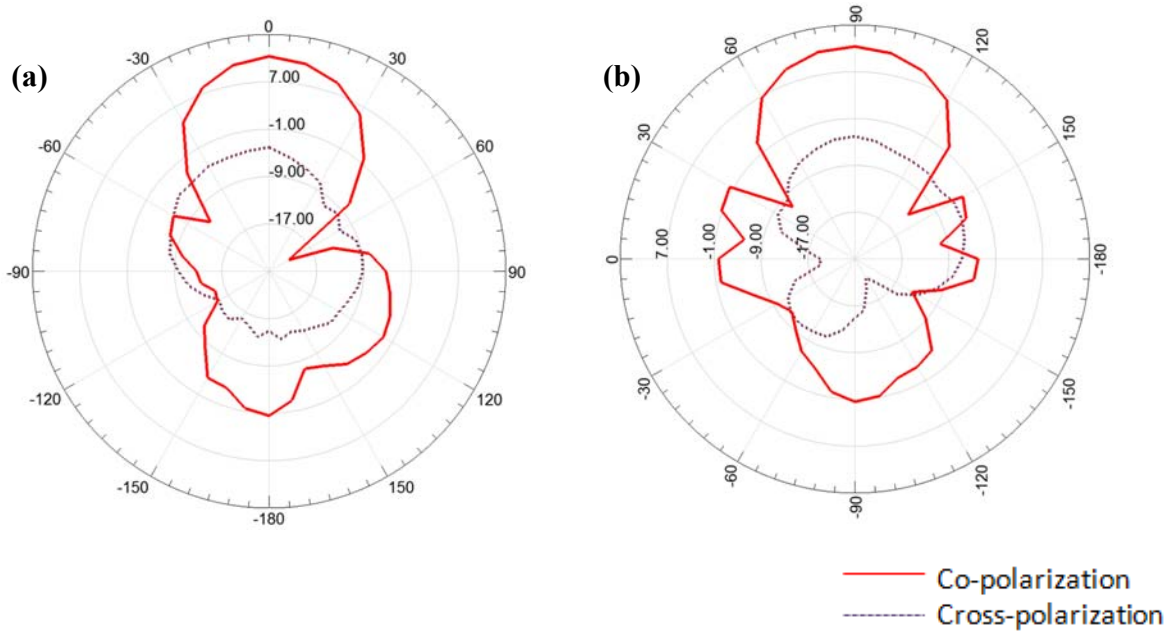

Figure 50 Simulated pattern of co- and cross-polarization in (a) E plane (b) H plane

Although the result is very desirable, there is still a major problem in this antenna design. For such a small system, certain mechanical strength is required. The substrate used here is only 10mil thick which exert great pressure on this issue and may not suitable for hand-held mobile devices. If we increase the thickness, for instance, from 10mil to 30mil, the end-fire gain will

drop significantly from 11 dB to 3dB as discussed in chapter 3. As suspected, the directors now behave more like reflectors. To prove this, four out of five directors are disabled and over 6dB end-fire gain is recovered. Thus, in practical antenna design, extra consideration is required when applying the directors and a compromise needs to be made between end-fire gain and mechanical strength.

4.4 Yagi on RO4350 Board

With a similar configuration, the Yagi structure can be transplanted on the RO4350 board with a slightly higher dielectric constant of 3.36 when the substrate is thinner than 4 mils. Instead of placing the antenna right at the center of the substrate with a restricted area, a more realistic model is proposed with a relatively large substrate and an off-centered feeding dipole ready for potential beamforming design or system integration as shown in Figure 51. It can be easily expanded into a 2×2 antenna system which will be an array example examined in chapter 5. Here the ground not only serves as reflector, it can be further extended backwardly as the ground of the whole SiP if needed. Directors are embedded in the substrate and another top-layer ground and integrated vias around the stripline are adopted for EMI concerns such as better shielding of backward radiation and mutual coupling. A single antenna requires a volume of 8.24mm× 2.375mm×0.376mm. The simulated return loss is plotted in Figure 52 indicating a full coverage of the 60GHz band, while Figure 53 compares the simulated and measured radiation pattern of co- and cross-polarization at 60GHz. For both E and H plane, simulated and measured co-

polarization levels are all roughly 20dB over the cross-polarization ones. As it is noticed the measured H-plane beam is a little tilted away from the end-fire direction. This may be due to the alignment of the receiver during the test.

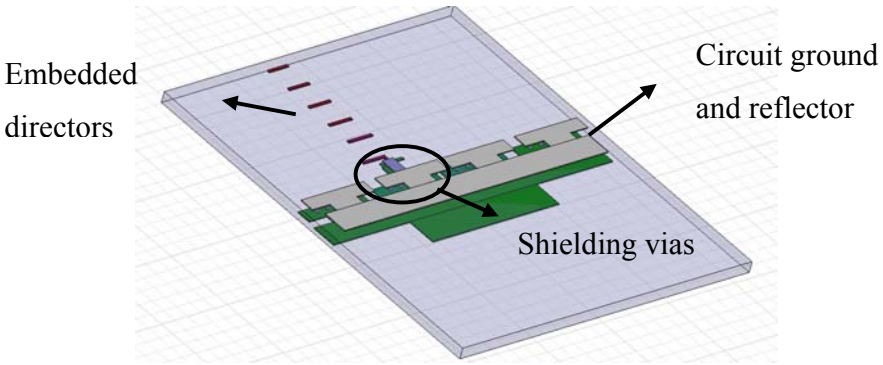

Figure 51 6-element Yagi antenna on RO4350

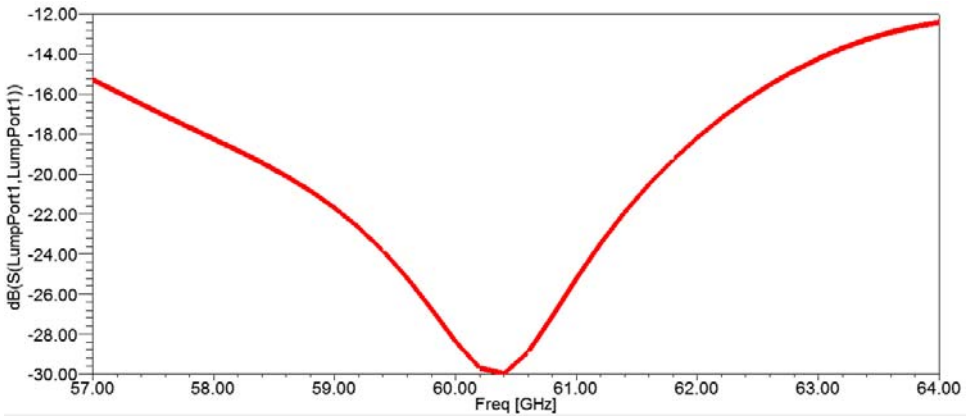

Figure 52 Simulated return loss of Yagi on RO4350

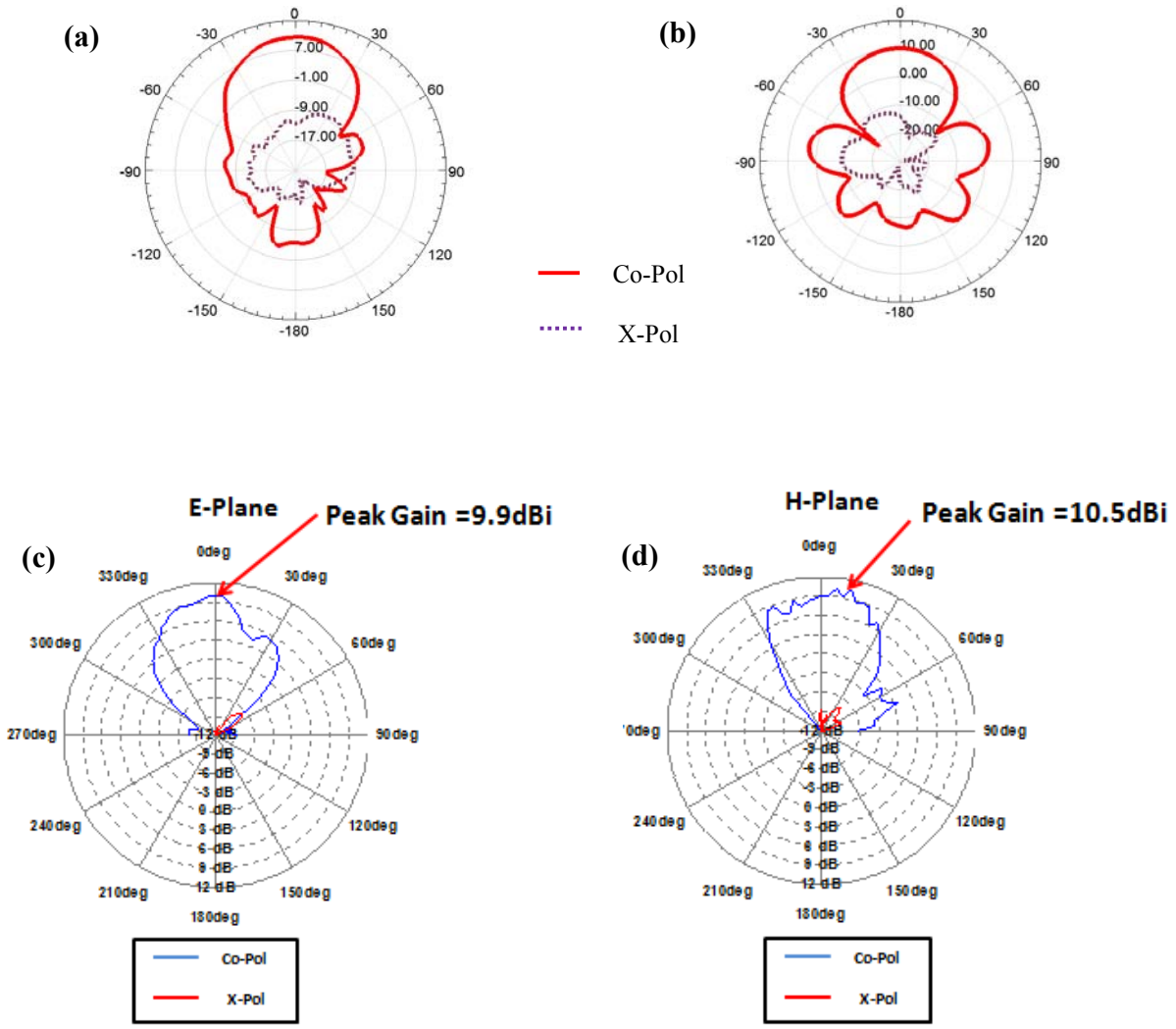

Figure 53 Simulated pattern of co- and cross-polarization in (a) E plane (b) H plane Measured pattern of co- and cross-polarization in (c) E plane (d) H plane at 60GHz

In order to show the advantages of such antennas in applications in mm-wave range, another very popular structure of linear tapered slot antenna (LTSA) is designed here and

compared with the performance of the antenna above. Both antennas use RO4350 as the substrate with the same thickness of 0.376mm. The detailed layout of the LTSA is shown in Figure 54. It is also placed on a large substrate ready to be extended to antenna system. Vias at back helps suppress backside radiation. Its simulated return loss and E-plane pattern are shown in Figure 55 with a 10.4dB end-fire gain and a bandwidth of only 7.7%.

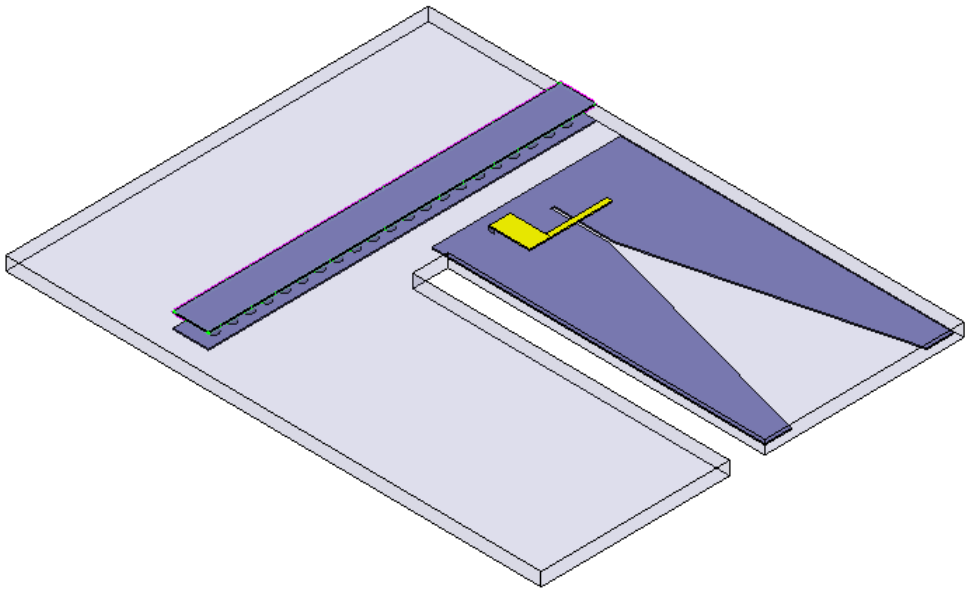

Figure 54 Layout of Rogers-based LTSA

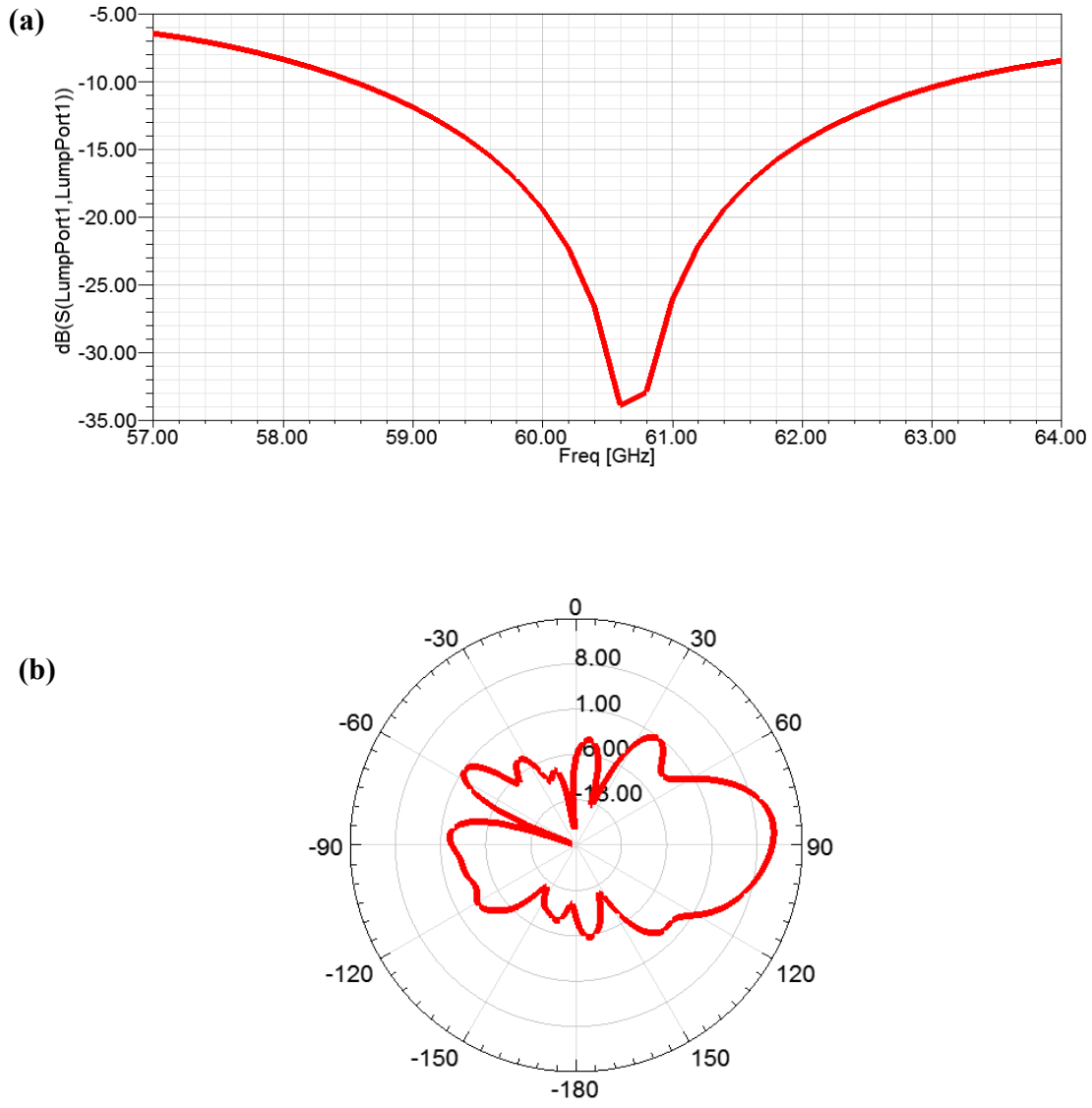

Figure 55 Simulated (a) return loss and (b) E-plane radiation pattern

It is quite straightforward to see that the planer Yagi has a much wider bandwidth that covers the whole 60GHz band. The single antenna only requires an area of 8.24mm×2.375mm at

such thickness, while the LTSA needs 11.45mm×5.65mm. Furthermore, the Yagi does not require a center cut for element isolation which greatly reduced the complexity and the total cost of the fabrication. Also, most of the planar Yagi antenna is dielectric-based which limits the use of metal. This not only increases the efficiency, but also makes the antenna lighter for the portable device.

4.5 LTCC-based Antenna

As has been pointed out earlier, LTCC material has a relatively higher dielectric constant with the potential of making a more compact single-antenna or beam forming system. This is a major advantage for integrating the antenna into hand-held devices for high-speed communication system in mm-wave range.

Two LTCC-based antenna examples will be provided with different dimensions shown in Figure 56. Antenna I has a dimension of $l \times w \times h$=8mm×7mm×0.35m and antenna II of $l \times w \times h$=7mm×4mm×0.35mm. Note that both LTCC substrates share the same thickness with different cross-section areas and the dielectric constant is 7.5. This again proves the design flexibility of rectangular DRA that multiple dimensions can result in the same resonant frequency. The feeding dipole length is slightly different for the upper and lower arm due to the asymmetric effective permittivity above and below the feed. The first antenna still adopts directors like a Yagi structure, while the second one is without director and functions as a DRA. Based on the knowledge on this topic so far, the performance of these two antennas can be

properly understood. Antenna II is wide enough with TE_{31l}^{y} modes excited. Thus the end-fire gain will suffer. However, antenna I has no disturbance of the transverse mode resulting in a better overall performance.

(a)

(b)

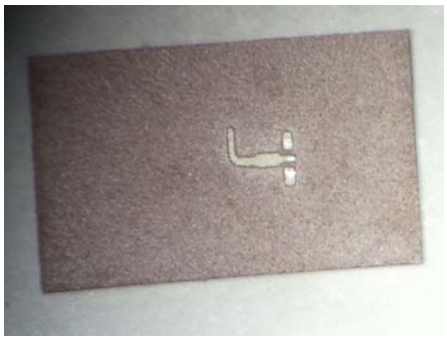

Figure 56 (a) Antenna I with dimension of $l \times w \times h$=8mm×7mm×0.35mm (b) antenna II with dimension of $l \times w \times h$=7mm×4mm×0.35mm

The simulated and measured data of these two antennas are shown respectively in Figure 57 and 58. It turns out they all provide an excellent wideband matching. Antenna I is able to maintain a gain of over 6dB with a peak of 8.2dB below 60GHz. However, the gain drops to 4dB as soon as it enters the higher half band which is not predicted by the simulation. This data mismatch and the slight resonant frequency shift of antenna II may due to the fabrication error since the antenna performance is very sensitive for such a small dimension especially over the whole band. On the other hand, antenna II achieves an average of 9dB measured end-fire gain

over the entire 60GHz band. This agrees with what has been expected and the conclusion of using narrower DR to achieve more stable performance over the band. Again the measured 9dB gain is mainly due to the dielectric resonant effect without the assistance of any directors.

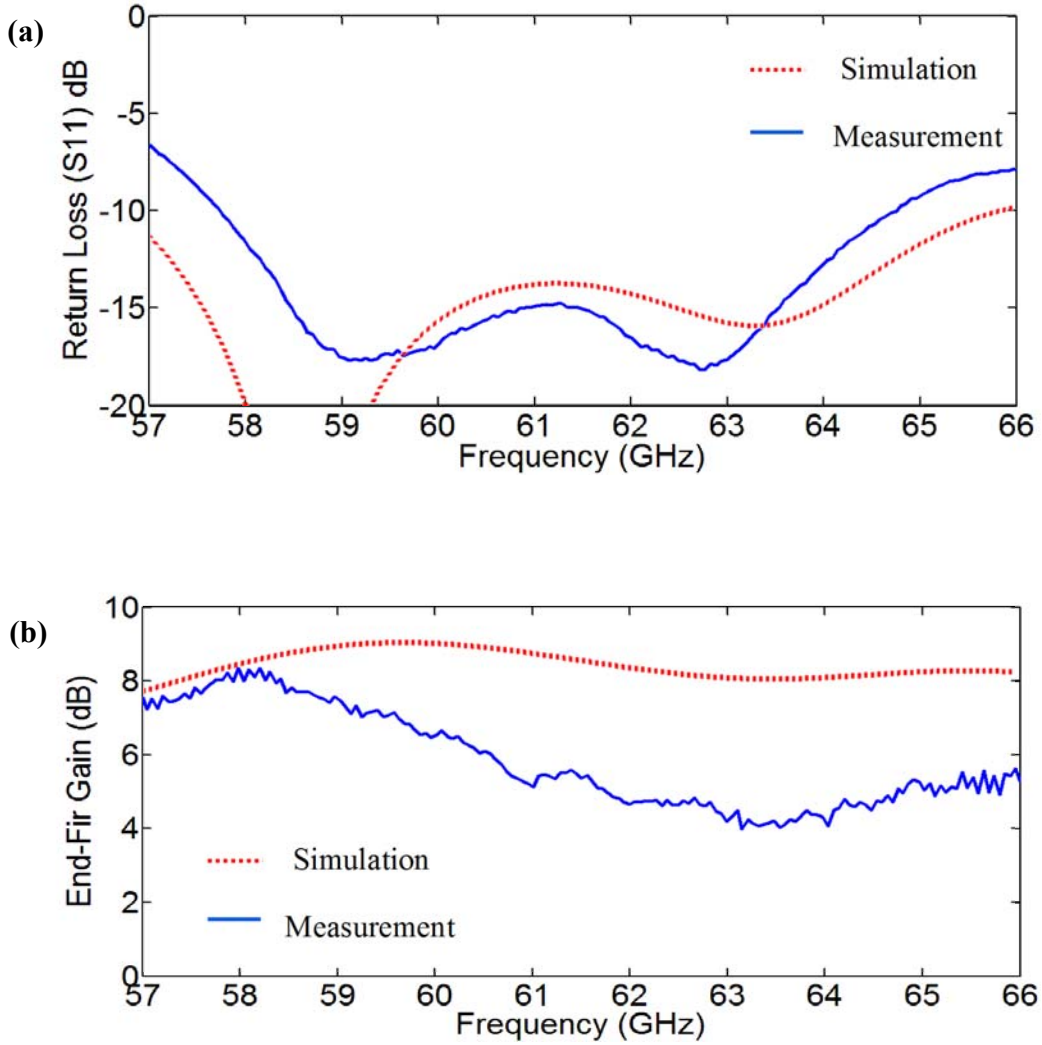

Figure 57 Simulated and measured (a) return loss (b) gain over the band of antenna I

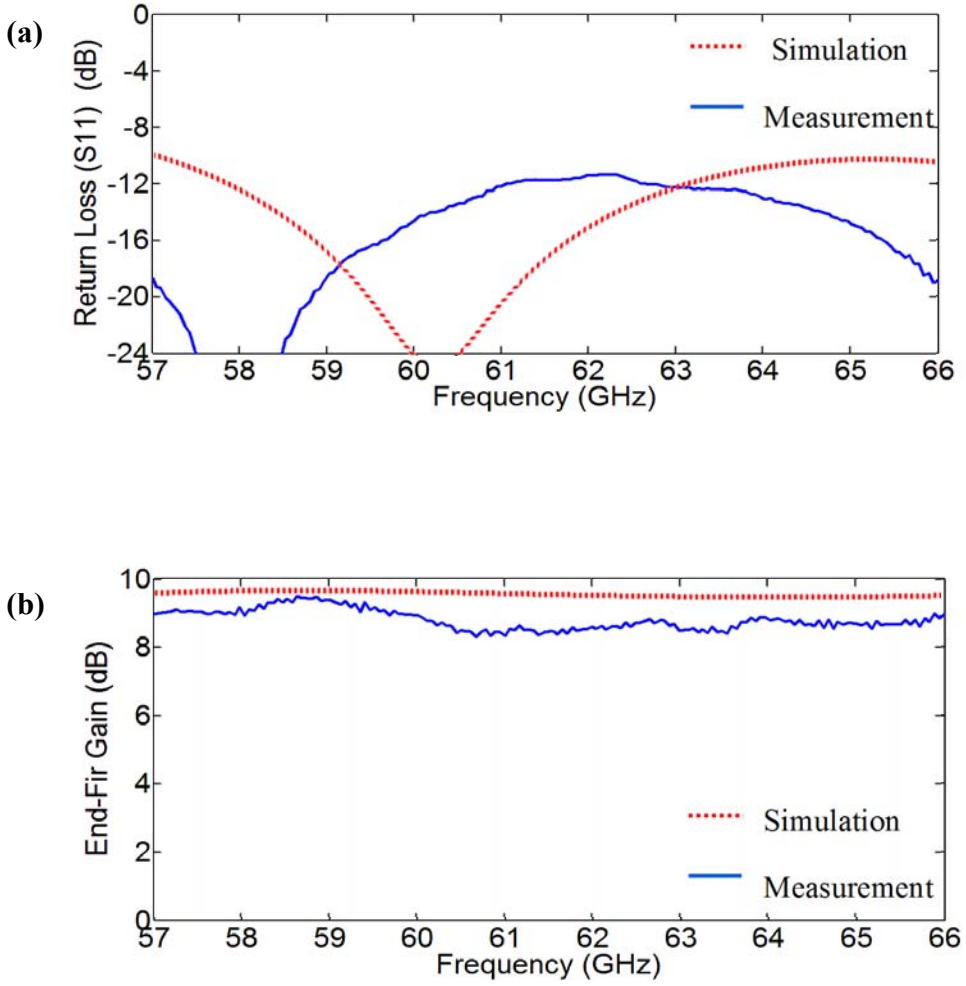

Figure 58 Simulated and measured (a) return loss (b) gain over the band of antenna II

So far, several single-antenna systems are designed and tested which show promising results in achieving high-gain end-fire radiation covering the 60GHz band. However, there are still many challenges ahead. For the concern of mechanical strength and minimum required

routing layers, the substrate cannot be very thin. Even the LTCC case above using 0.35mm is considered not thick enough. Thus certain compromise needs to be made. A complete antenna system should contain at least two antennas (transceiver and receiver). If two antennas are placed on the same board, the feeding dipole cannot be center-placed transversely. Furthermore, other IC chips need to be integrated with the antenna board which leads to inevitable EMI issues. A proper system integration scheme needs to be carefully chosen. Each technology has certain design rules one have to obey. Certain methods may be good solutions to some problems. However, they may not be cost-efficient for mass-production.

4.6 Conclusions

In this chapter, the design background, such as the main technologies and the materials used presents were first reviewed. Measurement setup is introduced for the 60GHz antenna test. Then several single antenna examples based on different materials were designed and simulated. Some of the antennas are fabricated and tested to prove the validity of the conclusions made previously. Another very popular structure of linear tapered slot antenna was designed and its performance was compared with the antennas proposed, the advantages of which in mm-wave range is very obvious.

5. ANTENNA SYSTEM DESIGN

5.1 Introduction of System Integration Methods

In chapter 4, several single antenna modules have been designed proving that the DRA with a proper feed is a good candidate for high-gain end-fire point-to-point wireless systems. After all, antenna is one part of the communication system and needs to be integrated with the RF front circuit. Thus a system-level design considerations needs to be addressed carefully.

Two ideas have been developed over the years for system integration: System-on-Chip (SoC) and System-in-Package (SiP). A SoC is a highly integrated, single-chip design using third party and internal intellectual property. It can contain analogue, digital or mixed-signal circuits [117]. A key advantage of SoC technology is the ability to reduce the performance limitations that result from the system board delays of going on- and off-chip. This also increases reliability for the system and lowers overall system costs, because of fewer discrete components on the board. In addition, where board real estate and low power are top priorities, such as in mobile devices, SoCs are often the only solutions that are cost-effective. When it comes to antenna integration, the common term becomes AoC. The AoC solution features the integration of antennas or arrays together with other front-end circuits on the same chip in mainstream silicon technologies such as SiGe or CMOS [118]. The largest die size of the current 60GHz radio in silicon is about 6.4 mm^2. It is believed that high-directivity AoC is not practical at 60GHz with the expected die size. Thus the biggest challenge for the AoC solution is its low efficiency due to large ohmic losses and surface waves of the substrate. As a matter of fact, low resistivity is the

dominant factor to poor AoC efficiency. Thus several techniques have been developed to improve the efficiency, including substrate thinning, proton implantation, micromachining and superstrate focusing. Some of these exotic techniques have undoubtedly increased the cost of the total solution. However, the idea of truly integrate the whole system on a single chip is still very appealing to encourage engineers to pursue new methods to overcome the shortcomings of SoC. On the other hand, A SiP is characterized by any combination of more than one active electronic component (package or die) of different functionality, plus optional passive devices and other devices such as MEMS or optical components. An example SiP can contain several chips—such as a specialized processor, DRAM, flash memory—combined with passive components—resistors and capacitors—all mounted on the same substrate. This means that a complete functional unit can be built in a multi-chip package, so that few external components need to be added to make it work. This is particularly valuable in space constrained environments like MP3 players and mobile phones as it reduces the complexity of the printed circuit board and overall design. AiP solution refers to the antenna integration technique which combines an antenna (or antennas) with a highly integrated radio die into a standard surface mounted chip-scale package device, which is a recent innovative and important development in the miniaturization of wireless systems. There are two major configurations depicted in Figure 59. In the first scenario, the radio die is placed horizontally by the side of the antenna. The antenna is most likely backed by air cavity or holes for broadside radiation and the interconnection between the radio die and the antenna is usually wire-bond. The second choice is to integrate these two parts in a vertically-stacking configuration. Flip-chip technique is adopted for the interconnection. Interconnection

using the electromagnetic- or capacitive-coupling techniques directly between the radio die and the antenna for both configurations is also possible at even higher frequencies. Materials such as silicon, Teflon, ceramics, polymers are all possible candidates in realizing the AiP.

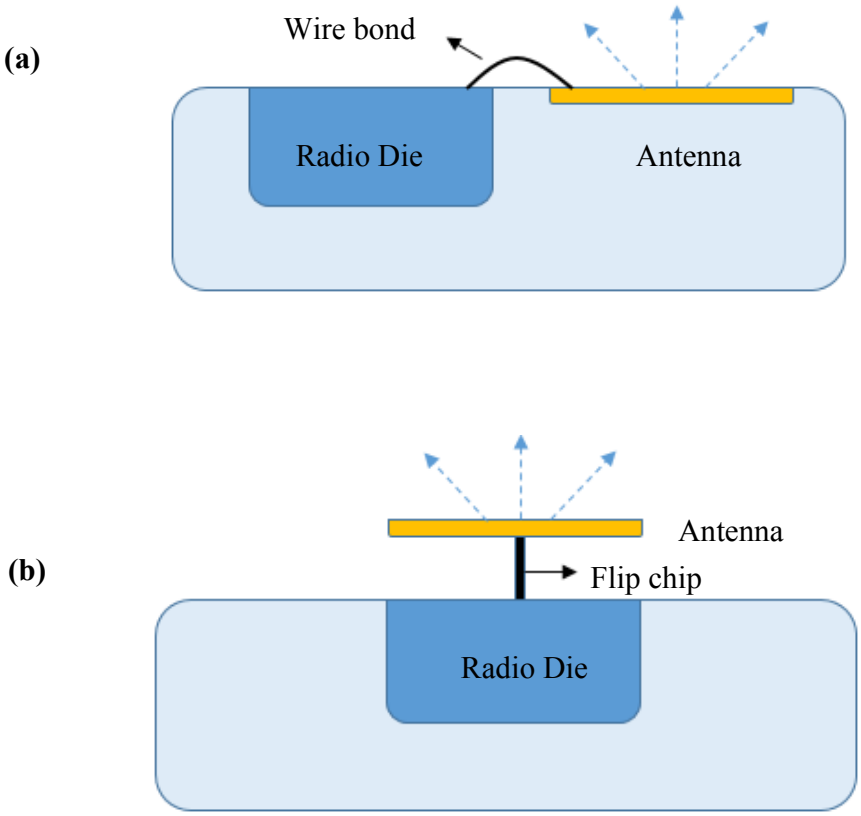

Figure 59 Two configurations of AiP (a) horizontal (b) vertical

Interconnections should provide good return loss and low insertion loss over the frequency of interest. As mentioned, wire-bond and flip chip are the two most popular interconnections for the integration. Fundamentally, they are both inductive at high frequency. Wire bond is simply a short metal stub connecting the contacts on the radio die and antenna in which the chip is mounted upright. This technique is the most widely used one due to its robust and inexpensive. In addition, it has the advantage of being tolerant on chip thermal expansion, an important requirement for many applications. However it appears to be a real challenge at mm-wave range for its vast influence on the antenna performance due to the inductive effect which needs to be tuned out by additional circuits. On the other hand, flip chip connects the antenna to external circuitry with solder bumps that have been deposited onto the chip pads as shown in Figure 60. In order to mount the chip to external circuitry, it is flipped over so that its top side faces down, and aligned so that its pads align with matching pads on the external circuit, and then the solder is flowed to complete the interconnect. The resulting completed flip chip assembly is much smaller than a traditional carrier-based system. Since the bump height is kept smaller than the length of the bond wire and the bump diameter is thicker than that of the bond wire, the inductive effect is mitigated resulting in higher-speed signals. They also conduct heat better. Despite of all these intriguing features, flip chips have several disadvantages. The lack of a carrier means they are not suitable for easy replacement, or manual installation. They also require very flat surfaces to mount to, which is not always easy to arrange, or sometimes difficult to maintain as the boards heat and cool. Also, the short connections are very stiff, so the thermal expansion of the chip must be matched to the supporting board or the connections can crack.

Considering for 60GHz band in which high speed is a priority, a high-gain antenna is in demand which has probably ruled out the option of AOC. Thus all the examples in this chapter will adopt the idea of AiP and the flip-chip technology.

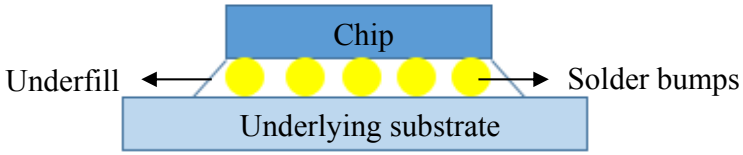

Figure 60 Schematic of flip chip

5.2 1×1 T/R Antenna System Design

Usually a complete antenna system includes at least two antennas, one for transmitting and one for receiving. Based on the single DRA model, the 1×1 T/R antenna system can be further constructed. Figure 61 indicates the earliest version of the system. Initially two antennas are placed side by side with certain distance between them on the board. The antenna here is based on the LTCC substrate ($\varepsilon_r = 7.5$) with dimension of $l \times w \times h$=7mm×4mm×0.35mm. The blue frame in the figure indicating the place reserved for the flip chip. Figure 62 shows the simulated and measured return loss and over-the-band gain of this structure. As one can see, the 7GHz of the 60GHz band is partially covered by this antenna from 58.5 to 64GHz and two data matches quite well. However, the simulated gain is higher than the measured one especially at

the lower half band. This inconsistency is quite similar as the single LTCC antenna I in chapter 4. Simulation at the lower band shows a hint of beam tilt which may not be a problem if the fabricated antenna is exactly the same as the simulated model. However, once fabrication error is introduced, it magnifies this effect and the gain performance is greatly influenced. Another explanation can be seen in Figure 63. Although the gain at the lower band is not precisely predicted, the isolation between two antennas is much worse than the one at the higher frequency indicating a stronger coupling that could affect both antennas. In fact, with the increasing thickness of the LTCC-based antenna system, the beam-tilting and mutual coupling effect are more obvious that proper measure needs be taken to ensure the antenna performance.

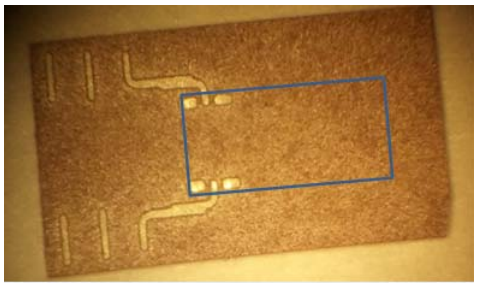

Figure 61 Fabricated T/R antennas integrated on LTCC board

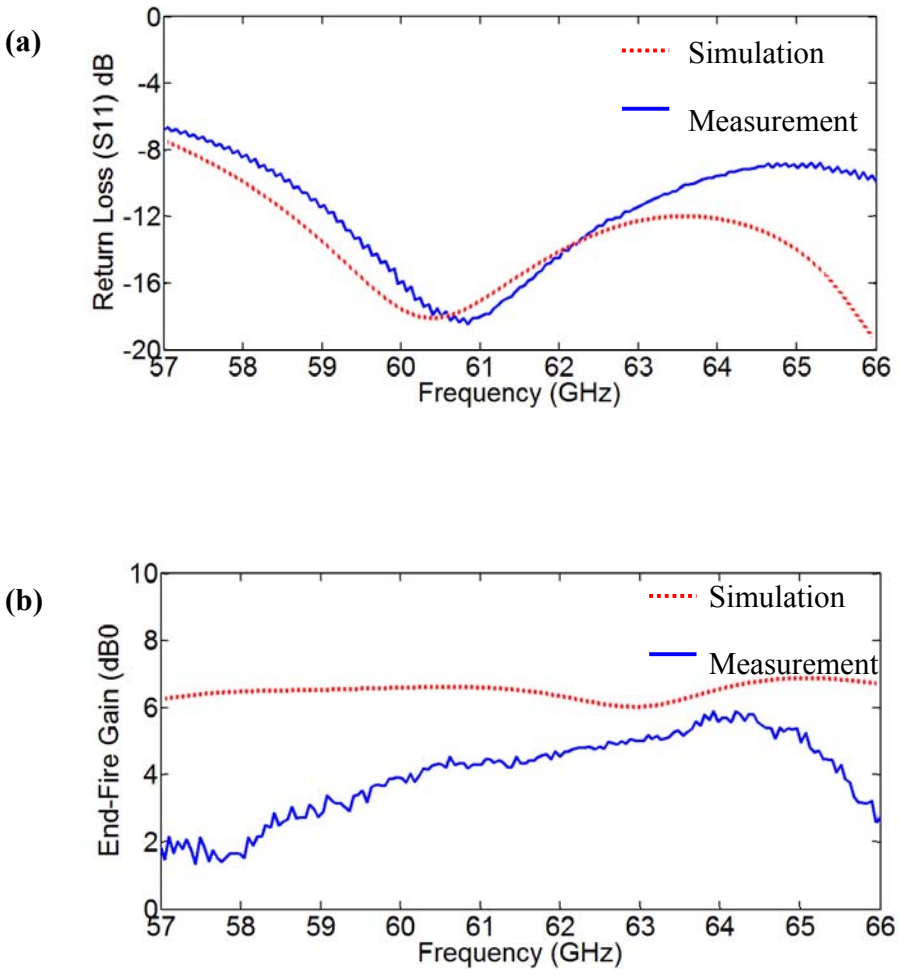

Figure 62 Simulated and measured (a) return loss (b) gain over the band

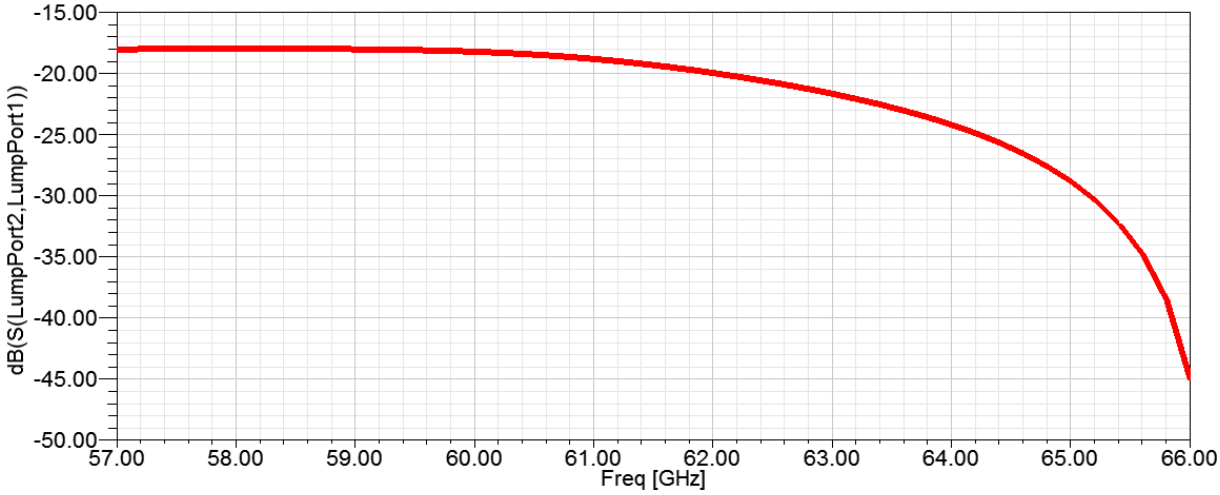

Figure 63 Simulated S21 of the T/R antennas

Although the EMI is still a big issue in the LTCC-based antenna, if such antennas are realized by Rogers board, the mutual coupling will be suppressed significantly. As a result, a 4-layer AiP using both Rogers RO 4450 (ε_r=3.36) and RO 4350 (ε_r=3.66) with the latter is sandwiched in the middle of two thin layers of 4450. The thickness is 0.376mm which is similar as the last case of LTCC. The total dimension accounts for antenna part is $l \times w$ =8.47mm × 9mm. The whole system-in-package structure using flip chip and its layer configuration are described in Figure 64. The top chip is flipped on the Rogers board via BGA, one of which originates from the PA output and serves as the signal line and pinned down to the impedance transformer. The other two contact the top ground which connects to the bottom ground through vias. The antenna still adopts the Yagi structure and its simulation results are

summarized in Figure 65. Notice that an end-fire gain of 8.86 dB at 61GHz and an ultra-wide bandwidth for impedance matching are achieved. Although the T/R antennas are placed quite close, the coupling between them is not severe enough to degrade the antenna performance due to its low permittivity and relatively small thickness.

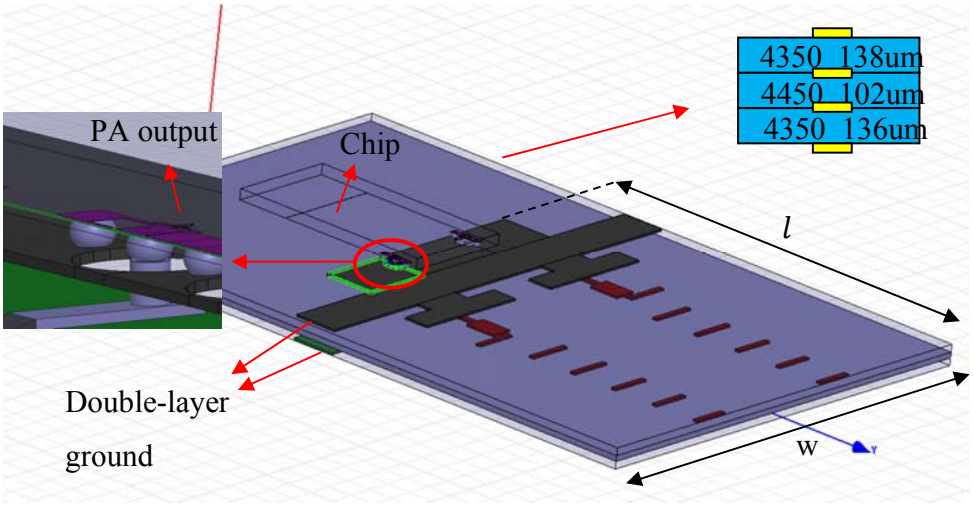

Figure 64 Layout of 4-layer AiP using multiple Rogers boards

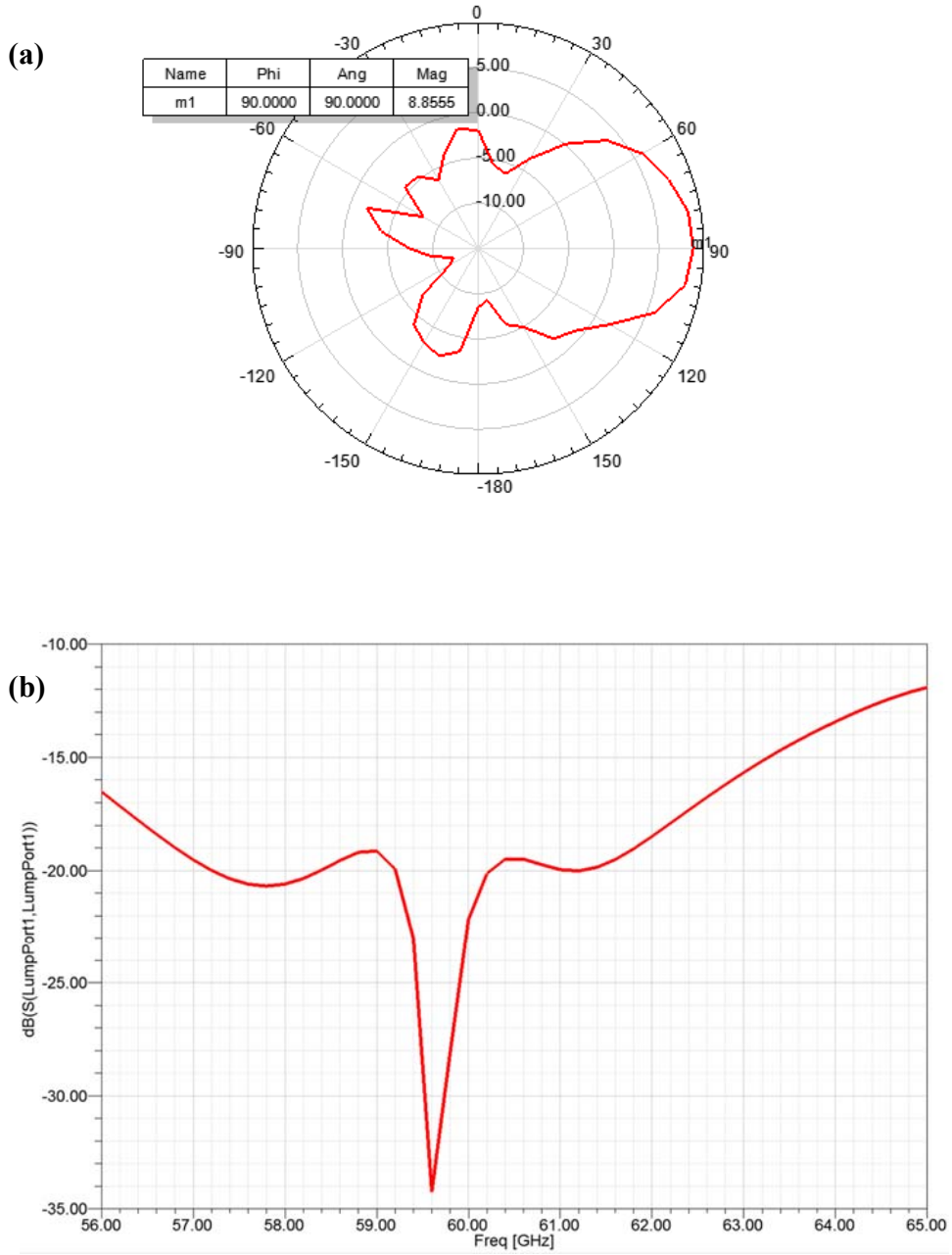

Figure 65 Simulated (a) radiation pattern at 61GHz (b) return loss at 61GHz

In hand-held mobile devices, mechanical strength is one of the key features in evaluating the system stability. In order to improve this while still maintain a certain level of isolation between antennas, the most straightforward way is to add on the substrate thickness. Single-antenna examples in chapter 4 already implies the disadvantage of thick substrate. Thus, a compromising choice is to use a material with relatively low dielectric constant, such as RO4000 series laminate to compensate for the thicker substrate. Hence a 6-layer Rogers-based AiP is designed with a total thickness of 0.605mm, the layout and layer configuration of which is shown in Figure 66 with a dimension of $l \times w$ =8.47mm×9mm same as the 4-layer case. It is worth mentioning that for different thickness, the dielectric constant of one material is not necessarily constant. For instant, here the dielectric constant of RO 4450 and 4350 are 3.3 and 3.36 which are in fact lower than the ones in 4-layer case. In addition, compared with the 4-layer one, certain changes need to be made. The tilting effect of the beam cannot be ignored any more due to the thicker substrate. That is why a center-cut gap between T/R antennas are used. The gap is greater than 1mm due to the fabrication limitation. Since we need to leave as much space as possible for other routing layers, the tuning stripline needs to have two bends to use the whole package space more efficiently. Tilted or rounded straight line is recommended to decrease the unwanted spurious radiation. However, it introduced considerable radiation at side and back direction which decrease the end-fire gain. Therefore vias at back and along the tuning transmission line are needed to suppress the unwanted radiation. One additional director is adopted for gain boosting. The simulated results are shown in Figure 67 in which end-fire gain is

about 9.13dB at 60GHz and maximum is 9.44dB at a tilted angle which is negligible. Again the wideband tuning is achieved around 60GHz.

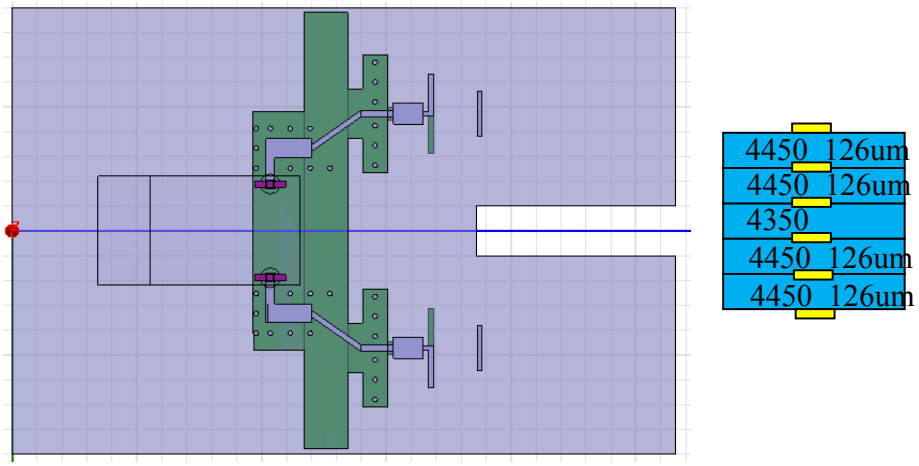

Figure 66 Layout of 6-layer AiP using multiple Rogers boards

(a)

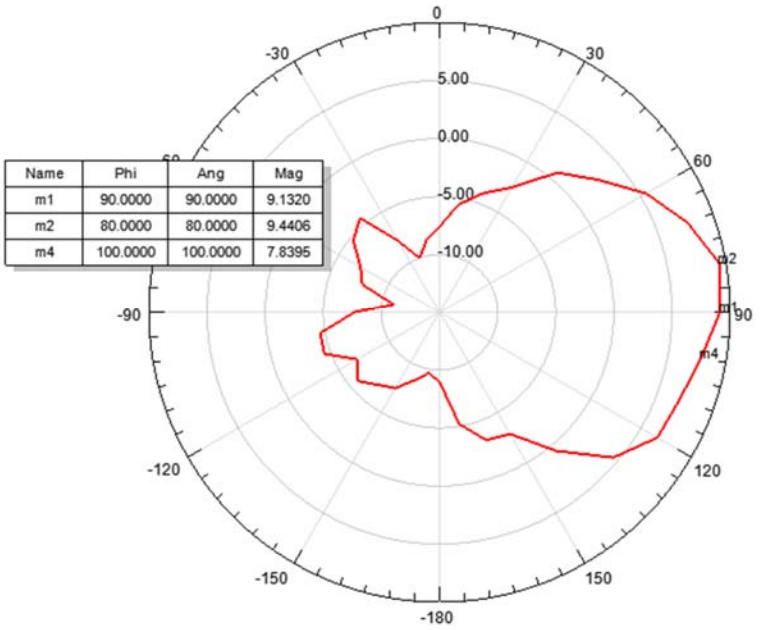

Name	Phi	Ang	Mag
m1	90.0000	90.0000	9.1320
m2	80.0000	80.0000	9.4406
m4	100.0000	100.0000	7.8395

(b)

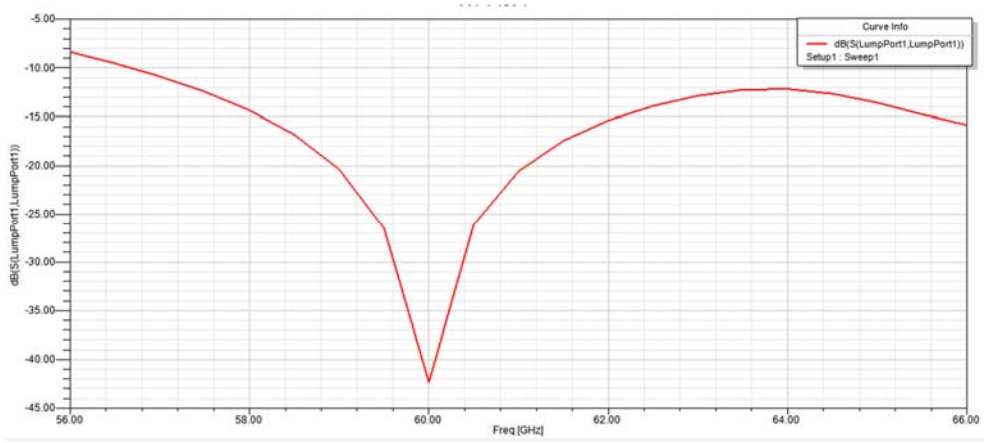

Figure 67 Simulated (a) radiation pattern (b) return loss at 60GHz

With a minimum number of layers is required, certain mechanical strength standard needs to be met, and a compact system is desired. An antenna designed on a relatively thick substrate like the last example can also be realized by LTCC. As a matter of fact, since the minimum thickness of LTCC technology is smaller than the Rogers board, more layers are available for the system integration for a fixed total thickness. Here 16–layer LTCC-based AiP systems are designed with two configurations. Antenna I has only signal layer and one ground layer as in Figure 68(a) while antenna II has two ground layers as in (b). Figure 69 shows the fabricated antenna I. The total dimension is $8.24\text{mm} \times 5.5\text{mm}$ with only $4.2\text{mm} \times 5.5\text{mm}$ accounts for antenna. Again, a center cut is applied in the center of the LTCC board. The total thickness of the LTCC including metal layers is 0.765mm sufficient for mechanical concern. To ensure accuracy, BGA and the contact pad are modeled in detail. The final measurement should also include bumps and chip interconnects and pads for consistency with the simulation.

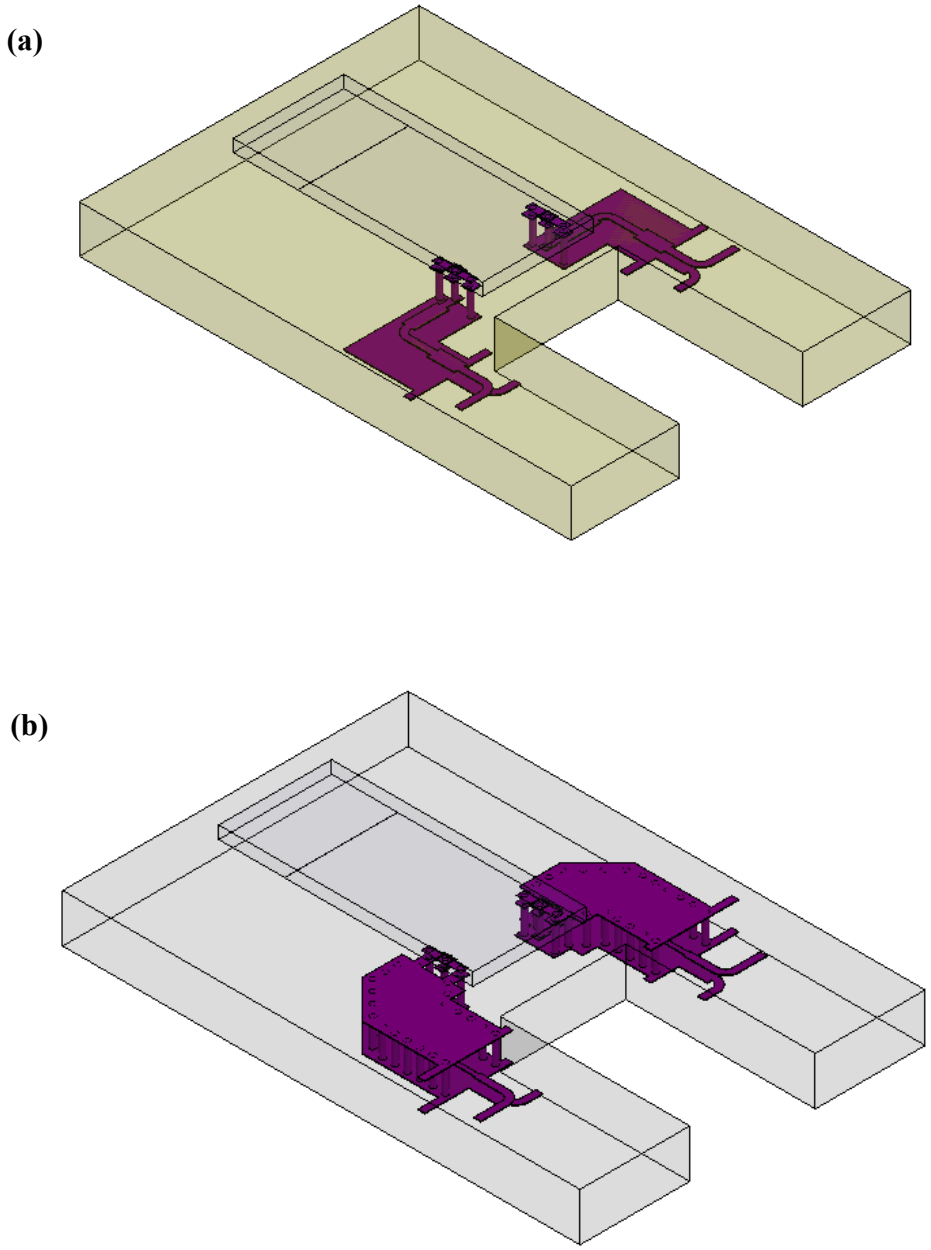

Figure 68 Configuration of (a) antenna I (b) antenna II

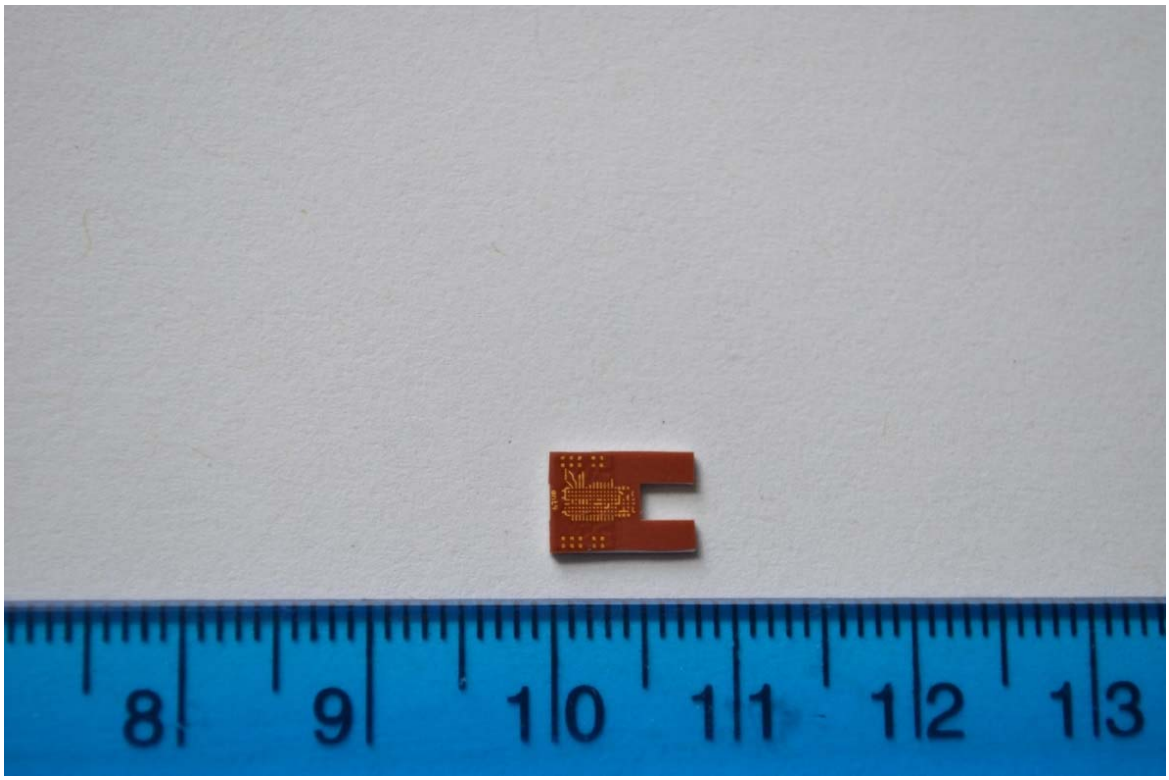

Figure 69 Layout of 16-layer AiP using LTCC

The simulated and measured performance of these two antenna systems are shown in Figure 70 and Figure 71, respectively. The measured resonant frequency agrees with the simulated one and the impedance is matched over a wide bandwidth. As one can expected, the gain performance is degraded for such thick substrate, especially when frequency is higher than 62GHz. The HFSS simulation well predicted the end-fire gain of antenna I while it did not show the fast gain drop for antenna II.

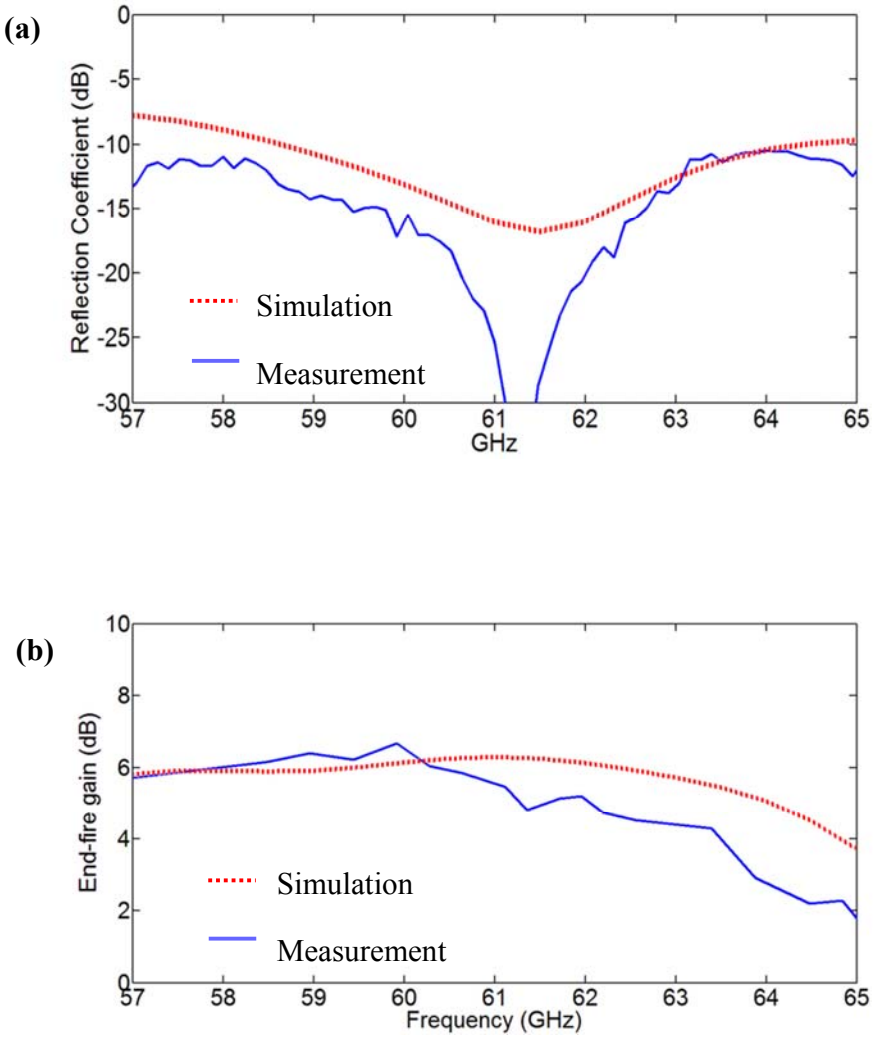

Figure 70 Measured (a) return loss (b) gain over the band of antenna I

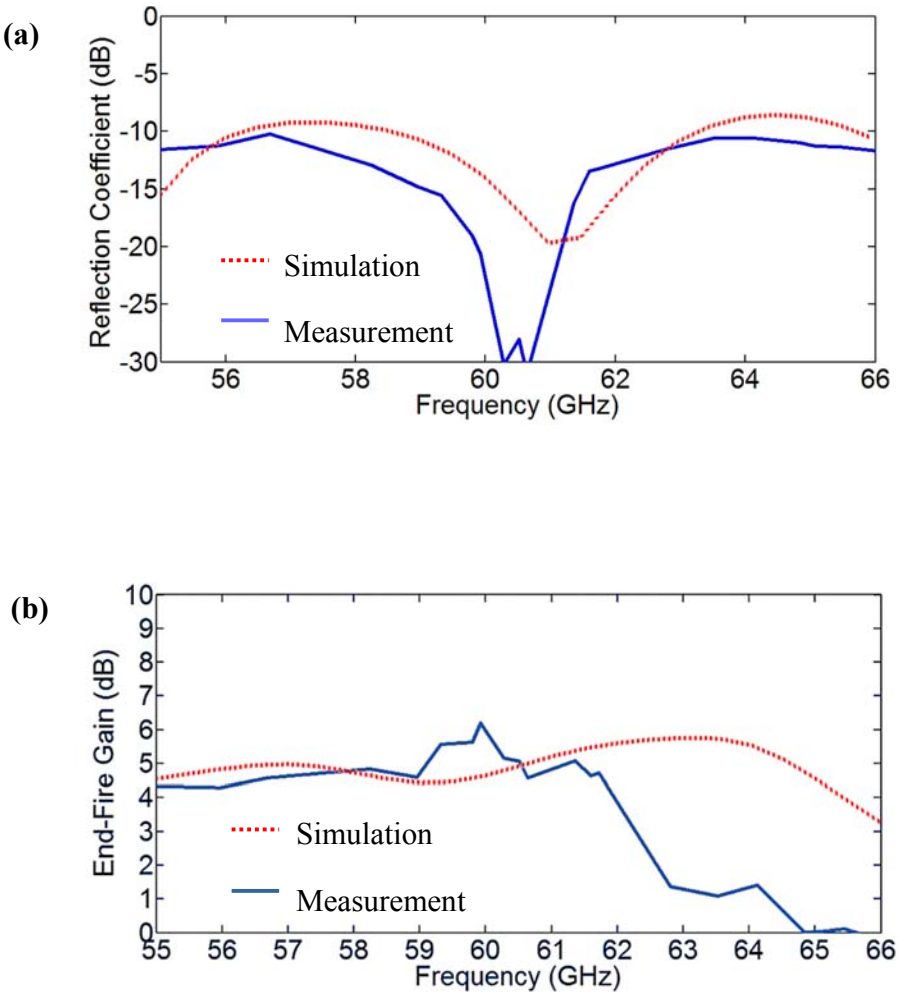

(b)

Figure 71 Measured (a) return loss (b) gain over the band of antenna II

As a matter of fact, this raises another problem resulted from mm-wave compact design. In mm-wave, miniaturization sometimes is not an advantage any more. The ultra-small size

makes the antenna more sensitive to the fabrication error. Furthermore, with the introduction of air cavity or gap in the substrate, it further challenges product's mechanical strength, let alone the increased possibility of chipping or bending which makes the antenna system more vulnerable. Reshaping the substrate also adds up to the total cost of the process. Thus, it is crucial to choose the right technique for the right application.

5.3 2×2 T/R Antenna System Design

Practically speaking, within a limited area, the end-fire gain which a single antenna can provide is far from sufficiency for mm-wave high-speed point-to-point communication. Thus, the ultimate solution is to use beamforming. Based on knowledge of all the single antenna boards and 1×1 T/R antenna system design, a high-gain linear or planer array system can be designed accordingly. Here, two 2×2 T/R antenna systems with different characteristics are proposed based on the RO4350 material with dielectric constant of 3.36. The layout of system I are shown in Figure 72 with dimension of 11mm×8.4mm×0.376mm. Beamforming E-plane pattern is shown in Figure 73. The phase of the antenna on the inner side is fixed at 0° while the phase of the outer one scans from -180° to 180° with each phase representing a curve in the figure. Each set of transmitting and receiving antenna can achieve a higher end-fire gain of 11.6dB when the two elements are in phase. Half-power beam widths of E plane and H plane are 38 and 52 degree. Beamforming range is $\pm 36^{\circ}$ away from end-fire direction.

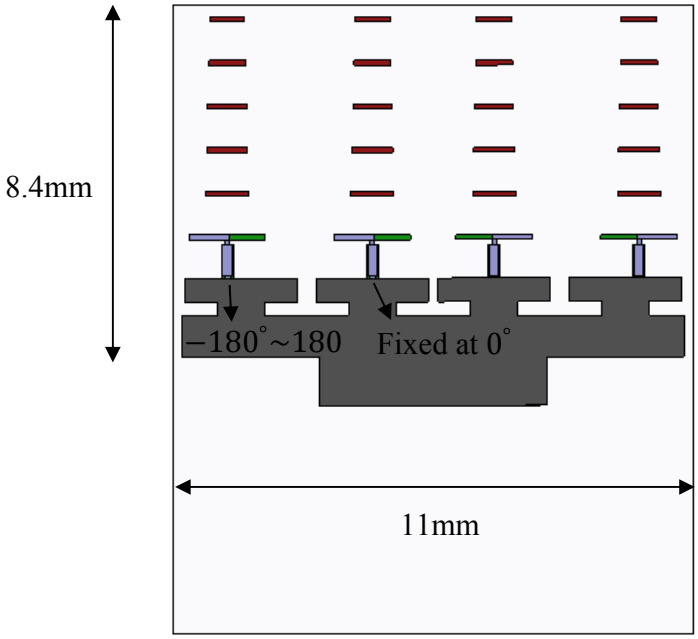

Figure 72 2×2 antenna system with higher gain

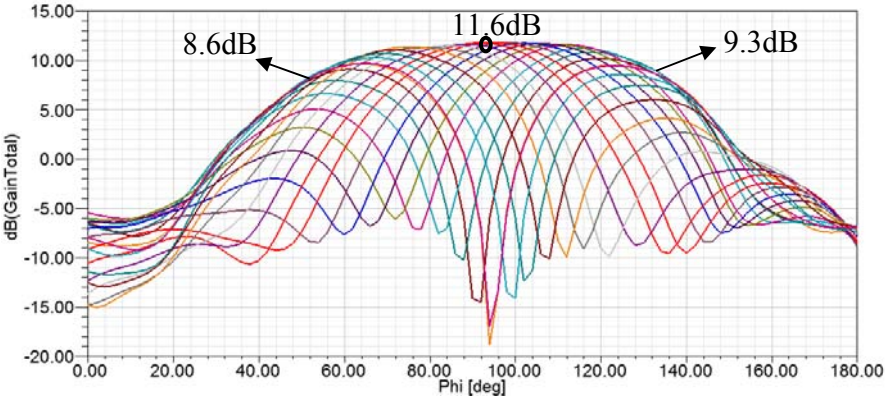

Figure 73 Beamforming E-plane pattern with higher gain

The layout of system II are shown in Figure 74 with dimension of 11mm×3.7mm×0.376mm with beamforming E-plane pattern shown in Figure 75. Each set of transmitting and receiving antenna gives an end-fire gain of 7.4dB with half-power beam widths of 40 and 176 degree on E plane and H plane. However, it provides a wider beamforming range of $\pm 55^{\circ}$ away from end-fire direction. From the layout of the antennas, it is quite clear that system I is made of element with higher gain, thus giving a higher overall gain and narrow scanning range and vice versa for system II. It is worth mentioning that the substrate material is relatively thin with lower dielectric constant. Hence the coupling between the antenna elements are not very strong. For LTCC case or the same case with thicker substrate, measures need to be taken such as cutting gaps between the elements to ensure certain isolation level. However, this will increase the complexity and total cost of the fabrication.

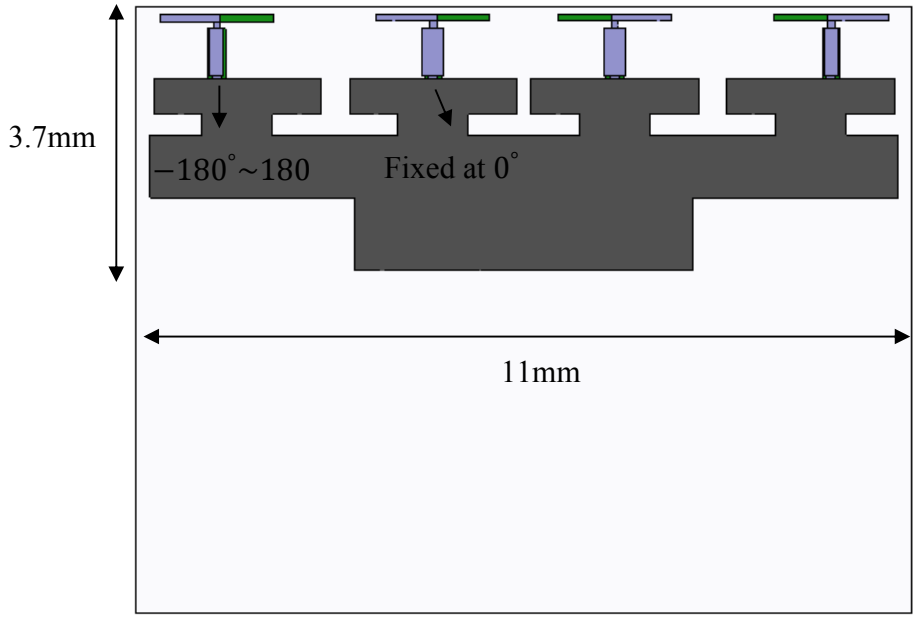

Figure 74 2×2 antenna system with wider range

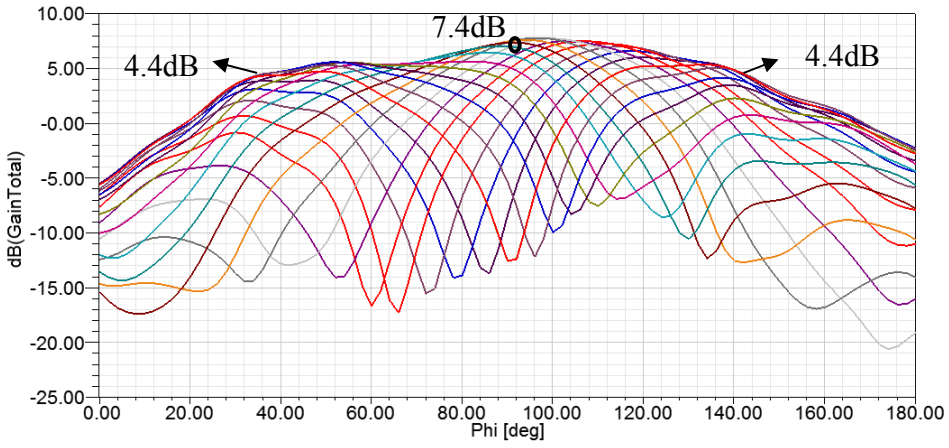

Figure 75 Beamforming E-plane pattern with wider range

5.4 Conclusions

In this chapter, the knowledge of single DRA was applied onto the mm-wave antenna system design. The idea of Antenna-in-Package was introduced as well as the flip-chip technology. Several 1×1 T/R antenna systems were successfully designed and fabricated. The measured results agreed with the simulated ones. Finally, the method was extended to the linear array design and two 2×2 antenna systems were presented with different operation modes suitable for different end-fire applications.

6. CONCLUSION AND FUTURE WORK

The demand of high-speed high-quality communication is very high within these several years. There is an urgent need to explore the possibilities in mm-wave range, such as the 7 GHz unlicensed spectrum at 60 GHz. This work was intended to provide design considerations of low-profile end-fire rectangular DRA in 60GHz band. Typically, the radiation pattern of a DRA is determined by the modes. In order to determine the modes excited in a DRA, DWM method was chosen as a first-order solution. Eigenmode simulation was carried out using HFSS to validate its accuracy on an isolated DRA. Then a more practical model with planar excitation was presented and this method was applied with certain reasonable modification. Since point-to-point applications require an antenna which can provide high gain and the operation of hand-held devices prefer an antenna with an end-fire pattern, several methods concerning these issues are introduced. The method of using higher-order modes is more suitable in this case and the characteristics of end-fire gain was thoroughly studied with respect to DRAs with different dimensions using LTCC material as the substrate. It was proven that the antenna with relatively low dielectric constant (<10) and thin substrate share certain properties of both the surface-wave antenna and the DRA. In fact, the knowledge of the surface-wave antenna was successfully applied to the antenna of interest and the gain curve provided by the HFSS simulation matched our expectations. As the substrate got thicker, the cavity effect caused ripple on the gain curve which slightly changed the location where the maximum gain occurred. Also, the transverse modes need to be avoided. Based on these, a design curve was presented and examples antenna was designed to prove its validity. The effect of additional directors and beam tilt due to an off-

centered feed were properly discussed as well. Several single antennas and 1×1 T/R systems were designed and fabricated using different materials. Simulated and measured results were compared and agreed well. Finally, the method was extended to the linear array design and two 2×2 antenna systems were presented with different operation modes suitable for different end-fire applications.

During the study, there are certain problems worth additional effort. For example, the partial ground effect, especially when the DRA is thick, was not properly modeled in this work. In this case, the surface wave is stronger that the ground is not as effective as a reflector. Thus the assumption of a perfect conductor is not valid any more. Also, the connection between the flip chip and the antenna board needs a better modeling as well since this not only affects the performance of the antenna, but also the one of the power amplifier. However, the biggest challenge in the future mm-wave antenna design lies in the antenna array which is the ultimate way to achieve high gain. This includes the topics of stripline routing, beamforming and isolation which become more critical in mm-wave range.

CITED LITERATURE

[1] E. H. Lim and K. W. Leung, “Use of the dielectric resonator antenna as a filter element,” IEEE Trans. Antennas Propag., vol. 56, no. 1, pp. 5–10, 2008.

[2] Guillon, Pierre, Y. Garault, and J. Farenc. "Dielectric resonator dual modes filter." Electronics Letters 16, no. 17 (1980): 646-647.

[3] Oh, Soon-Soo, Seung-Ho Chang, Dong-Chul Lim, and Gyoo Chul An. "FDTD modeling of cylindrical dielectric resonator filters." In TENCON 99. Proceedings of the IEEE Region 10 Conference, vol. 1, pp. 15-18. IEEE, 1999.

[4] Kajfez, Darko, and Pierre Guillon. "Dielectric resonators." Norwood, MA, Artech House, Inc., 1986, 547 p. No individual items are abstracted in this volume. 1 (1986).

[5] Mongia, Rajesh K., and Prakash Bhartia. "Dielectric resonator antennas—A review and general design relations for resonant frequency and bandwidth." International Journal of Microwave and Millimeter‐Wave Computer‐Aided Engineering 4, no. 3 (1994): 230-247.

[6] Petosa, Aldo, and Apisak Ittipiboon. "Dielectric resonator antennas: A historical review and the current state of the art." Antennas and Propagation Magazine, IEEE 52, no. 5 (2010): 91-116.

[7] Long, Stuart A., Mark W. McAllister, and Liang C. Shen. "The resonant cylindrical dielectric cavity antenna." IEEE Transactions on Antennas and Propagation 31 (1983): 406-412.

[8] McAllister, M. W., S. Andrew Long, and G. L. Conway. "Rectangular dielectric resonator antenna." Electronics Letters 19, no. 6 (1983): 218-219.

[9] McAllister, M. W., and S. Andrew Long. "Resonant hemispherical dielectric antenna." Electronics Letters 20, no. 16 (1984): 657-659.

[10] Junker, Gregory P., Ahmed Kishk, and Allen W. Glisson. "Input impedance of dielectric resonator antennas excited by a coaxial probe." Antennas and Propagation, IEEE Transactions on 42, no. 7 (1994): 960-966.

[11] Shum, Shiu-Ming, and Kwai-Man Luk. "FDTD analysis of probe-fed cylindrical dielectric resonator antenna." Antennas and Propagation, IEEE Transactions on 46, no. 3 (1998): 325-333.

CITED LITERATURE (continued)

[12] Luk, K. M., K. W. Leung, S. M. Shum, and K. F. Lee. "Numerical study of dielectric resonator antenna." Advances in microstrip and printed antennas(1997): 553-592

[13] Luk, Kwai Man, and Kowk Wa Leung, eds. Dielectric resonator antennas. Research Studies Press, 2003.

[14] Mongia, R. K. "Resonant frequency of cylindrical dielectric resonator placed in an MIC environment." Microwave Theory and Techniques, IEEE Transactions on 38, no. 6 (1990): 802-804.

[15] Glisson, Allen W., Darko Kajfez, and Joseph James. "Evaluation of modes in dielectric resonators using a surface integral equation formulation." IEEE transactions on microwave theory and techniques 31, no. 12 (1983): 1023-1029.

[16] Petosa, Aldo. Dielectric resonator antenna handbook. Artech House Publishers, 2007.

[17] Hady, Laila K., Darko Kajfez, and Ahmed Kishk. "Triple mode use of a single dielectric resonator." Antennas and Propagation, IEEE Transactions on 57, no. 5 (2009): 1328-1335.

[18] Liang, Xiao-Peng, and Kawthar Zaki. "Modeling of cylindrical dielectric resonators in rectangular waveguides and cavities." Microwave Theory and Techniques, IEEE Transactions on 41, no. 12 (1993): 2174-2181.

[19] Kobayashi, Yoshio, and Tomohiro Senju. "Resonant modes in shielded uniaxial-anisotropic dielectric rod resonators." Microwave Theory and Techniques, IEEE Transactions on 41, no. 12 (1993): 2198-2205.

[20] Shum, S. M., and K. M. Luk. "Analysis of aperture coupled rectangular dielectric resonator antenna." Electronics Letters 30, no. 21 (1994): 1726-1727.

[21] K.P. Esselle, "Circular Polarized Dielectric Resonator Antennas: Analysis of Near and Far Fields using the FDTD Method," URSI Radio Science Meeting, June 1995, Newport Beach, CA, pp. 28.

[22] Junker, G. P., Ahmed Kishk, A. W. Glisson, and Darko Kajfez. "Effect of fabrication imperfections for ground-plane-backed dielectric-resonator antennas." Antennas and Propagation Magazine, IEEE 37, no. 1 (1995): 40-47.

[23] Van Bladel, Jean. "On the resonances of a dielectric resonator of very high permittivity." IEEE Transactions on Microwave Theory Techniques 23 (1975): 199-208.

CITED LITERATURE (continued)

[24] Van Bladel, Jeant. "The excitation of dielectric resonators of very high permittivity." IEEE Transactions on Microwave Theory Techniques 23 (1975): 208-217.

[25] Mongia, Rajesh Kumar, and Apisak Ittipiboon. "Theoretical and experimental investigations on rectangular dielectric resonator antennas." Antennas and Propagation, IEEE Transactions on 45, no. 9 (1997): 1348-1356.

[26] Birand, M. T., and R. V. Gelsthorpe. "Experimental millimetric array using dielectric radiators fed by means of dielectric waveguide." Electronics Letters17, no. 18 (1981): 633-635.

[27] Petosa, A., R. K. Mongia, A. Ittipiboon, and J. S. Wight. "Investigation of various feed structures for linear arrays of dielectric resonator antennas." InAntennas and Propagation Society International Symposium, 1995. AP-S. Digest, vol. 4, pp. 1982-1985. IEEE, 1995.

[28] Lin, Song. "Dielectric Resonator Antennas fed by Image Guide Lines." In 2006 IEEE Antennas and Propagation Society International Symposium, pp. 2205-2208. 2006.

[29] Chua, Chee-Parng, P. A. Pavlovich, and Mook-Seng Leong. "A compact and wideband rectangular dielectric resonator antenna." In 8th Electron. Packag. Technol. Conf, pp. 313-316. 2005.

[30] Gao, Yuan, C-P. Chua, Alexandre P. Popov, and B-L. Ooi. "Integrated wideband rectangular dielectric resonator antenna for WLAN." (2005).

[31] Bijumon, P. V., Sreedevi Menon, M. N. Suma, B. Lethakumari, M. T. Sebastian, and P. Mohanan. "T-strip-fed high-permittivity rectangular dielectric resonator antenna for broadband applications." Microwave and optical technology letters 47, no. 3 (2005): 226-228.

[32] Bit-Babik, G., C. Di Nallo, and A. Faraone. "Multimode dielectric resonator antenna of very high permittivity." In Antennas and Propagation Society International Symposium, 2004. IEEE, vol. 2, pp. 1383-1386. IEEE, 2004.

[33] Gao, Yuan, Ban-Leong Ooi, Wei-Bin Ewe, and Alexandre P. Popov. "A compact wideband hybrid dielectric resonator antenna." Microwave and Wireless Components Letters, IEEE 16, no. 4 (2006): 227-229.

[34] Yohannan, Jaimon, Anil Lonappan, G. Bindu, T. Vinu, V. Hamsakkutty, and K. T. Mathew. "Microstripline fed circular sector dielectric resonator antenna." InAntennas and

CITED LITERATURE (continued)

Propagation Society International Symposium, 2005 IEEE, vol. 2, pp. 192-195. IEEE, 2005.

[35] Yohannan, Jaimon, Anil Lonappan, G. Bindu, T. Vinu, V. Hamsakkutty, and K. T. Mathew. "Microstripline fed circular sector dielectric resonator antenna." InAntennas and Propagation Society International Symposium, 2005 IEEE, vol. 2, pp. 192-195. IEEE, 2005.

[36] Hamsakutty, V., Jaimon Yohannan, and K. T. Mathew. "A wideband conical beam cylindrical dielectric resonator antenna." Antennas and Wireless Propagation Letters, IEEE 6 (2007): 15-17.

[37] Alhalabi, Ramadan, and Gabriel M. Rebeiz. "High-efficiency angled-dipole antennas for millimeter-wave phased array applications." Antennas and Propagation, IEEE Transactions on 56, no. 10 (2008): 3136-3142.

[38] Lamminen, Antti, and Jussi Säily. "Wideband millimetre wave end-fire antenna and array for wireless short-range applications." In Antennas and Propagation (EuCAP), 2010 Proceedings of the Fourth European Conference on, pp. 1-5. IEEE, 2010.

[39] Yoshida, Sigeru, Yuya Suzuki, Tuan Thanh Ta, Suguru Kameda, Noriharu Suematsu, Toshiyuki Takagi, and Kazuo Tsubouchi. "A 60-GHz band planar dipole array antenna using 3-D SiP structure in small wireless terminals for beamforming applications." Antennas and Propagation, IEEE Transactions on61, no. 7 (2013): 3502-3510.

[40] Wu, Jiangniu, Zhiqin Zhao, Zaiping Nie, and Qing-Huo Liu. "Bandwidth enhancement of a planar printed quasi-Yagi antenna with size reduction."Antennas and Propagation, IEEE Transactions on 62, no. 1 (2014): 463-467.

[41] Lo, H. Y., K. W. Leung, and K. M. Luk. "Slot-line-excited equilateral-triangular dielectric resonator antenna of very high permittivity." Microwave and Optical technology letters 29, no. 4 (2001): 230-231.

[42] Buerkle, Amelia, Kamal Sarabandi, and Hossein Mosallaei. "Compact slot and dielectric resonator antenna with dual-resonance, broadband characteristics."Antennas and Propagation, IEEE Transactions on 53, no. 3 (2005): 1020-1027.

[43] Almpanis, G., C. Fumeaux, and R. Vahldieck. "Dual mode slot coupled cylindrical dielectric resonator antenna." In Antennas and Propagation Society International Symposium 2006, IEEE, pp. 2511-2514. IEEE, 2006.

CITED LITERATURE (continued)

[44] Leung, K. W., and C. K. Leung. "Wideband dielectric resonator antenna excited by cavity-backed circular aperture with microstrip tuning fork." Electronics Letters 39, no. 14 (2003): 1033-1035.

[45] Leung, K. W., K. M. Luk, E. K. N. Yung, and S. Lai. "Characteristics of a low-profile circular disk DR antenna with very high permittivity." Electronics Letters31, no. 6 (1995): 417-418.

[46] Tam, Matthew TK, and Ross D. Murch. "Compact cylindrical sector dielectric resonator antennas." In Antennas and Propagation Society International Symposium, 1998. IEEE, vol. 4, pp. 1958-1961. IEEE, 1998.

[47] Mongia, R. K., A. Ittipiboon, M. Cuhaci, and D. Roscoe. "Circularly polarised dielectric resonator antenna." Electronics Letters 30, no. 17 (1994): 1361-1362.

[48] Huang, Chih-Yu, Kin-Lu Wong, Cheng-Fu Yang, and Jian-Yi Wu. "Planar array composed of two linearly polarized dielectric resonator antennas for circular polarization." Microwave and Optical Technology Letters 21, no. 5 (1999): 323-324.

[49] Hwang, Y., Y. P. Zhang, K. M. Luk, and E. K. N. Yung. "Gain-enhanced miniaturised rectangular dielectric resonator antenna." Electronics Letters 33, no. 5 (1997): 350-352.

[50] Luk, K. M., K. W. Leung, and K. Y. Chow. "Bandwidth and gain enhancement of a dielectric resonator antenna with the use of a stacking element."Microwave and Optical Technology Letters 14, no. 4 (1997): 215-217.

[51] Shum, S. M., and K. M. Luk. "Stacked annular ring dielectric resonator antenna excited by axi-symmetric coaxial probe." Antennas and Propagation, IEEE Transactions on 43, no. 8 (1995): 889-892.

[52] Petosa, A., M. Cuhaci, N. Simons, A. Ittipiboon, and R. Larose. "A Novel Microstrip-Fed Multi-Segment Dielectric Resonator Antenna." ANTEM (1996): 705-708.

[53] Petosa, Aldo, R. K. Mongia, M. Cuhaci, and Jim S. Wight. "Magnetically tunable ferrite resonator antenna." Electronics Letters 30, no. 13 (1994): 1021-1022.

[54] Kingsley, S. P., and Steven Gregory O'Keefe. "Beam steering and monopulse processing of probe-fed dielectric resonator antennas." IEE Proceedings-Radar, Sonar and Navigation 146, no. 3 (1999): 121-125.

CITED LITERATURE (continued)

[55] Lim, E. H., and K. W. Leung. "Experimental Study on the Dualfunction Dielectric-Resonator-Antenna-Filter." In Microwave Conference, 2007. APMC 2007. Asia-Pacific, pp. 1-4. IEEE, 2007.

[56] Hady, Laila K., Darko Kajfez, and Ahmed Kishk. "Dielectric resonator antenna in a polarization filtering cavity for dual function applications." Microwave Theory and Techniques, IEEE Transactions on 56, no. 12 (2008): 3079-3085.

[57] Gao, Yuan, Alexandre P. Popov, Ban-Leong Ooi, and Mook-Seng Leong. "Integrated hybrid dielectric resonator antenna for system-in-package application." In Microwave Symposium, 2007. IEEE/MTT-S International, pp. 1653-1656. IEEE, 2007.

[58] Popov, Alexander Pavlovich, Mihai Dragos Rotaru, and Mahadevan Krishna Iyer. "Packaged integrated antenna for circular and linear polarizations." U.S. Patent 6,879,287, issued April 12, 2005.

[59] Oh, Jungsuek, Taejong Baek, Donghoon Shin, Jinkoo Rhee, and Sangwook Nam. "60-GHz CPW-fed dielectric-resonator-above-patch (DRAP) antenna for broadband WLAN applications using micromachining technology." Microwave and Optical Technology Letters 49, no. 8 (2007): 1859-1861.

[60] Bijumon, P. V., A. P. Freundorfer, M. Sayer, and Y. M. M. Antar. "On-chip silicon integrated cylindrical dielectric resonator antenna for millimeter wave applications." In Signals, Systems and Electronics, 2007. ISSSE'07. International Symposium on, pp. 489-492. IEEE, 2007.

[61] Doan, Chinh H., Sohrab Emami, David Sobel, Ali M. Niknejad, and Robert W. Brodersen. "Design considerations for 60 GHz CMOS radios." Communications Magazine, IEEE 42, no. 12 (2004): 132-140.

[62] Lo, Yuen T., and S. W. Lee. Antenna Handbook: Volume III Applications. Springer Science & Business Media, 2012.

[63] Rappaport, By Theodore S., James N. Murdock, and Felix Gutierrez. "State of the art in 60-GHz integrated circuits and systems for wireless communications." Proceedings of the IEEE 99, no. 8 (2011): 1390-1436.

[64] Daniels, Robert C., James N. Murdock, Theodore S. Rappaport, and Robert W. Heath Jr. "60 GHz wireless: Up close and personal." Microwave Magazine, IEEE 11, no. 7 (2010): 44-50.

CITED LITERATURE (continued)

[65] URL http://www.ieee802.org/15, “IEEE 802.15 Working Group for WPAN”.

[66] Giannetti, Filippo, Marco Luise, and Ruggero Reggiannini. "Mobile and personal communications in the 60 GHz band: A survey." Wireless Personal Communications 10, no. 2 (1999): 207-243.

[67] Anderson, Christopher R., and Theodore S. Rappaport. "In-building wideband partition loss measurements at 2.5 and 60 GHz." Wireless Communications, IEEE Transactions on 3, no. 3 (2004): 922-928.

[68] Millimeter Wave Wireless Communications: The Renaissance of Computing and Communications, 2014 International Conference on Communications, Keynote presentation, Sydney, Australia, June 13, 2014

[69] Gutierrez Jr, Felix, Shatam Agarwal, Kristen Parrish, and Theodore S. Rappaport. "On-chip integrated antenna structures in CMOS for 60 GHz WPAN systems." Selected Areas in Communications, IEEE Journal on 27, no. 8 (2009): 1367-1378.

[70] Zhang, Yue Ping, M. Sun, Kai Meng Chua, L. L. Wai, and Duixian Liu. "Antenna-in-package design for wirebond interconnection to highly integrated 60-GHz radios." Antennas and Propagation, IEEE Transactions on 57, no. 10 (2009): 2842-2852.

[71] Zwick, Thomas, Duixian Liu, and Brian P. Gaucher. "Broadband planar superstrate antenna for integrated millimeterwave transceivers." Antennas and Propagation, IEEE Transactions on 54, no. 10 (2006): 2790-2796.

[72] Seki, Tomohiro, Naoki Honma, Kenjiro Nishikawa, and Kouichi Tsunekawa. "Millimeter-wave high-efficiency multilayer parasitic microstrip antenna array on teflon substrate." Microwave Theory and Techniques, IEEE Transactions on53, no. 6 (2005): 2101-2106.

[73] Zhang, Yue Ping, and Duixian Liu. "Antenna-on-chip and antenna-in-package solutions to highly integrated millimeter-wave devices for wireless communications." Antennas and Propagation, IEEE Transactions on 57, no. 10 (2009): 2830-2841.

[74] Sun, M., Y. P. Zhang, K. M. Chua, L. L. Wai, D. Liu, and B. P. Gaucher. "Integration of Yagi antenna in LTCC package for differential 60-GHz radio."IEEE transactions on antennas and propagation 56, no. 8 (2008): 2780-2783.

CITED LITERATURE (continued)

[75] Seki, Tomohiro, Kenjiro Nishikawa, and Kazuyasu Okada. "60-GHz multi-layer parasitic microstrip array antenna with stacked rings using multi-layer LTCC substrate." In Radio and Wireless Symposium, 2008 IEEE, pp. 679-682. IEEE, 2008.

[76] Zwick, Thomas, Arun Chandrasekhar, Christian W. Baks, Ullrich R. Pfeiffer, Steven Brebels, and Brian P. Gaucher. "Determination of the complex permittivity of packaging materials at millimeter-wave frequencies." Microwave Theory and Techniques, IEEE Transactions on 54, no. 3 (2006): 1001-1010.

[77] Kim, Il Kwon, Stephane Pinel, Joy Laskar, and Jong-Gwan Yook. "Circularly & linearly polarized fan beam patch antenna arrays on liquid crystal polymer substrate for V-band applications." In Microwave Conference Proceedings, 2005. APMC 2005. Asia-Pacific Conference Proceedings, vol. 4, pp. 3-pp. IEEE, 2005.

[78] Kam, Dong Gun, Duixian Liu, Arun Natarajan, Scott Reynolds, and Brian Floyd. "Low-cost antenna-in-package solutions for 60-GHz phased-array systems." InElectrical Performance of Electronic Packaging and Systems (EPEPS), 2010 IEEE 19th Conference on, pp. 93-96. IEEE, 2010.

[79] Chen, I., Hwann-Kaeo Chiou, and Nan-Wei Chen. "V-band on-chip dipole-based antenna." Antennas and Propagation, IEEE Transactions on 57, no. 10 (2009): 2853-2861.

[80] Bijumon, P. V., Y. M. M. Antar, A. P. Freundorfer, and M. Sayer. "Integrated dielectric resonator antennas for system on-chip applications." InMicroelectronics, 2007. ICM 2007. Internatonal Conference on, pp. 275-278. IEEE, 2007.

[81] Yang, HY David, and S. S. Zhao. "Millimeter-wave antennas on a LTCC cavity." In Antennas and Propagation Society International Symposium (APSURSI), 2012 IEEE, pp. 1-2. IEEE, 2012.

[82] Zhang, Yue Ping, Mei Sun, and L. H. Guo. "On-chip antennas for 60-GHz radios in silicon technology." Electron Devices, IEEE Transactions on 52, no. 7 (2005): 1664-1668.

[83] Wai, Lai L., Kai M. Chua, Albert CW Lu, Y. P. Zhang, and M. Sun. "Ultra compact LTCC based AiP for 60 GHz applications." In Electronics Packaging Technology Conference, 2007. EPTC 2007. 9th, pp. 595-599. IEEE, 2007.

[84] Kim, Il K. WO, Stephan Pinel, John Papapolymerou, Manos M. Tentzeris, Joy Laskar, and Jong-Gwan Yook. "Linear tapered slot antennas on LTCC substrate for millimeter-

CITED LITERATURE (continued)

wave applications." In Antennas and Propagation Society International Symposium, 2005 IEEE, vol. 2, pp. 483-486. IEEE, 2005.

[85] Gong, Ke, Zhi Ning Chen, Xianming Qing, Peng Chen, and Wei Hong. "Substrate integrated waveguide cavity-backed wide slot antenna for 60-GHz bands." Antennas and Propagation, IEEE Transactions on 60, no. 12 (2012): 6023-6026.

[86] Almpanis, Georgios, Christophe Fumeaux, and Ruediger Vahldieck. "The trapezoidal dielectric resonator antenna." Antennas and Propagation, IEEE Transactions on 56, no. 9 (2008): 2810-2816.

[87] Lim, Eng Hock, and Kwok Wa Leung. "Novel application of the hollow dielectric resonator antenna as a packaging cover." Antennas and Propagation, IEEE Transactions on 54, no. 2 (2006): 484-487.

[88] Soren, Dipali, Rowdra Ghatak, Rabindra Kishore Mishra, and Dipak Ranjan Poddar. "Dielectric Resonator Antennas: Designs and Advances." Progress In Electromagnetics Research B 60 (2014): 195-213.

[89] Baghaee, Reza Mohammadi, Mohammad H. Neshati, and Jalil Rashed Mohassel. "Rigorous analysis of rectangular dielectric resonator antenna with a finite ground plane." Antennas and Propagation, IEEE Transactions on 56, no. 9 (2008): 2801-2809.

[90] Li, Bin, and Kwok Wa Leung. "On the differentially fed rectangular dielectric resonator antenna." Antennas and Propagation, IEEE Transactions on 56, no. 2 (2008): 353-359.

[91] Okaya, A., and L. F. Barash. "The dielectric microwave resonator."Proceedings of the IRE 50, no. 10 (1962): 2081-2092.

[92] Van Bladel, Jean. "On the resonances of a dielectric resonator of very high permittivity." IEEE Transactions on Microwave Theory Techniques 23 (1975): 199-208.

[93] Marcatili, Enrique AJ. "Dielectric rectangular waveguide and directional coupler for integrated optics." Bell System Technical Journal 48, no. 7 (1969): 2071-2102.

[94] Itoh, Tatsuo, and Chen Chang. "Resonant characteristics of dielectric resonators for millimeter-wave integrated circuits." In 1978 IEEE-MTT-S International Microwave Symposium Digest, pp. 121-122. 1978.

CITED LITERATURE (continued)

[95] Mongia, R. K. "Theoretical and experimental resonant frequencies of rectangular dielectric resonators." In IEE Proceedings H (Microwaves, Antennas and Propagation), vol. 139, no. 1, pp. 98-104. IET Digital Library, 1992.

[96] Collin, Robert E. Foundations for microwave engineering. John Wiley & Sons, 2007.

[97] Almpanis, Georgios, Cristophe Fumeaux, and Rüdiger Vahldieck. "Offset cross-slot-coupled dielectric resonator antenna for circular polarization."Microwave and Wireless Components Letters, IEEE 16, no. 8 (2006): 461-463.

[98] Liang, Xian-Ling, and Tayeb Denidni. "H-shaped dielectric resonator antenna for wideband applications." Antennas and Wireless Propagation Letters, IEEE 7 (2008): 163-166.

[99] Birand, M. T., and R. V. Gelsthorpe. "Experimental millimetric array using dielectric radiators fed by means of dielectric waveguide." Electronics Letters17, no. 18 (1981): 633-635.

[100] Hwang, Y., Y. P. Zhang, K. M. Luk, and E. K. N. Yung. "Gain-enhanced miniaturised rectangular dielectric resonator antenna." Electronics Letters 33, no. 5 (1997): 350-352.

[101] Esselle, K. P. "Antennas with dielectric resonators and surface mounted short horns for high gain and large bandwidth." IET Microwaves, Antennas & Propagation 1, no. 3 (2007): 723-728.

[102] Antar, Yahia MM. "Antennas for wireless communication: recent advances using dielectric resonators." IET circuits, devices & systems 2, no. 1 (2008): 133-138.

[103] El-Deen, Emad, S. H. Zainud-Deen, H. A. Sharshar, and M. A. Binyamin. "The effect of the ground plane shape on the characteristics of rectangular dielectric resonator antennas." In 2006 IEEE Antennas and Propagation Society International Symposium. 2006.

[104] Li, Bin, and Kwok Wa Leung. "Strip-fed rectangular dielectric resonator antennas with/without a parasitic patch." Antennas and Propagation, IEEE Transactions on 53, no. 7 (2005): 2200-2207.

[105] DeYoung, C., and Stuart Long. "Wideband cylindrical and rectangular dielectric resonator antennas." IEEE Antennas and Wireless Propagation Letters 1, no. 5 (2006): 426-429.

CITED LITERATURE (continued)

[106] Chang, Tze-Hsuan, and Jean-Fu Kiang. "Dualband split dielectric resonator antenna." Antennas and Propagation, IEEE Transactions on 55, no. 11 (2007): 3155-3162.

[107] Esselle, Karu P. "Circularly polarised higher-order rectangular dielectric-resonator antenna." Electronics Letters 32, no. 3 (1996): 150-151.

[108] Petosa, Aldo, Soulideth Thirakoune, and Apisak Ittipiboon. "Higher-order modes in rectangular DRAs for gain enhancement." In 2009 13th International Symposium on Antenna Technology and Applied Electromagnetics and the Canadian Radio Science Meeting. 2009.

[109] Petosa, Aldo, and Soulideth Thirakoune. "Rectangular dielectric resonator antennas with enhanced gain." IEEE transactions on antennas and propagation59, no. 4 (2011): 1385-1389.

[110] Pan, Yong-Mei, Kwok Wa Leung, and Kwai-Man Luk. "Design of the millimeter-wave rectangular dielectric resonator antenna using a higher-order mode."Antennas and Propagation, IEEE Transactions on 59, no. 8 (2011): 2780-2788.

[111] Lamminen, Antti EI, Jussi Säily, and Antti R. Vimpari. "60-GHz patch antennas and arrays on LTCC with embedded-cavity substrates." antennas and propagation, ieee transactions on 56, no. 9 (2008): 2865-2874.

[112] Yeap, Siew Bee, Xianming Qing, Mei Sun, and Zhi Ning Chen. "140-GHz 2× 2 SIW horn array on LTCC." In Antennas and Propagation (APCAP), 2012 IEEE Asia-Pacific Conference on, pp. 279-280. IEEE, 2012.

[113] Brown, J., and J. O. Spector. "The radiating properties of end-fire aerials."Proceedings of the IEE-Part B: Radio and Electronic Engineering 104, no. 13 (1957): 27-34.

[114] Balanis, Constantine A. Antenna Theory: Analysis and Design. John Wiley & Sons, 2012.

[115] Clarke, R. H. "A method of estimating the power radiated directly at the feed of a dielectric-rod aerial." Proceedings of the IEE-Part B: Radio and Electronic Engineering 104, no. 17 (1957): 511-514.

[116] Johnson, Richard C., and Henry Jasik. "Antenna engineering handbook." New York, McGraw-Hill Book Company, 1984, 1356 p. No individual items are abstracted in this volume. 1 (1984).

CITED LITERATURE (continued)

[117] URL http://www.eetindia.co.in/STATIC/PDF/200810/EEIOL_2008OCT09_EDA_TA_01.pdf?SOURCES=DOWNLOAD, “SoC vs SiP: design alternatives and challenges”

[118] Zhang, Yue Ping, and Duixian Liu. "Antenna-on-chip and antenna-in-package solutions to highly integrated millimeter-wave devices for wireless communications." Antennas and Propagation, IEEE Transactions on 57, no. 10 (2009): 2830-2841.

APPENDIX: DESIGN CURVE AND MATLAB CODE

The design curve in this thesis serves as a practical tool for the design of low-profile end-fire rectangular DRA in 60GHz using LTCC ($\varepsilon_r = 7.5$). Since it has been proven that the thickness is the dimension that affects the antenna performance the most, the figure is a cluster of curves with respect to different thickness. For each width shown on the horizontal axis, there is an optimized length associated with it for the highest end-fire gain available on the vertical axis according to the equation (21) and (22) in chapter 3. In addition, the three dimensions of the DRA should avoid the occurrence of the transverse modes in order not to deteriorate the end-fire gain.

As an example, the following matlab code was used to generate the curve with a thickness of 0.45mm.

'Design Curve. m'

```
%plot the design curve
clear all;
b=0.45*10^(-3);
er=7.5;
c=0.3;
f0=60;
m=1;
n=1;
k0=2*pi*f0/c;
l0=c/f0;
astart=2*10^(-3);
astep=0.01*10^(-3);
astop=l0;
p=1;
```

APPENDIX (continued)

```
size=(astop-astart)/astep;
width=zeros(size);
lmax=zeros(size);
dopt=zeros(size);
deg=zeros(size);
root3=zeros(size);
root4=zeros(size);
kz=zeros(size);
lg=zeros(size);
l=zeros(size);
for a=astart:astep:astop
y3=@(x1) x1*a-m.*pi+2*atan(x1./(er*((er-1)*k0.^2-x1.^2).^0.5));
y4=@(y1) y1*b-n.*pi+2*atan(y1./((er-1)*k0.^2-y1.^2).^0.5);
%bisection is a function for analytical solution
root3(p)=bisection(y3,0,5000,0.001,0);
root4(p)=bisection(y4,0,5000,0.001,0);
kz(p)=sqrt(er*k0.^2-root3(p).^2-root4(p).^2);
lg(p)=2*pi./kz(p);
l(p)=fix(2*l0./(l0-lg(p)));
if rem(l(p),2)==1
   lmax(p)=l(p);
else lmax(p)=l(p)+1;
end
dopt(p)=1./kz(p).*(0.5*lmax(p).*pi-atan(kz(p)./(er*((er-1)*k0.^2-kz(p).^2).^0.5)));
width(p)=a;
deg(p)=getfr(a,b,dopt(p));
if deg(p)==1
   break;
end
p=p+1;
end
x=find(width);
y=find(dopt);
plot(width(x),dopt(y));
axis([2*10^(-3),5*10^(-3),2*10^(-3),9*10^(-3)]);
‘bisection.m’
function root = bisection(fname,a,b,delta,display)
% The bisection method.
%
```

APPENDIX (continued)

```
%input: fname is a string that names the function f(x)
% a and b define an interval [a,b]
% delta is the tolerance
% display = 1 if step-by-step display is desired,
% = 0 otherwise
%output: root is the computed root of f(x)=0
%
fa = feval(fname,a);
fb = feval(fname,b);
if sign(fa).*sign(fb) > 0
disp('function has the same sign at a and b')
return
end
if fa == 0,
root = a;
return
end
if fb == 0
root = b;
return
end
c = (a+b)/2;
fc = feval(fname,c);
e_bound = abs(b-a)/2;
if display,
disp(' ');
disp(' a b c f(c) error_bound');
disp(' ');
disp([a b c fc e_bound])
end
while e_bound > delta
if fc == 0,
root = c;
return
end
if sign(fa).*sign(fc) < 0 % a root exists in [a,c].
b = c;
fb = fc;
else % a root exists in [c,b].
```

APPENDIX (continued)

```
a = c;
fa = fc;
end
c = (a+b)/2;
fc = feval(fname,c);
e_bound = e_bound/2;
if display, disp([a b c fc e_bound]), end
end
root = c;
```

'getfr.m'

```
function root = getfr(a,b,d)
%this code tells you whether fr of TE311y is below 60G
c=0.3;
f0=60;
er=7.5;
f=[f0,f0+0.1];
k0=2*pi*f/c;
y6=@(x2) x2*a-3.*pi+2*atan(x2./(er*((er-1)*k0.^2-x2.^2).^0.5));
y7=@(y2) y2*b-pi+2*atan(y2./((er-1)*k0.^2-y2.^2).^0.5);
y8=@(z2) z2*2*d-pi+2*atan(z2./(er*((er-1)*k0.^2-z2.^2).^0.5));
%bisection is a function for analytical soluiton
root6=bisection(y6,0,7000,0.001,0);
root7=bisection(y7,0,5000,0.001,0);
root8=bisection(y8,0,5000,0.001,0);
x=abs(root6.^2+root7.^2+root8.^2-er*k0.^2);
if x(1)>x(2)
   root=0;
else root=1;
end
```

VITA

NAME	SHANSHAN ZHAO
EDUCATION	PhD, University of Illinois at Chicago, 2015 BS, Nanjing University of Sci. & Tech., China, 2010
EXPERIENCE	Research Assistant in Electrical and Computer Engineering Department, UIC, 2011-2015 Teaching Assistant in Electrical and Computer Engineering Department, UIC, 2011-2015 Lecturer of ECE 322: Communication Electromagnetics in Electrical and Computer Engineering Department, UIC, 2015 Summer Intern in Tensorcom Inc., CA, 2012, 2013
AFFILIATIONS	IEEE Student Member, 2011-2015 Member of Society of Women Engineers, 2011-2015
HONORS	Hewlett-Packard Fellowship, UIC, 2010
PUBLICATIONS	Zhao, S.S.; Yang, H.Y.D., "Analysis of LTCC Millimeter-Wave Dielectric Slab Antennas", IEEE Antennas and Propagation Society International Symposium (APSURSI), pp. 1872 - 1873, 2013 Yang, H.Y.D.; Zhao, S.S., "Millimeter-Wave Antennas on a LTCC Cavity", IEEE Antennas and Propagation Society International Symposium (APSURSI), pp. 1-2, 2012 ShanShan Zhao and H.Y. David Yang, "Millimeter-Wave Printed Yagi-Uda Antennas", URSI, 2012 Zhao, S.S.; Yang, H.Y.D., "Design Considerations of Low-profile End-fire Dipole Dielectric Antenna at 60GHz", in submission Wang, J.; Xu, L.-J.; Zhao, S.; Guo, Y.-X.; Wu, W., "Compact Quasi-elliptic Microstrip Lowpass Filter with Wide Stopband", Electronics Letters, Vol. 46, pp. 1384 - 1385, 2010 Jianpeng Wang; Jia-Lin Li; Jia Ni; Shanshan Zhao; Wen Wu; Dagang Fang, "Design of Miniaturized Microstrip Dual-Mode Filter with Source-Load Coupling", IEEE Microwave and Wireless Components Letters, Vol. 20, pp. 319 - 321, 2010 J. Wang, J. Ni, S. Zhao, Y. X. Guo, "Compact Microstrip Ring Branch-line Coupler with Harmonic Suppression", J. of Electromagn. Waves and Appl., pp. 2119-2126, 2009